FUNCTIONAL CHARACTERIZATION OF CHARGED RESIDUES IN THE β10-β11 RECEPTOR-BINDING LOOP OF *Bacillus thuringiensis* Cry4Aa AND Cry4Ba TOXINS

SARINPORN VISITSATTAPONGSE

A THESIS SUBMITTED IN PARTIAL FULFILLMENT
OF THE REQUIREMENTS FOR
THE DEGREE OF DOCTOR OF PHILOSOPHY
(MEDICAL TECHNOLOGY)
FACULTY OF GRADUATE STUDIES
MAHIDOL UNIVERSITY
2014

Thesis
entitled

FUNCTIONAL CHARACTERIZATION OF CHARGED RESIDUES IN THE β10-β11 RECEPTOR-BINDING LOOP OF *Bacillus thuringiensis* Cry4Aa AND Cry4Ba TOXINS

Sarinporn Visitsattapongse

Miss Sarinporn Visitsattapongse
Candidate

Prof. Chanan Angsuthanasombat, Ph.D.
Major advisor

Asst. Prof. Chamras Promptmas, Ph.D.
Co-advisor

Lect. Somphob Leetachewa, Ph.D.
Co-advisor

Lect. Chalermpol Kanchanawarin, Ph.D.
Co-advisor

Prof. Banchong Mahaisavariya,
M.D., Dip. Thai Board of Orthopidic
Dean
Faculty of Graduate Studies
Mahidol University

Prof. Virapong Prachyasittikul, Ph.D.
Program Director
Doctor of Philosophy Program in
Medical Technology
Faculty of Medical Technology
Mahidol University

Thesis
entitled

FUNCTIONAL CHARACTERIZATION OF CHARGED RESIDUES IN THE β10-β11 RECEPTOR-BINDING LOOP OF *Bacillus thuringiensis* Cry4Aa AND Cry4Ba TOXINS

was submitted to the Faculty of Graduate Studies, Mahidol University
for the degree of Doctor of Philosophy (Medical Technology)
on
April 30, 2014

Sarinporn Visitsattapongse
.....
Miss Sarinporn Visitsattapongse
Candidate

Kosum Chansiri
.....
Assoc. Prof. Kosum Chansiri, Ph.D.
Chair

Somphob Leetachewa
.....
Lect. Somphob Leetachewa, Ph.D.
Member

C. Angsuthanasombat
.....
Prof. Chanan Angsuthanasombat, Ph.D.
Member

Chamras Promptmas
.....
Asst. Prof. Chamras Promptmas, Ph.D.
Member

.....
Lect. Chalermpol Kanchanawarin, Ph.D.
Member

B. Mahaisavariya
.....
Prof. Banchong Mahaisavariya,
M.D., Dip. Thai Board of Orthopedics
Dean
Faculty of Graduate Studies
Mahidol University

Virapong Prachyasittikul
.....
Prof. Virapong Prachyasittikul, Ph.D.
Dean
Faculty of Medical Technology
Mahidol University

ACKNOWLEDGEMENTS

I would like to thank my advisor, Assoc. Prof. Chanan Angsuthanasombat, for his patronize of valuable guide and encouragement in various stages of this project. I am also graceful to my co-advisors, Asst. Prof. Chamras Promptmas, Dr. Somphob Leetachewa and Dr. Chalermpol Kanchanawarin.

My appreciation is extended to Ms. Somsri Sakdee and Miss Chompounoot Imtong, for providing research facilities and concerning in my work through this research project.

I would like to thank the Commission on Higher Education, Thailand for financial support throughout my study in this project.

Finally, I would like to thank my parents for their love and encouragement.

Sarinporn Visitsattapongse

FUNCTIONAL CHARACTERIZATION OF CHARGED RESIDUES IN THE β10-β11 RECEPTOR-BINDING LOOP OF *Bacillus thuringiensis* Cry4Aa AND Cry4Ba TOXINS

SARINPORN VISITSATTAPONGSE 5037437 MTMT/D

Ph.D. (MEDICAL TECHNOLOGY)

THESIS ADVISORY COMMITTEE: CHANAN ANGSUTHANASOMBAT, Ph.D., CHAMRAS PROMPTMAS, Ph.D., SOMPHOB LEETACHEWA, Ph.D., CHALERMPOL KANCHANAWARIN, Ph.D.

ABSTRACT

Cry4Aa and Cry4Ba, two closely related mosquito-active toxins produced by *Bacillus thuringiensis* subsp. *israelensis* during sporulation, are highly specific to different target mosquito-larvae, according to high dissimilarity between their receptor-binding domain (II). Single-alanine substitutions of five amino-acid residues within the β10-β11 loop of Cry4Aa-domain II revealed that only Lys^{514} is required for Cry4Aa toxicity against *Culex* larvae. Opposite to that of Cry4Aa, the β10-β11 loop of Cry4Ba which is less toxic to *Culex* larvae contains a negative residue–Asp^{454}. Target specificity analysis *via* charge reversal mutagenesis of the Cry4Ba-Asp^{454} revealed that D454K and D454R substitutions can introduce *Culex* toxicity to the Cry4Ba toxin, although D454A mutation showed no effect on toxicity against *Culex* larvae. Consistent with data from bioassays, *in situ* binding analysis *via* immunohistochemical assay displayed that both D454K and D454R mutants, but not the D454A mutant, showed a significant increase in binding to *Culex*-larval gut membrane. These data suggest that charge within the β10-β11 loop is a determinant for different *Culex* toxicity between Cry4Ba and Cry4Aa toxins, thus suggesting that both toxins bind to *Culex* receptor through ionic interactions.

KEY WORDS: LARVICIDAL ACTIVITY/RECEPTOR-BINDING LOOP/ CHARGE-REVERSAL MUTATION/Cry4Aa/Cry4Ba

130 pages

การศึกษาเชิงหน้าที่ของกรดอะมิโนชนิดที่มีขั้วในส่วนเชื่อมต่อ เบต้าที่ 10 และ 11 โปรตีนสารพิษ Cry4Aa และ Cry4Ba จาก *Bacillus thuringiensis*

FUNCTIONAL CHARACTERIZATION OF CHARGED RESIDUES IN THE β10-β11 RECEPTOR-BINDING LOOP OF *Bacillus thuringiensis* Cry4Aa AND Cry4Ba TOXINS

สรินพร วิสิฐสัทธาพงศ์ 5037437 MTMT/D

ปร.ด. (เทคนิคการแพทย์)

คณะกรรมการที่ปรึกษาวิทยานิพนธ์: ชนันท์ อังศุธนสมบัติ, Ph.D., จำรัส พร้อมมาศ, Ph.D., สมภพ ลีตะชีวะ, Ph.D., เฉลิมพล กาญจนวรินทร์, Ph.D.

บทคัดย่อ

โปรตีนสารพิษฆ่าลูกน้ำยุง ชนิด Cry4Aa และ Cry4Ba จากแบคทีเรียชนิด *Bacillus thuringiensis* มีความจำเพาะต่อลูกน้ำยุงที่แตกต่างกัน อันเป็นผลมาจากความแตกต่างทางโครงสร้างในส่วนบริเวณที่ 2 (Receptor-binding domain) ของโปรตีนสารพิษทั้งสองชนิดนี้ การศึกษาด้วยการแทนที่กรดอะมิโนในส่วนเชื่อมต่อเบต้าที่ 10 และ 11 ในบริเวณส่วนที่ 2 ของโปรตีน Cry4Aa ด้วย alanine พบว่าเฉพาะโปรตีนกลายพันธุ์ชนิด K514A ที่สูญเสียความเป็นขั้วบวกเท่านั้นที่ออกฤทธิ์ฆ่าลูกน้ำยุง *Culex quinquefasciatus* ลดลง เป็นที่น่าสังเกตว่าในทางตรงกันข้าม โปรตีน Cry4Ba ซึ่งมีความเป็นพิษน้อยต่อลูกน้ำยุง *C. quinquefasciatus* นั้นมีกรดอะมิโนที่มีความเป็นขั้วลบ (Asp^{454}) ในส่วนเชื่อมต่อเบต้า 10 และ 11 และจากการศึกษาเพิ่มเติมพบว่าโปรตีนกลายพันธุ์ D454R และ D454K ของโปรตีน Cry4Ba มีความเป็นพิษต่อลูกน้ำยุง *C. quinquefasciatus* เพิ่มขึ้นอย่างชัดเจนเมื่อเปรียบเทียบกับโปรตีนกลายพันธุ์ D454A นอกจากนี้ผลจากการทดลองด้วยวิธี immune-histochemistry แสดงให้เห็นว่า เฉพาะโปรตีนกลายพันธ์ชนิด D454R และ D454K เท่านั้นที่สามารถจับกับส่วนบนสุดของเซลล์บุผิวของกระเพาะลูกน้ำยุง *C. quinquefasciatus* ได้ในปริมาณที่เพิ่มขึ้นกว่าเดิม จากผลทดลองในครั้งนี้จึงได้เสนอว่าชนิดของความเป็นขั้วที่ตรงกันข้ามของส่วนเชื่อมต่อเบต้า ที่10 และ 11 ของโปรตีนฆ่าลูกน้ำยุงทั้ง 2 ชนิดนี้มีผลต่อความจำเพาะในการฆ่าลูกน้ำยุงชนิด *C. quinquefasciatus*

130 หน้า

CONTENTS

CONTENTS (cont.)

CONTENTS (cont.)

CONTENTS (cont.)

LIST OF TABLES

LIST OF FIGURES

LIST OF FIGURES (cont.)

LIST OF FIGURES (cont.)

LIST OF FIGURES (cont.)

CHAPTER I
INTRODUCTION

Bacillus thuringiensis subsp. *israelensis* (*Bti*), a Gram-positive spore-forming bacterium, has been used for controlling insect pests for many decades [1]. During sporulation, it produces at least four major types of insecticidal proteins (Cry4Aa, Cry4Ba, Cry11Aa and Cyt1Aa) as crystalline inclusions which are highly toxic against mosquito larvae of the genera *Aedes*, *Culex* and *Anopheles* [2, 3]. However, individual insecticidal proteins expressed in *Escherichia coli* were found to be toxic towards mosquito larvae of certain genus, *e.g.*, Cry4Ba shows major toxicity to *Aedes* sp. and *Anopheles* sp. while Cry4Aa shows major toxicity to *Culex* sp.

After ingestion by susceptible mosquito-larvae, inclusions of the insecticidal proteins are solubilized under alkaline conditions of larval midgut and subsequently activated by gut proteases [3]. The activated proteins then bind to specific receptors located on the midgut cell membrane prior insertion into the membrane to form ion-leakage pore, resulting in osmotic cell lysis and ultimately mosquito larvae died before becoming adults.

Among *Bti* toxin, Cry4Aa and Cry4Ba (both of ca. 130 kDa) are the most closely related toxin. The identity of their N-terminal and C-terminal amino-acid sequences share ~55% similarity [4]. As previously showed, *in vitro* activation of both 130-kDa Cry4Aa and Cry4Ba toxins by trypsin yielded 65-kDa activated toxins comprising two non-covalently associated fragments of ca. 20 and ca. 47 kDa [5]. The two trypsin-resistant fragments (20- and 47-kDa) were produced by cleavage at Arg^{235} and Arg^{203} located in surface-exposed α5-α6 loop of domain I of Cry4Aa and Cry4Ba, respective [5]. Structural data obtained by X-ray crystallographic analysis revealed that the 65-kDa Cry4Aa and Cry4Ba toxins are composed of three distinct domains (**Fig. 1.1**): a helical bundle domain (I), a β-prism of three antiparallel β-sheets (domain II) and a β-sandwich of two antiparallel β-sheets (domain III).

Domain II of Cry toxin is the most variable region. It consists of three anti-parallel β-sheets ending with surface-exposed loops (β1-α8, β2-β3, β4-β5, β6-β7, β8-β9 and β10-β11 loops). Many research groups have investigated the role in toxicity and specificity of such domain-II surface-exposed loops of Cry toxins using site-directed mutagenesis strategy and found that these loops are involved in receptor binding and thus confer insect specificity [6-8]. Moreover, replacement of surface-exposed β2-β3 loop of non-*Aedes* larvae toxic Cry19Aa with that of *Aedes* larvae toxic Cry4Ba resulted in a great improvement of Cry19Aatoxicity to *Aedes* larvae [9].

Previous studies demonstrated that β6-β7, β8-β9 and β10-β11 loops of Cry4Ba-domain II are involved in toxicity against *Aedes* larvae. [6, 7]. In addition, it was shown that toxicity of Cry4Ba against Culex larvae could be increased by replacement of Asp^{454} located in the β10-β11 loop of Cry4Ba with a variety of tripeptides [10]. In the present study, we have focused on charged residues within the β10-β11 loop of non-*Culex* toxic Cry4Ba and *Culex*- toxic Cry4Aa (Cry4Ba-Asp^{454} and Cry4Aa-Lys^{514}) and found that positive charge at such loop is required for *Culex* toxicity of both toxins.

Thesis Objective:

The objectives of this thesis are:

1. To examine whether there is a residue within the β6-β7 loop (**Fig. 1.2** and **1.5**) and the β10-β11 loop (**Fig. 1.3** and **1.6**) of the Cry4Aa-domain II that is critical for *C. quinquefasciatus* larval toxicity.

2. To investigate an involvement of a negatively charged residue within the β10-β11 loop (**Fig. 1.4** and **1.6**) of the Cry4Ba-domain II in *C. quinquefasciatus* larvae toxicity.

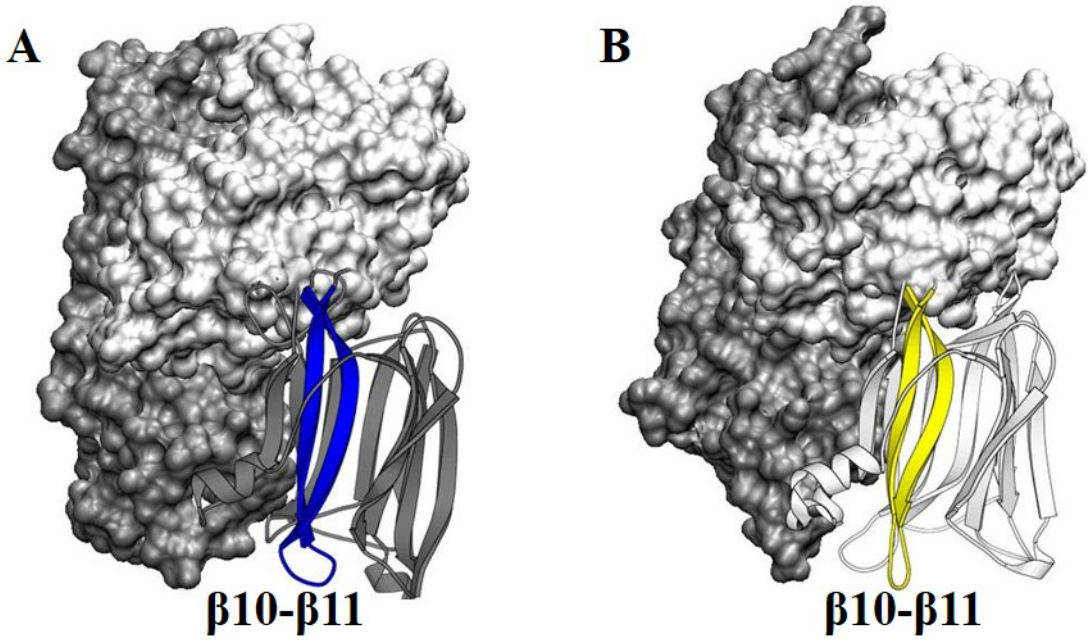

Figure 1.1: Ribbon and surface representation of Cry4Aa and Cry4Ba toxins

(A) The Cry4Ba toxin [11] is shown in three-domain organization; domains I and III (surface model), and domain II (schematic ribbon). The β10 - β11 hairpin in domain II is depicted as blue ribbon.

(B) The Cry4Aa toxin [12] is shown in three-domain organization; domains I and III (surface model), and domain II (schematic ribbon). The β10 - β11 hairpin in domain II is depicted as yellow ribbon.

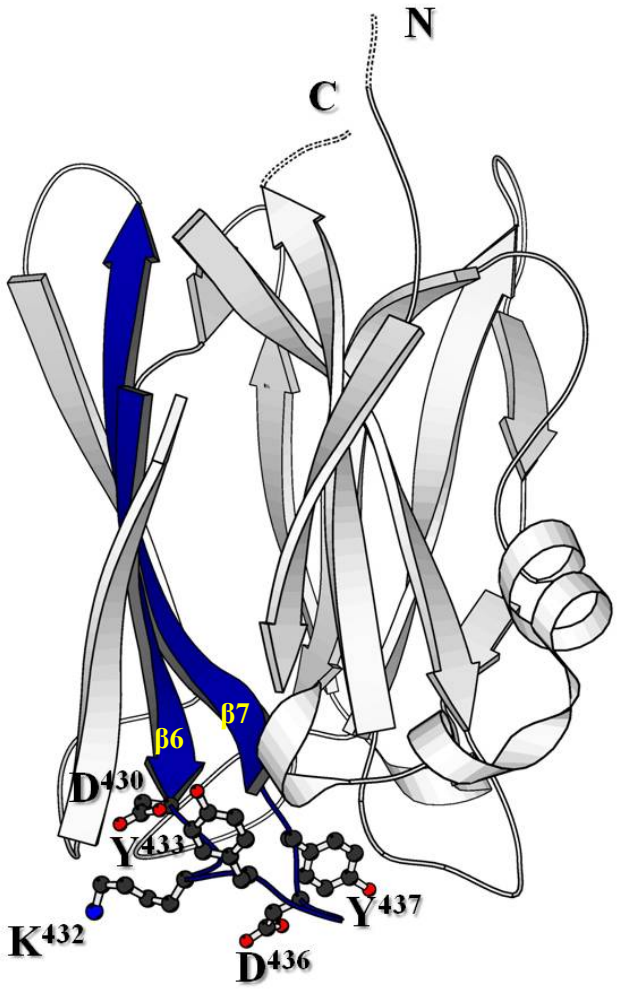

Figure 1.2: β6-β7 loop of Cry4Aa-domain II

The figure shows ribbon representation of the Cry4Aa-domain II. Five residues (D^{430}, K^{432}, Y^{433}, D^{436} and Y^{437}) in the β6-β7 loop (blue-colored) are shown in ball-and-stick representation.

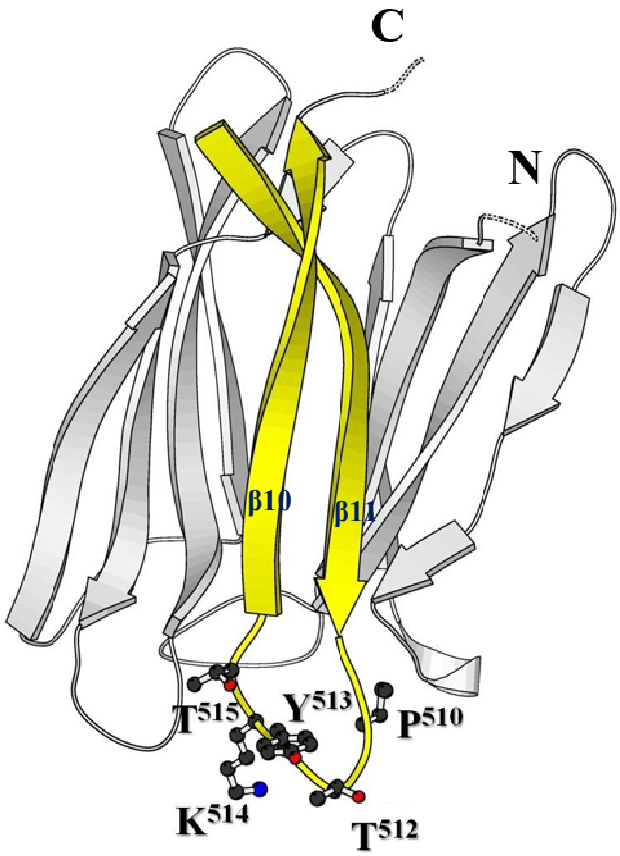

Figure 1.3: β10-β11 loop of Cry4Aa – domain II

The figure shows ribbon representation of the Cry4Aa-domain II. Five residues (P^{510}, T^{512}, Y^{513}, K^{514} and T^{515}) in the β10-β11 loop (yellow-colored) are shown in ball-and-stick representation.

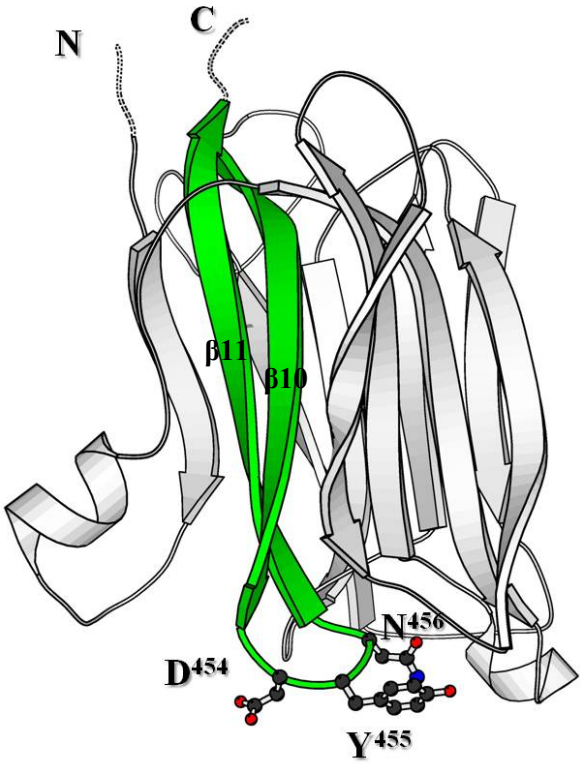

Figure 1.4: β10-β11 loop of Cry4Ba toxin-domain II

The figure shows ribbon representation of the Cry4Ba-domain II. Three residues (D^{454}, Y^{455} and N^{456}) in the β10-β11 loop (green-colored) are shown in ball-and-stick representation.

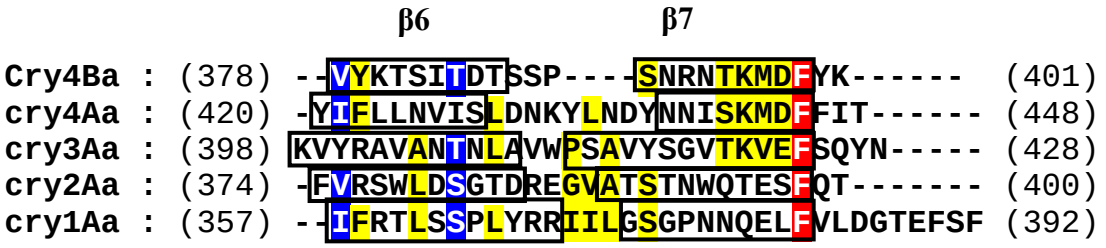

Figure 1.5: Multiple sequence alignments of the β6-β7 loop in domain II of Cry4Ba, Cry4Aa, Cry3Aa, Cry2Aa and Cry1Aa toxins

The degree of conservation among the five sequence is represented by background shading of the residues with red, blue and yellow shading for 100%, 80% and 60% sequence homology, respectively.

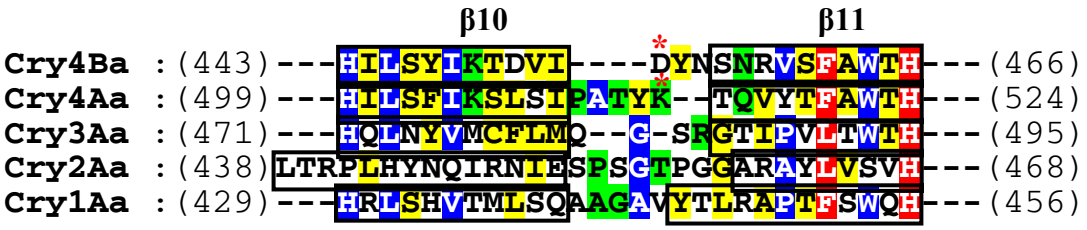

Figure 1.6: Multiple sequence alignments of the β10-β11 loop in domain II of Cry4Ba, Cry4Aa, Cry3Aa, Cry2Aa and Cry1Aa toxins

The degree of conservation among the five sequences is represented by background shading of the residues with red, blue, yellow and green shading for 100%, 80%, 60% and 40% sequence homology, respectively.

CHAPTER II
LITERATURE REVIEW

2.1 General background of *Bacillus thuringiensis*

Bacillus thuringiensis (*Bt*) is a Gram-positive, rod shape, soil bacterium. *Bt* has been used commercially for many years to control insect pests of several orders, such as Lepidoptera (butterflies and moths), Diptera (flies and mosquitoes) [13, 14] and Coleoptera (beetles) [15]. *Bt* is an alternative insecticide to synthetic chemical pesticides which continue to pose significant risks in many parts of the world [16]. During sporulation, It produces parasporal crystalline inclusions consisting of one or more insecticidal proteins known as δ-endotoxins of different shape and molecular masses.

Bacillus thuringiensis subsp. *israelensis* (*Bti*) was first isolated in 1977 by Goldberg and Margalit [17]. It produces at least four types of larvicidal proteins, i.e., Cry4Aa (134 kDa), Cry4Ba (128 kDa), Cry11Aa (72 kDa) and Cyt1Aa (27 kDa), in three different inclusion forms assembled into a spherical parasporal body held together by lamellar envelope (**Fig. 2.1**). *Bti* is specifically toxic to *Aedes*, *Anopheles* and *Culex* mosquito vectors with various degrees.

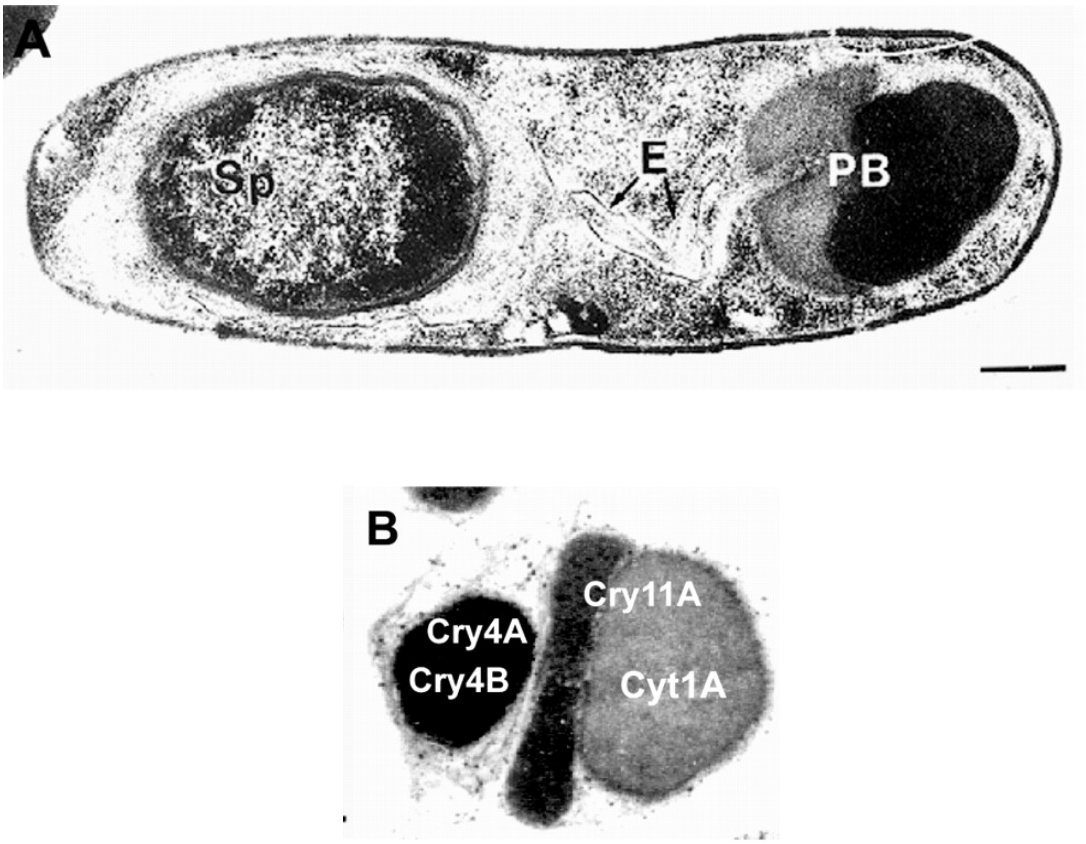

Figure 2.1: Transmitted electron micrograph of *Bacillus thuringiensis* subsp. *israelensis* during sporulation [1]

(A) A sporulating cell of *Bacillus thuringiensis* subsp. *israelensis*

(B) A parasporal body, showing individual toxin inclusions and their toxin composition (Cry4Aa, Cry4Ba, Cry11Aa and Cyt1Aa). Sp, Spore; E, Exosporium; PB, Parasporal body.

2.2 Nomenclature of *Bt* δ-endotoxins

The *Bt* δ-endotoxins have been categorized into two types. *Bt* crystal protein nomenclature (Cry and Cyt toxins) was initially based on insecticidal activity for the primary ranking criterion [16]. According to the revised system, the δ-endotoxins were assigned a new name by changing Roman numerals of class name to Arabic numerals (*e.g.* CryIVB became Cry4Ba). Genes of *Bt* crystal proteins have been classified into several major classes and subclasses characterized by both the insecticidal spectra of the encoded protein and the proteins structural similarities [2, 3].

2.3 Structure of Cry toxins

To date, tertiary structures of seven crystal proteins- Cry1Aa [18], Cry2Aa [19], Cry3Aa [20], Cry3Bb [21], Cry4Ba [12], Cry4Aa [11] and Cry8Ea [22] have been determined by X-ray crystallography. Despite the fact that these proteins show comparatively low amino acid sequence similarity, all the activated Cry toxins show a globular molecule of three distinct domains with high degree of overall similarity (**Fig. 2.2**).

Domain I (N-terminal domain) is a bundle of seven α-helice in which helix 5 is central helix. It has been shown to play a critical role in lytic pore formation and membrane insertion [23-25].

Domain II is made of three antiparallel β-sheets, each ending with surface-exposed loops which are the most variable region among the seven Cry toxin structures. Mutagenic studies of domain II have shown that some residues are essential for receptor- binding step [26-28].

Domain III is two antiparallel β-sheets of β-sandwich structure. It has been shown to play a critical role in structured intrigity, and insect specificity [29-31].

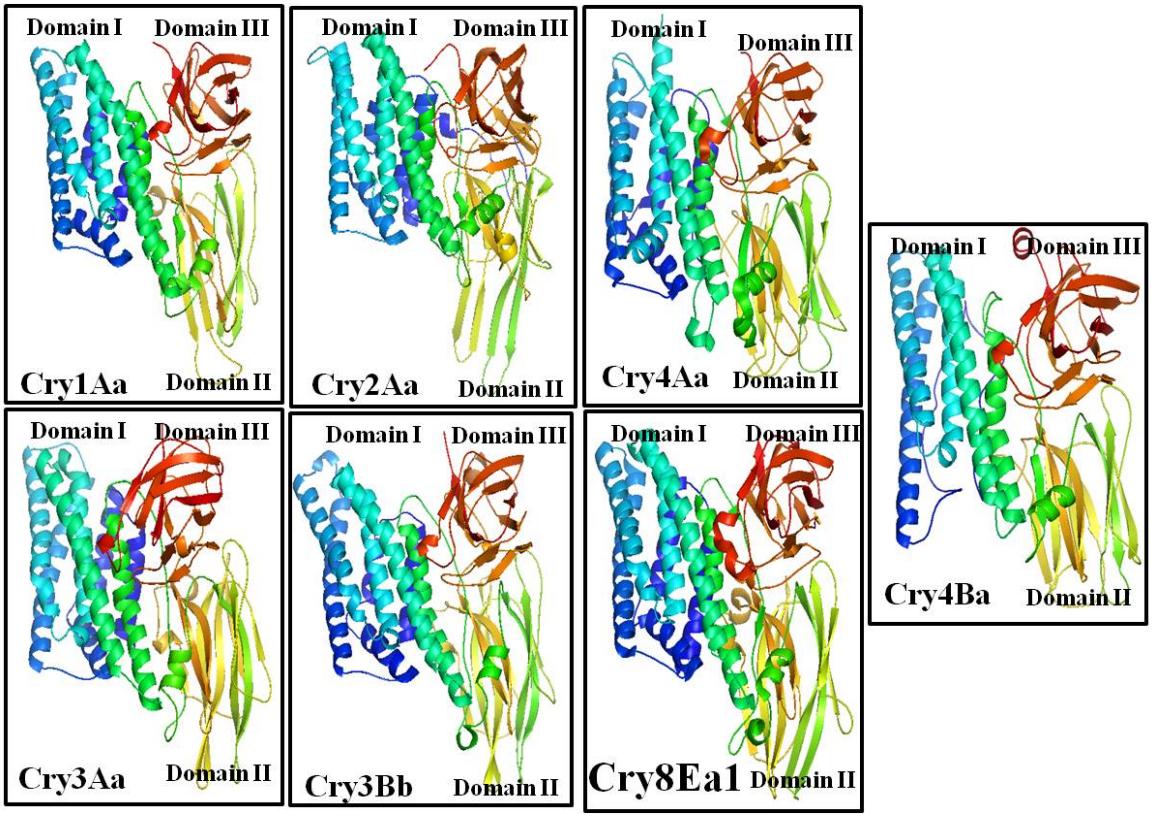

Figure 2.2: Ribbon representations of various Cry toxins

The X-ray crystal structures of Cry1Aa [18], Cry2Aa [19], Cry3Aa [20], Cry3Bb [21], Cry4Aa [11], Cry4Ba [12] and Cry8Ea1 [22] toxins. All Cry toxin tertiary structures show high similarity in their three domain organization.

2.4 Cry4Aa mosquito-larvicidal protein

Cry4Aa toxin exhibits a high level of toxicity against *Culex* and *Aedes* larvae and is slightly less toxic to *Anopheles* larvae [32]. All these mosquito larvae are the vector of West Nile virus, Japanese encephalitis virus and dengue fever. The Cry4Aa toxin is a rather compact molecule composed of three distinct domains [11].

Domain I (residues 68 to 321) is composed of seven amphipathic helices. The most hydrophobic helix (α5) is surrounded by the six remaining helices. The α2 is interrupted by a short loop section and thus can be divided into α2 and α2b, as in Cry3Aa and Cry1Aa (**Fig. 2.3**) [18, 20]. The domain I organization is evocative of the organization of other pore-forming proteins composed of α-helices, such as colicin A [33] or hemolysin E from *E. coli* [34]. In Cry4Aa-domain I, a larger number of electrostatic charges are found at the surface of α-helices 1, 6, and 7 than the surface of helices 3 and 4. Proteolytic cleavage between helices 5 and 6 of Cry4Aa was proposed to trigger the conformational changes essential for membrane insertion [5].

Domain II (residues 322 to 524) is composed of three antiparallel β-sheets packed through formation of a central hydrophobic core. Sheet 1 (β5, β2, β3, and β4) and sheet 2 (strands β8, β7, β6, and β9) adopt a "Greek key" topology. Three β strands of sheet 3 (β1, β11, and β10), which is augmented by α-helix 8 and a short 3_{10} helix 8a, adopts a fold similar to that of other known Cry protein structures (**Fig. 2.3**). The interface between domains I and II is composed of a mixture of hydrogen bonds, van der Waals interactions and salt bridges.

Domain III (residues 525 to 679) consists of two antiparallel β-sheets, fold with the jelly roll topology. The outer sheet comprises of six strands, β12, β13b, β16, β22, β18, and β19, which are exposed to the solvent. The inner sheet is composed of seven strands (β20, β17, β23, β21, β13, β14, and β15) (**Fig. 2.3**).

2.5 Cry4Ba mosquito-larvicidal protein

Cry4Ba is specifically toxic against the larvae of *Aedes* and *Anopheles* mosquitoes [35], the vectors of dengue fever, yellow fever and malaria. Amino acid sequence alignment of the Cry toxins showed that Cry4Ba contains the five conserved blocks [16] that form the structural core of activated Cry3Aa and Cry1Aa. Therefore, activated Cry4Ba is expected to show a topology similar to those of these toxins.

Cry4Ba is composed of three structurally distinct domains [12]. Domain I (residues 84-282) is a bundle of five α-helices and has been shown to be responsible for toxin insertion into the cell membrane, leading to the formation of ion-leakage pore. These helices correspond to helices 3-7 (**Fig**. **2.4**). Although the N-terminal residue generated by chymotrypsin activation was identified as Gly34 [36] which aligns with the N-terminus of α1 in homologous toxins, well-connected densities interpretable as the 34-83 peptide were not visible in the electro density map. This suggests that the N-terminal fragment has undergone proteolysis during crystallization [12]. Helix α3 contains 39 amino acid residues, making it the longest helix in Cry4Ba. The central helix α5 is contained in the first conserved sequence block [16] (residues 170-199) of the Cry toxin. This helix has the least amphipathic character and is relatively hydrophobic. Helix α5 is followed by a single-turn helix (residues 195-200) before the protease-sensitive connection to helix α6. Helix α7 (residues 249-267) is kinked by 21° at residues 257 and its C-terminal residues (residues 263-267) are in the 3_{10} helical conformation.

Domain II is the most diverse part of the Cry toxins. This domain has been demonstrated to be involved in receptor binding, and insect specificity determination [8]. Cry4Ba-domain II, extending from residues 283 to 466, is a β-prism of three anti-parallel β-sheets. Sheet 1 (strands β5, β2, β3 and β4) and sheet 2 (strands β8, β7, β6 and β9) show the Greek-key motif, while sheet 3, (strands, β1, β11 and β10) together with the α8 helix form a Greek-key-like motif (**Fig. 2.4**). The domain also displays six surface-exposed loops which are highly variable in length and amino acid sequence.

Domain (III), comprising of residues 467 to 641, is a β-sandwich consisting of two anti-parallel β-sheets arranged in a jelly-roll-like topology. The exact role of this domain is still not clearly elucidated, however it has been implicated to participate in toxin-receptor recognition [37]. This domain stacks on top of domain II

and against the side of domain I (**Fig. 2.4**). The β20 and β21 together make up its top edge, followed by β17, β23, then β13 and β15 together with the next strand, and finally β14 at the bottom edge. The outer sheet, facing the solvent, also has five strands from top to bottom: β19, β18, β22, β16, and β12 and β13b together forming the edge strand.

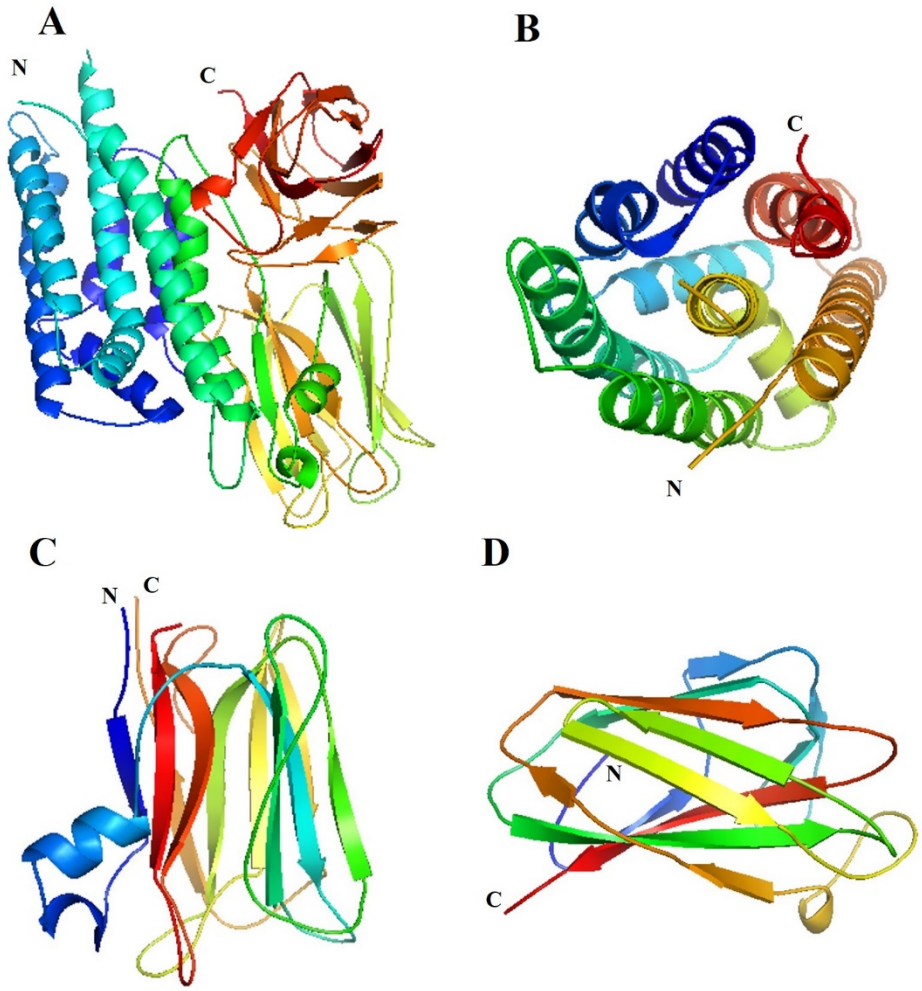

Figure 2.3: Ribbon representation of the Cry4Aa structure

(A) Overview of the Cry4Aa toxin showing domain I, II and III. The individual domains of the toxin; (B) a helix bundle of domain I is viewed from the top; (C) a prism of three antiparallel β-sheets of domain II; (D) a β-sandwich of domain III. All ribbon diagrams are colored rainbow.

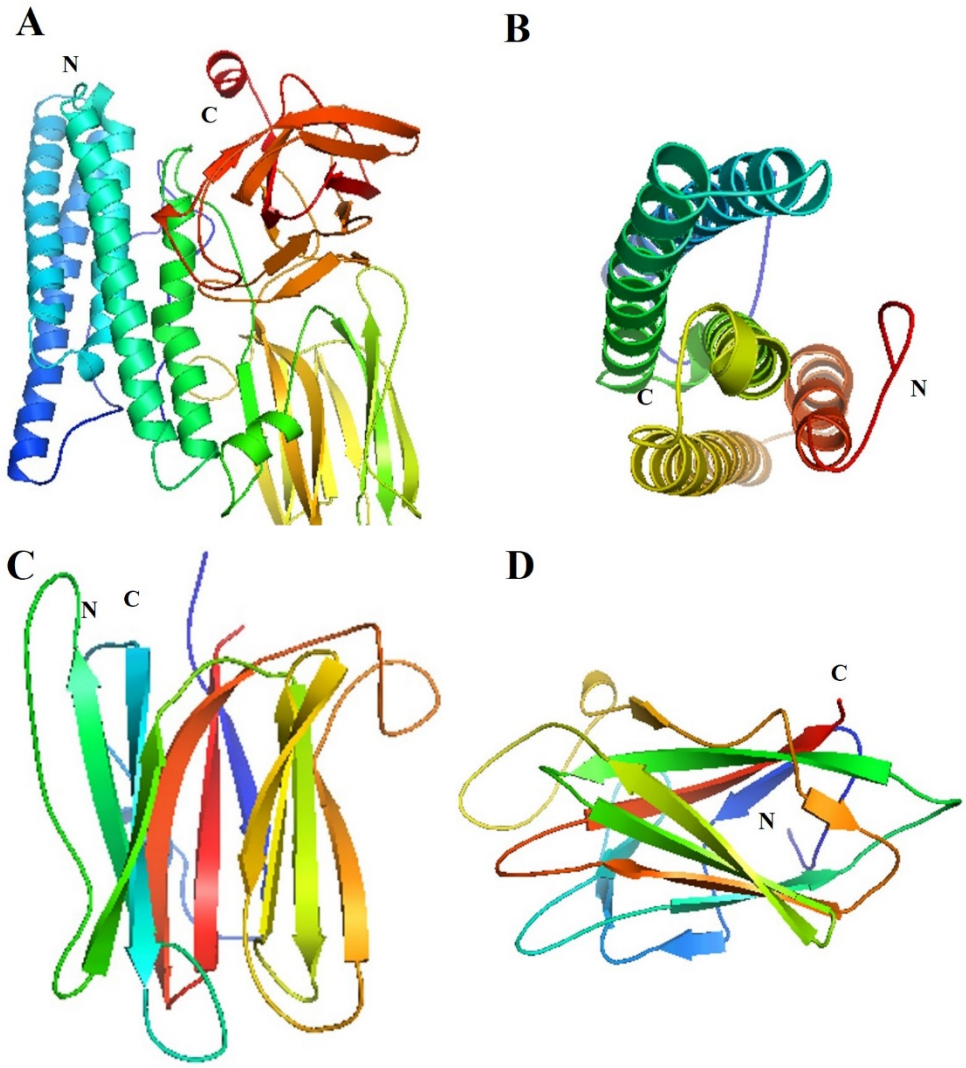

Figure 2.4: Ribbon representation of the Cry4Ba structure

(A) Overview of the Cry4Aa toxin showing domain I, II and III. The individual domains of the toxin; (B) a helix bundle of domain I is viewed from the top; (C) a prism of three antiparallel β-sheets of domain II; (D) a β-sandwich of domain III. All ribbon diagrams are colored rainbow.

2.6 Mechanism of action of Cry toxins

After the *Bt* toxins are ingested by susceptible insect larvae, the Cry toxin inclusion is solubilised under alkaline conditions in the larval midgut lumen. The resulting soluble protoxin will be processed by midgut proteases to yield the active toxin which subsequently bind to midgut receptors and insert into the membrane to form ion-leakage pore, the cause of osmotic cell lysis and larval death [38] (**Fig. 2.5**).

2.7 Solubilisation of Cry toxin inclusions

Most Cry inclusions are solubilised under reducing conditions in the insect larval midgut. The solubility was shown to correlate directly with toxicity [39]. A reduction in the solubility was shown to be a potential mechanism of insecticide resistance [40]. Interchain disulphide bond were proposed to be involved in the in solubility [41]. It has been proposed that four salt bridges linking between polypeptide chains are involved in solubility of Cry3Aa [20].

2.8 Proteolytic processing of the Cry toxins

Based on molecular mass, Cry toxins are divided into two groups. The first one is protoxin of approximately 130 kDa, *e.g*. Cry1A, Cry4Aa and Cry4Ba, and the second one is protoxin of approximately 70 kDa, *e.g*. Cry2Aa, Cry3Aa and Cry11Aa. After proteolytic activation, approximately 25-30 amino acids of the N-terminus and the C-terminal half of the large Cry protoxins (~130 kDa) are removed, leaving an active toxin of around 65 kDa [42] while the smaller Cry protoxins (~70 kDa) are cleaved only at the N-terminus where approximately 50 residues are removed, resulting in an active toxin of around 65 kDa [14].

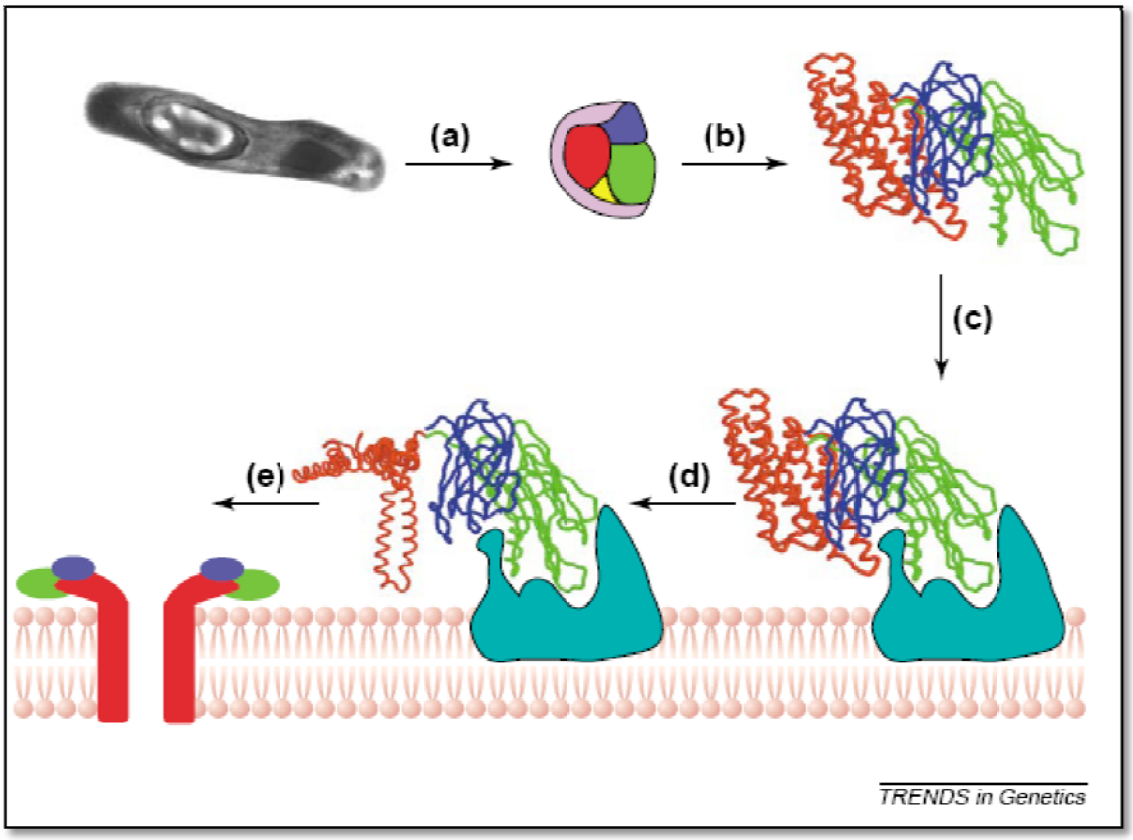

Figure 2.5: Mode of action of Cry toxins [43]

(a) After ingestion by the insect, crystals are dissolved in the gut juice. (b) Gut proteases subsequently clip off the C-terminal extension (purple) in the large Cry protein as well as a small N-terminal fragment (yellow). (c) The activated toxin binds to receptors on the epithelial cell membrane, a process in which both domain II and domain III are involved. (d) Structural rearrangement of domain I might allow a two-helix hairpin to insert into the membrane. (e) Inserted toxins form oligomeric pores.

2.9 Pore formation of Cry toxins

There are at least two alternative models suggested to describe the mechanism of pore formation. One is a penknife model [44], this model proposed that the strongly hydrophobic α5 and α6, which are joined by a loop at the top of the structure, open in a penknife fashion and insert into the membrane. Another model, an umbrella-like model (**Fig. 2.6**) [24], proposed that Cry proteins contain an amphipathic helical hairpin (α4-loop-α5) that initiates pore formation. Ion channels formed by the δ-endotoxin is appear to have more than one ion channel due to aggregation of toxins. Co-operating gating of more than one identical channel is observed, supporting the co-operative gating hypothesis [45].

2.10 Receptor binding of Cry toxin

2.10.1 Aminopeptidase N receptors

The aminopeptidase N (APN) family (EC3.4.11.2) has been identified as a putative receptor for the Cry toxins. APN, a class of enzymes, cleaves neutral amino acids from the N terminus of polypeptide and they have been divided into different five classes [46]. The average sequence identity within a class varies from 56% to 67%. As shown in **Figure 2.7**, the predicted number of O-linked glycosylation site differs considerably among the different classes of APN. To date, 17 different APNs have been reported to bind to Cry toxins, only 2 of them have been shown to mediate toxin susceptibility. Several different APNs are believed to be simultaneously expressed in the larval midgut. These protein have similarities in properties (molecular weight, glycosylation and enzymatic activity) and share sequence identity

The 120-kDa class 1 APN from *Bombyx mori* has been identified as a Cry1Aa-binding protein [47]. The interaction between Cry1Ab and *Manduca sexta* APN class 2 were demonstrated when APN was partially purified using a Cry1Ab affinity column [48]. APN class 3 from *Lymantria dispar* was shown to bind to Cry1Ac but this binding could be blocked by GalNAc [49]. 110-kDa APN class 4

from *Heliothis virescens* has been reported to be Cry1Ac-binding protein [50]. APN class 5 from *Plutella xylostella* could bind to Cry1Aa and Cry1Ab toxins [51]

2.10.2 Cadherin

Cadherin is highly diverse and serves a variety of functions, migration, cytoskeletal organization and morphogenesis. The cadherin, defined by the presence of repeating calcium-binding domains or cadherin repeats of approximately (**Fig. 6**) 110 amino acids in length. Lepidopteran cadherin-like proteins have been studied as Cry1A receptor. The 210-kDa BT-R_1 glycoprotein was identified as a receptor for Cry1Ab in *M.sexta* larvae [52]. The 175-kDa BtR175 glycoprotein was identified as a Cry1Aareceptor in *B.mori* [53]. The isoform of APN and cadherin-like proteins in brush border membrane of *Ostrinia nubilalis* larvae were shown to serve as Cry1Ab, Cry1Ac and Cry1F binding receptor [54].

2.10.3 Glycosylphosphatidyl-inositol (GPI) -anchor alkaline phosphatase (ALP)

The alkaline phosphatase (ALP) (EC3.1.3.1) has been identified as a putative receptor for the Cry toxins. ALP is a hydrolase enzyme responsible for removing phosphate groups from many types of molecules, including nucleotides, proteins, and alkaloids. A 65-kDa GPI-anchored ALP was characterized as a functional receptor of the *Bti* Cry11Aa toxin in *Ae. aegypti* midgut cells [55]. The 58-kDa GPI-anchored-ALP from *Ae. aegypti* was shown to mediate Cry4Ba toxicity against *Sf*9 cells, suggesting its role as a receptor for this mosquito-active toxin in *Ae. aegypti* larvae [56]. Moreover, Cry4Ba binding of this ALP is not occur *via* a sugar moiety as the non glycosylated ALP produced by *E.coli* still show high binding activity to Cry4Ba toxin [57].

2.10.4 Receptor-binding domain II of the Cry1Aa toxin

The receptor binding studies by Lee et al. [58] confirmed that the region of Cry1Aa toxin responsible for binding to *B. mori* receptor corresponds to the amino acids 332 to 450. Hong *et. al*. [28] demonstrated that substitutions or deletions of amino acids 365 to 371 (LYRRIIL) of the CryIAa toxin significantly reduce the

binding ability of the toxin to *B. mori* membrane vesicles and reduce its larvicidal potency by more than 1,000-fold, while mutations in β2-β3 loop showed no effect on initial binding [59]. In addition, mutagenesis studies in the region of 521 to 527 of Cry1Aa demonstrated that toxin plays a role in post binding events, particularly at the level of membrane permeabilisation.

2.10.5 Receptor-binding domain of the Cry1Ab toxin

The involvement of charged (^{368}RR^{369}) and aromatic residue (F^{371}) in initial and irreversible binding of the Cry1Ab toxin to *M. sexta* BBMV was previously shown [60, 61]. The triple mutation of N^{372} and ^{282}AL^{283} with smaller (A^{372}) and less hydrophobic residues ^{282}GS^{283} has significantly enhanced the toxin-receptor contact and the binding affinity [62]. Alanine-scanning experiments of residue ^{370}PFNIGI^{375} of Cry1Ab were also carried out. The F371A and G374A mutants lost most of the toxicity (400 time less) against *M. sexta* larvae, whereas N372A and I375A were only 2 times less toxic than the wild type toxin. These results suggested that mutations in residues 370 to 375 of CryIAb domain II did not affect overall binding but affect the irreversible association of the toxin to the midgut columna epithelial cell of *M. sexta* [60]. Alanine scanning study of ^{438}SGFSNS^{443} were also performed and it was found that G439A and F440A mutants had reduced toxicity to *M. sexta* and *H. virescens*. This was due to the loss of their initial binding activity [62]. Site-directed mutagenesis of trypsin residues of the Cry1Ab toxin showed that W316F, W316C and W455C mutants were less efficient to compete for the binding of the labeled Cry1Ab toxin, suggesting that these mutants are also affected in binding to receptors. Two of these three tryptophan residues are buried within domain II [63].

2.10.6 Receptor-binding domain II of the Cry2Aa and Cry2Ab toxins

The specificity-distinguishing residues are also indicated by comparison of the Cry2Aa structure with the structure of the highly homologous (87%) Cry2Ab that is inactive against some Cry2Aa target species. The substitutions of residues 278-340 of Cry2Aa resulted in a loss of dipteran-specific activity [64], while substitutions of residues 307-382 conferred dipteran-specific activity of Cry2Ab [65]. There are isosteric non H-bond residues in Cry2Ab that were replaced by hydrophilic residues in

Cry2Aa, one of them (A313T) in the β_2, and the other three residues A334S, L336N and A337S are in β_3. All are buried behind the β_4-β_5 loop and also make side chain-side chain hydrogen bonds between β_2 and β_3.

2.10.7 Receptor-binding domain II of the Cry3Aa toxin

Receptor binding studies of two mutants, A1 (R345A, Y350F and Y351F) and A2 (R345A, ΔY350 and ΔY351), demonstrated that these mutant toxins, A1 and A2, were more toxic than the wild-type Cry3Aa. It was suggested that deletion of Y^{350} and Y^{351} allows the aliphatic side chains of N^{353} and D^{354} to make better contact with the receptor, hence enhancing toxicity [26].

2.10.8 Receptor-binding domain II of the Cry4Aa and Cry4Ba toxins

Cry4Aa is toxic to both *Aedes* and *Culex* larvae, while Cry4Ba is highly toxic to *Aedes* but not *Culex* larvae (50). In Cry4Aa, replacement of four residues (TTPN) within β2-β3 loop with 4BL1YQDL, resulted in a marginal decrease in the toxicity against *A. dirus* and *C. quinquefasciatus* and show no effect on toxicity in *Ae. aegypti*. This suggests that β2-β3 loop does not participate in receptor binding interaction. In contrast, deletion of 4AL2ΔKY in β4-β5 loop resulted in a dramatically reduction in the toxicity against the three insect genera, suggesting that β4-β5 loop directly participates in receptor binding [11]. The β2-β3 loop mutant (T^{331}PNHM→T^{331}PNNL) of Cry4Ba had lost toxicity against both *Aedes* and *Culex* mosquito larvae, but still showed ion channel activity in lipid bilayer membranes. This data suggested that the loss of toxicity is likely to be due to inactivity of the Cry4Ba toxin to bind with receptor on larval midgut cells. In Cry4Ba, T^{338} and Y^{332} in the β_2-β_3 loop and F^{364} and T^{369} in the β_4-β_5 loop were suggested to be crucial residues for receptor recognition [66]. Moreover, Cry4Ba utilizes two critical aromatic loop-residues, Tyr^{332} in the β2-β3 loop and Phe^{364} in the β4-β5 loop for synergistic toxicity with its alternative receptor-Cyt2Aa2 [67]. The β6-β7 loop mutation (S^{388}PS→K^{388}YL) was shown to retain high toxicity of the Cry4Ba toxin against *Aedes* larvae but cause a slightly decreased toxicity against *Culex* larvae. It is possible that the β6-β7 loop is involved partly in receptor binding. In addition, the β10-β11

loop mutant (Cry4Ba-D^{454}YNS→ T^{454}YKS), lost toxicity against *Aedes* larvae, but not *Culex* mosquito larvae [68]. However, substitution of the Cry4Ba-D^{454} with a short peptide (PAT, GAT or GAV) did not suppress *Aedes* larvicidal activity of this toxin, but rather significantly increase toxicity against *Culex* larvae [10].

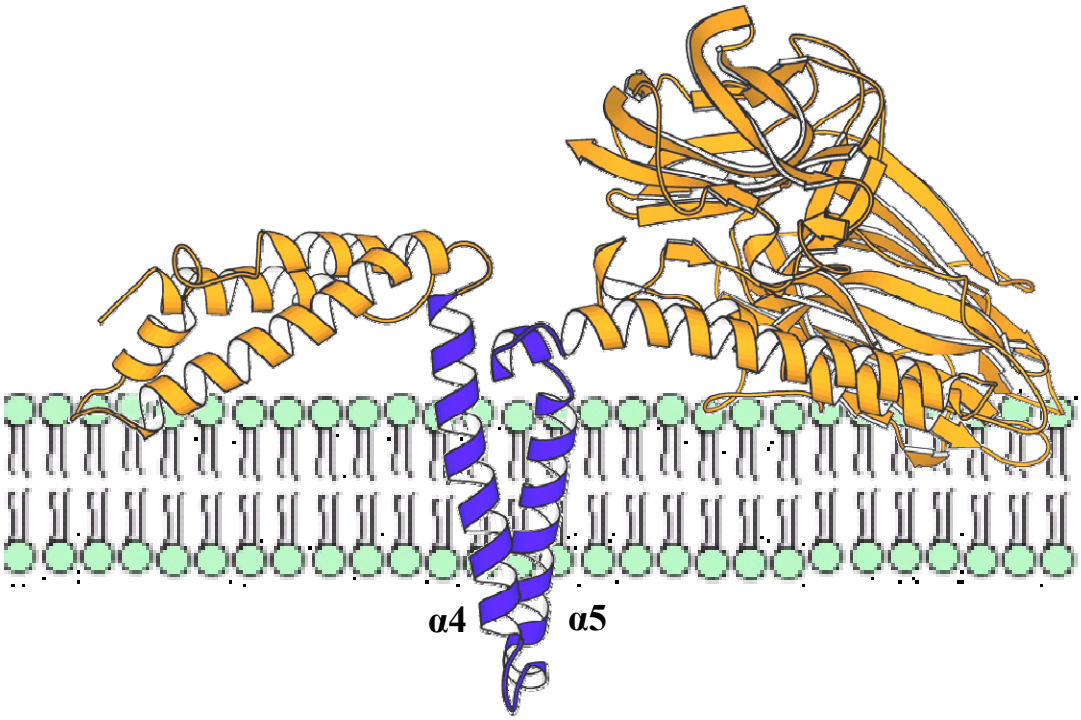

Figure 2.6: An umbrella-like model for Cry toxins [24]

An umbrella-like model has been proposed that helices α4 and α5 insert into the membrane as a helical hairpin in an antiparallel manner, while the other helices lie on the membrane surface like the ribs of an umbrella.

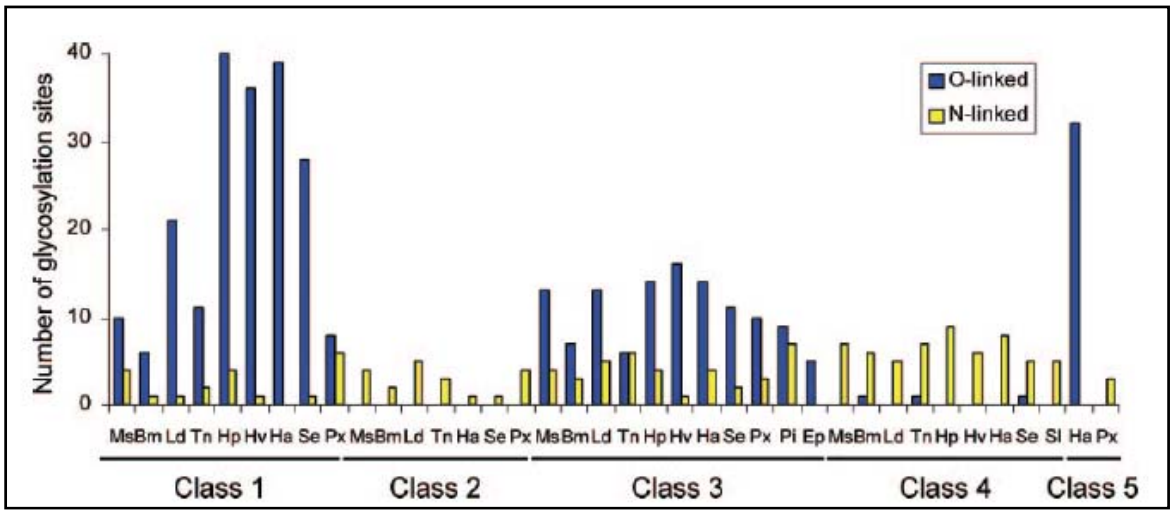

Figure 2.7: Comparison of predicted N-linked and O-linked glycosylation sites among lepidopteran midgut APNs, sorted by class [46]

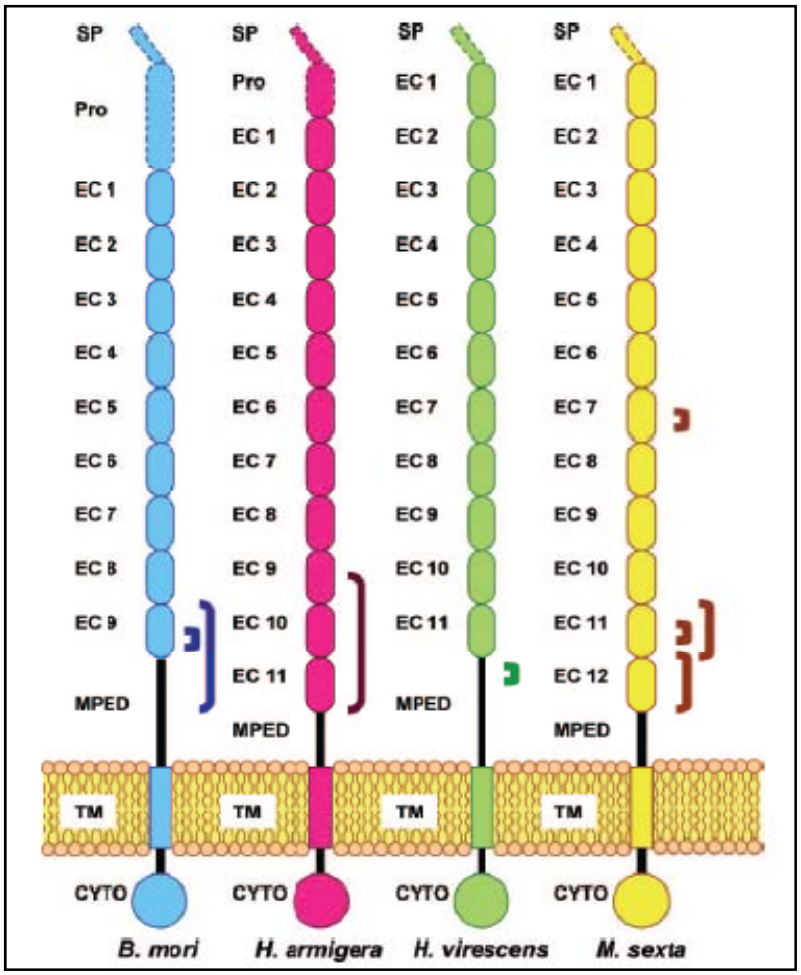

Figure 2.8: Domain structure and putative Cry1A toxin binding sites in lepidoptera cadherin-like proteins

(EC, ectoderm; MPED, membrane-proximal extracellular domain; TM, transmembrane domain; CYTO, cytoplasmic domain.

2.11 Biology of *Culex* sp.

Culex is a genus of mosquitoes and serves as vectors of important diseases, such as West Nile virus, Japanese encephalitis and filariasis. The adult mosquito can be measure from 4-10 mm and morphologically has three body parts common to insect: head, thorax and abdomen (**Fig.2.9**).

Life cycle of *Culex* start with egg as 100 or more eggs are laid on the water surface. The rafts remain afloat until hatching occur 2-3 day later. *Culex* sp. breed in a large variety of still waters, ranging from artificial containers to large bodies of permanent water. During the larval stage, the mosquito lives in water and feeds on organic matter and plants, then develops into a pupa. The pupa is comma shaped and also lives in water. It does not feed and becomes an adult after one or two days. In many developing countries *Culex quinquefasciatus* is common in rapidly expanding urban areas where drainage and sanitation are inadequate. *C. quinquefasciatus* is markedly domestic species. The adult females bite people and animals throughout the night, indoors and outdoors. During the day they are inactive and are often found resting in dark corners of rooms, shelters and culverts. They also rest outdoors on vegetation and in holes in trees in forested areas.

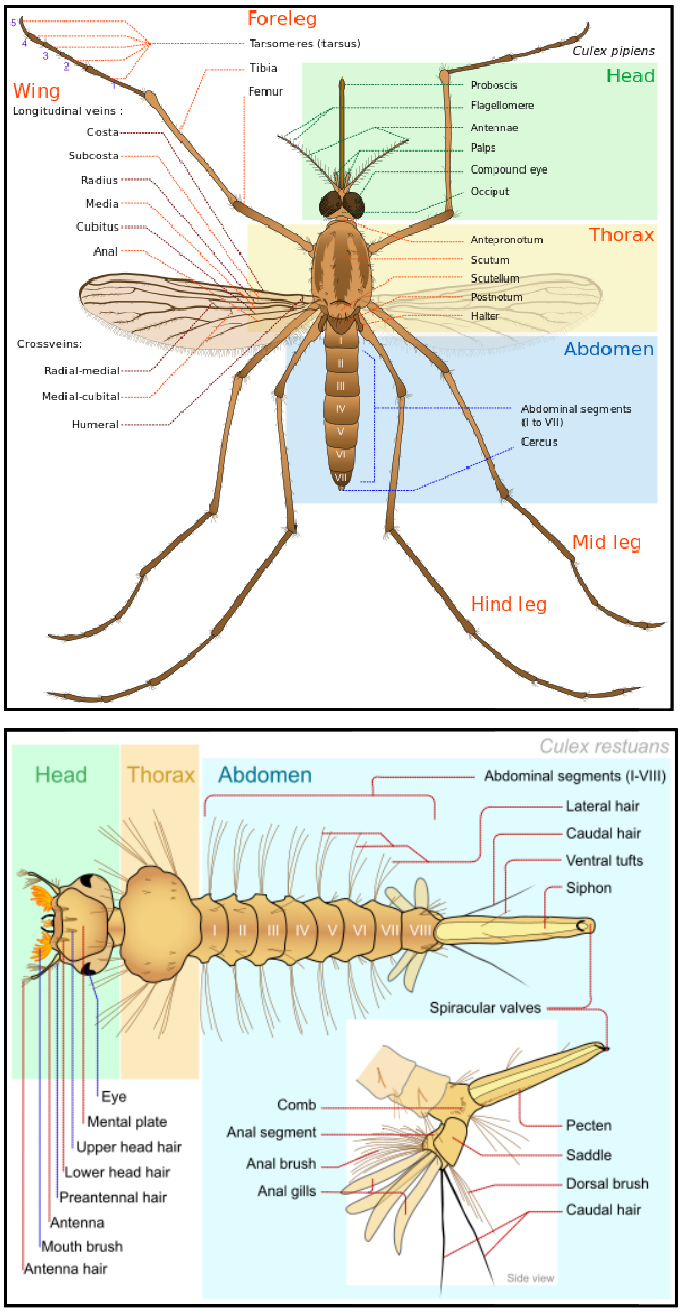

Figure 2.9: Diagram of morphology of adult and larvae of *Culex* sp.

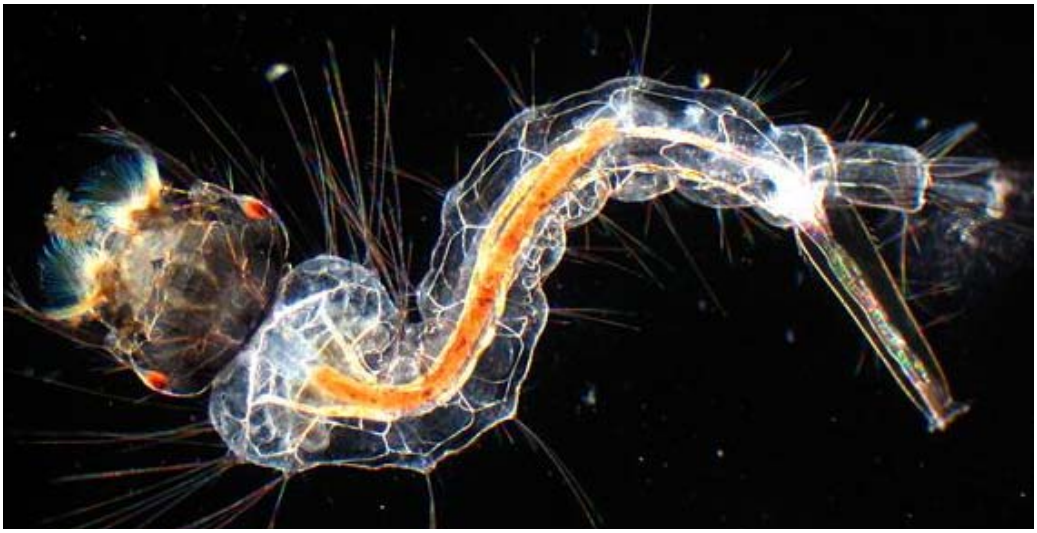

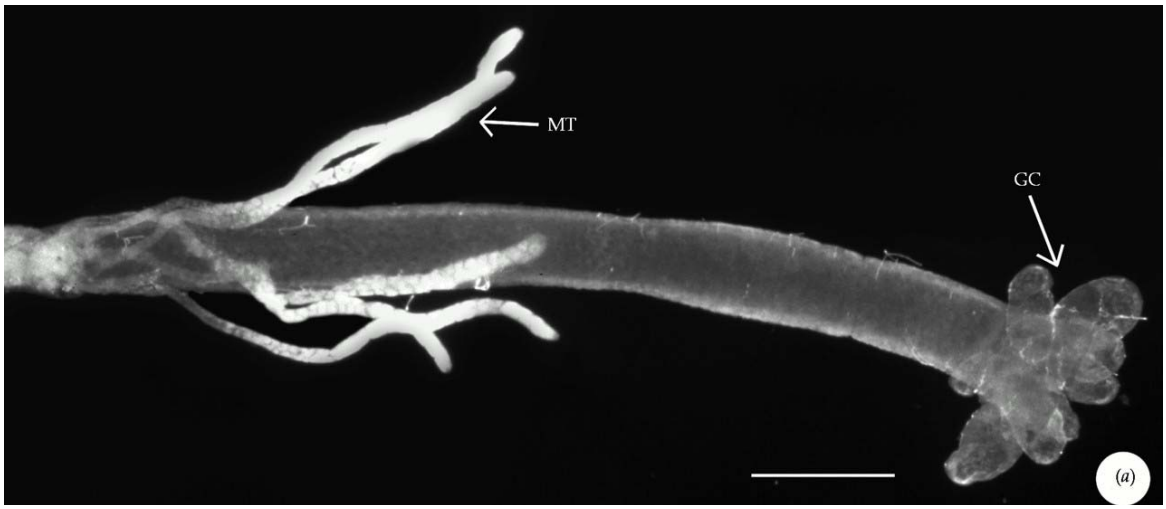

Figure 2.10: Morphology of *Culex* sp larvae

(A) Upper: Morphology of *Culex* sp. larvae

(B) Lower: Dissected midgets from Third-instar *Culex* sp. larvae. Stomach and gastric caeca (GC) with malpighian tubules (MT

CHAPTER III
MATERIALS

3.1 MATERIALS

Acrylamide	Sigma
Ammonium persulfate	Sigma
Ampicillin	Sigma
Bovine serum albumin (no. 23209)	Promega
Bradford protein assay reagent (no. 500-0006)	BIORAD
Bromophenol blue	Sigma
Cetyl trimethyl ammonium bromide (CTAB, C19H42NBr, FW: 364.5, Code H5882)	Sigma
Calcium choride	Sigma
Chloroform	Merck
Deoxynucleotide triphosphates	Pharmacia Biotech
3, 3´-diaminobenzidine (DAB)	Vector
Dithiothreitol (DTT, C4H10O2S2, MW: 154.25)	Merck
Ethanol	Merck
Glacial acetic acid	Merck
Glycerol	Merck
Isopropyl-β-D-thiogalactopyranoside (IPTG, C9H18O5S, MW: 238.31)	Sigma
Lamda-*Hin*d III digested DNA marker	GIBCO BRL
Methanol	Merck
N,N´-methylene bis acrylamide	Sigma
SDS-PAGE molecular mass standards (Broad range)	BIORAD
Sodium carbonate (Na_2CO_3, MW: 105.99, no. 71351)	Fluka
TEMED	BIORAD
Triton X-100	Sigma

3.2 Enzymes

Phusion DNA polymerase	Finnzymes
Lysozyme (EC 3.2.1.17, L-6876)	Sigma
Ribonuclease A (RNase A, EC 3.1.27.5)	Sigma
Trypsin Type XIII (TPCK treated)	Sigma
Restriction endonucleases	Promega, BioLabs
*Dde*I, *Dpn*I, *Pst*I, *Rsa*I, *Sca*I	Promega
*Bst*NI, *Bst*BI, *Hae*III, *Sna*BI	Biolabs

Streptavidin conjugated with horseradish peroxidase
(no. 21126, ImmunoPure® streptavidin, Pierce biotechnology, Inc.)

3.3 Buffer and solutions

3.3.1 Plasmid extraction solutions

0.5 M EDTA, pH 8.0 (100 ml)

EDTA ($2H_2O$ MW. 372.24) 18.61 g

The solution was adjusted pH to 8.0 with NaOH pellet, adjusted volume to 100 ml with distilled water; and then autoclaved at 121°C, for 20 min.

1 M Tris HCl, pH 8.0 (100 ml)

Tris 12.11 g

Distilled water

The solution was adjusted to pH 8.0 with 1 N HCl and adjusted volume to 100 ml with distilled water.

5% (w/v) CTAB (50 ml)

CTAB (FW 364.5) 2.5 g

Distilled water making final volume to 50 ml

The solution was autoclaved at 121°C, for 20 min.

STET buffer, pH 8.0 (50 ml)

1 M Tris-HCl, pH 8.0	2.5	ml
0.5 M EDTA, pH 8.0	1.25	ml
Triton-X 100	50	µl
Sucrose	0.4	g

Distilled water making final volume to 50 ml

10 mg/ml RNase A (1.5ml)

RNase A	0.163	g
Distilled water	1.5	ml

The solution was passed through 0.2 µm filter and aliquoted into 100µl/microcentrifuge tube for keeping at -20°C

10 mg/ml Lysozyme

Lysozyme	0.01	g
Distilled water	1	ml

1.2 M NaCl (100 ml)

NaCl (M.W 58.44)	7.2	g
Distilled water making final volume	100	ml

The solution was autoclaved at 121°C, for 20 min.

3.3.2 DNA gel electrophoresis solutions

50 ng/µl λ/*Hin*dIII DNA marker (100 µl)

λ/*Hin*dIII DNA marker (500 ng/µl)	10	µl
4X loading buffer	25	µl
Distilled water	65	µl

6X gel loading buffer (0.5 ml)

Bromophenol blue	0.05	g
Ficoll 400	7.5	g
0.5 M EDTA	0.5	ml

Distilled water was added to make up the volume to 0.5 ml.

3.3.3 Competent cell preparation solutions

0.1 M $CaCl_2$ (100 ml)

$CaCl_2.2H_2O$ (MW 147.02)	1.47	g

Distilled water making final volume to 100 ml

The solution was autoclaved at 121°C, for 20 min.

0.1M $MgCl_2$ (100 ml)

$MgCl_2$ ($6H_2O$)	20.33	g

Distlled water making final volume to 100 ml

The solution was autoclaved at 121°C, for 20 min.

3.3.4 Protein expression solutions

20% (w/v) IPTG (2ml)

IPTG	0.5	g
Distilled water	2	ml

The solution was passed through 0.2 μm filter and aliquoted into 1 ml/microcentrifuge tube for keeping at -20°C.

100 mg/ml Ampicillin (2 ml)

Ampicillin	0.2	g
Distilled water	2	ml

The solution was passed through 0.2 μm filter and aliquoted into 1 ml/microcentrifuge tube for keeping at -20°C.

3.3.5 Solutions for protein purification and solubilization

100 mM KH_2PO_4, pH 6.5, for inclusions washing (500 ml)

1 mM KH_2PO_4	50	ml
Distlled water making final volume to	500	ml

50 mM Na_2HCO_3, pH 10.0 (1 litre)

50 mM Na_2HCO_3 (MW 105.9)	5.3	g

The solution was adjusted to pH 10.0 with HCl
and distilled water was added to make up volume to 1 litre.

3.3.6 Solutions for SDS-PAGE analysis, gel staining solutions

10X Running buffer (1 litre)

Tris-base (MW 121.1)	30.0	g
Glycine	144.13	g
SDS	10.0	g
Distlled water making final volume to	1	litre

10% SDS (50 ml)

SDS (FW 288.38)	5	g
Distlled water making final volume to	50	ml

1.5 M Tris-HCl, pH 8.8 (100 ml)

Tris-base	18.17	g

The solution was adjusted to pH 8.8 with HCl and
distilled water was added to make up the volume to 100 ml.

0.5 M Tris-HCl, pH 6.8 (100 ml)

Tris-base	6.07	g

The solution was adjusted to pH 6.8 with HCl and
distilled water was added to make up the volume to 100 ml.

10% Ammonium persulphate (1ml)

Ammonium persulphate	0.1	g
Distilled water	1	ml

The solution was kept at 4°C

1M DTT (20 ml)

DTT (Sigma)	3	g
Distilled water	20	ml

The solution was passed through a 0.2 µm filter and aliquoted into 1 ml/microcentrifuge tube for keeping at -20°C.

4X sample buffer (100 ml)

SDS	1	g
Glycerol	15.5	ml
Tris	0.6055	g
Bromophenol blue	25	mg
Distilled water making final volume to	100	ml

1 M DTT was added before used to obtain 200 mM final concentration.

Broad range standard molecular mass markers (200 µl)

Broad range protein marker (65- 200 kDa)	10	µl
4X sample buffer	190	µl

Staining solution for acrylamide gel (1 litre)

Coomassie brilliant blue R-250	2	g
Ethanol	500	ml
Acetic acid	100	ml
Distilled water making final volume to	1	litre

Destaining solution for acrylamide gel (1 litre)

Ethanol	100	ml
Acetic acid	200	ml
Distilled water making final volume to	1	litre

3.3.7 Solution for immunohistochemistry

DAB substrate kit (5 ml)

Distilled water	5	ml
Buffer stock	2	drops
DAB solution	4	drops
H_2O_2	2	drops

Fixative (500 ml)

Paraformaldehyde	20	g

1X PBS pH 7.4

The solution was heat at 60°C until the solution turned to clear. After it was cooled down to approximately 50°C, sucrose was added to obtain 5% final concentration (w/v).

Fixative II (200 ml)

Sucrose	10	g

5% sucrose, 4% paraformaldehyde PBS, pH 7.4

3.3.8 Bacterial culture medium

LB broth medium (1 litre)

NaCl	10	g
Peptone	10	g
Yeast extract	5	g

The solution was autoclaved at 121°C, for 20 min and kept at 4°C.

1.5% LB agar (plate) (500 ml)

Agar	7.5	g
LB broth	500	ml

The solution was autoclaved at 121°C, for 20 min. and then kept at room temperature until it was harden.

3.4 Recombinant plasmids

pMU388 (**Fig. 3.1**): The recombinant plasmid containing the *cry4Ba* gene encoding the 130-kDa protoxin was employed as a template for site-directed mutagenesis.

pMEx-B4A (**Fig. 3.2**): The recombinant plasmid containing the *cry4Aa* gene encoding the 130-kDa protoxin was employed as a template for site-directed mutagenesis.

3.5 Antibodies

Rabbit anti 4B-R203Q and Rabbit anti 4A-R235Q antibodies which specifically recognises the Cry4Ba and Cry4Aa respectively, was provided by Dr. Watchara Kasinrerk, Faculty of Associated Medical Sciences, Chiang Mai University. Goat anti rabbit IgG (H+L) conjugated with biotin (product number: 31820) was purchased from Pierce biotechnology, Inc.

3.6 DNA sequencing primers

The primer for sequencing Cry4Ba mutant plasmids:

Y266A-f: 5’ GCCAGTGCGGATCCACGTC 3’

The primer for sequencing Cry4Aa mutant plasmids:

D200P-f: 5’ TGATTGCCCGTACTACTATAACATACTAG 3’

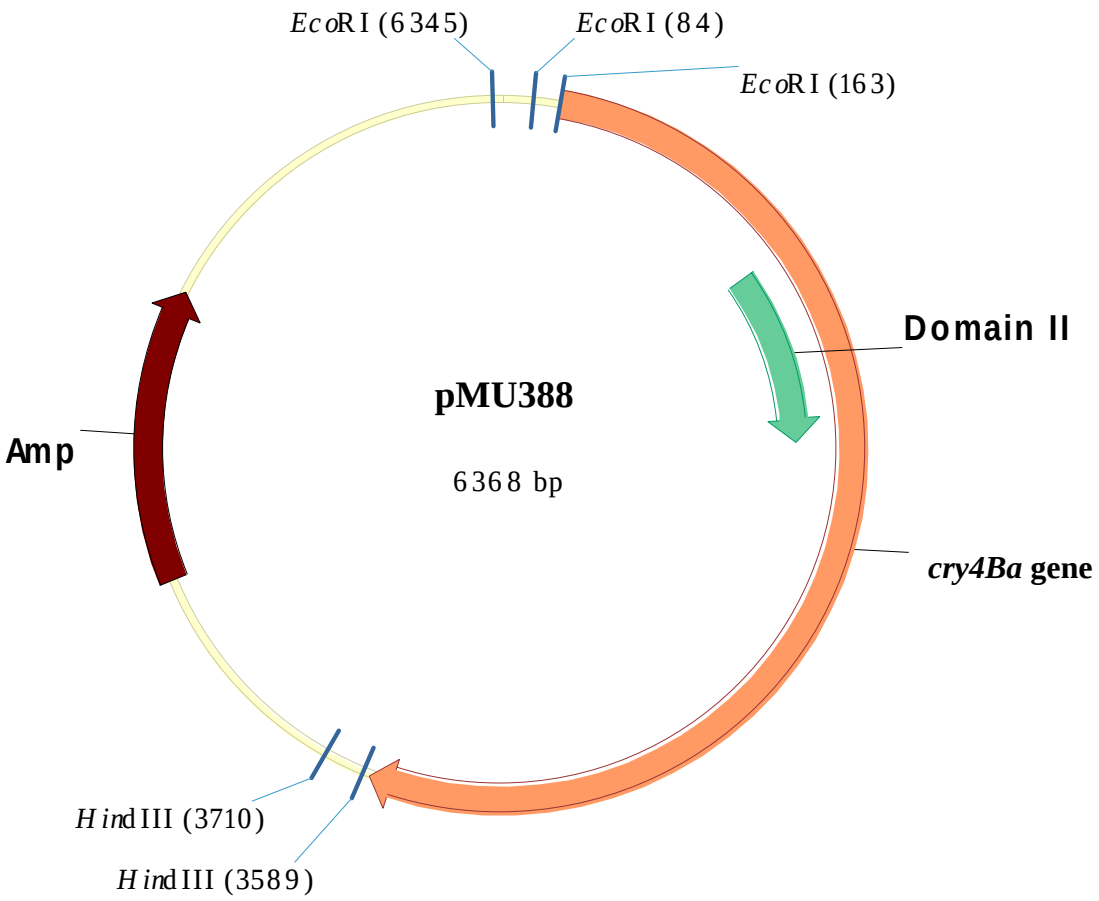

Figure 3.1: Physical map of pMU388 plasmid

The Figure shows the recombinant pMU388 plasmid containing the *cry4Ba* gene (orange arrow). Green arrow represents part of the *cry4Ba* gene that encodes Cry4Ba-domain II.

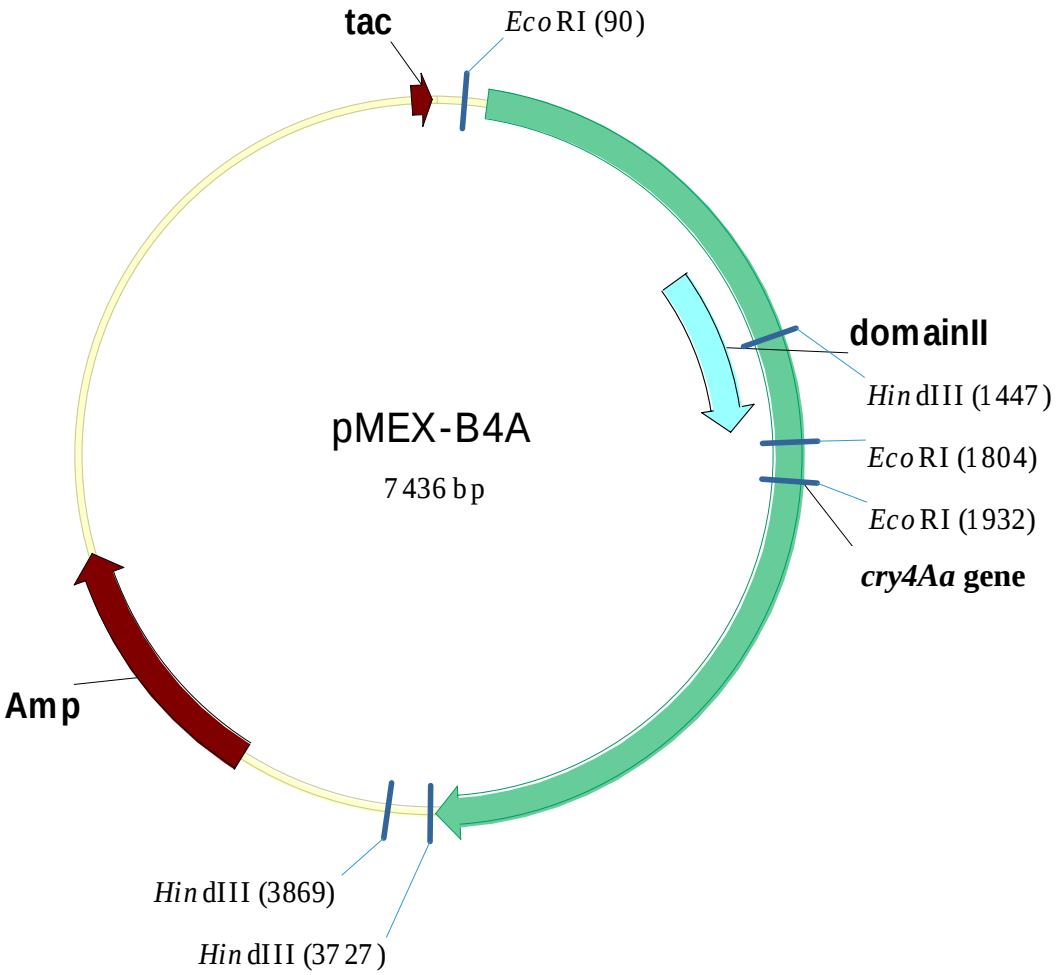

Figure 3.2: Physical map of pMEx-B4A plasmid

The Figure shows the recombinant pMEX-B4A plasmid containing the *cry4Aa* gene (green arrow). Blue arrow represents part of the *cry4Aa* gene that encodes Cry4Aa-domain II.

3.7 Oligonucleotide primers

3.7.1 Cry4Aa primers

All synthetic oligonucleotide primers were purchased from Sigma Proligo (Singapore). The sequences of all oligonucleotides are shown below. [a]Recognition sites introduced for restriction enzyme analysis are underlined. Bold letters indicate mutated nucleotide residues; f and r represent forward and reversed primers, respectively.

*Dde*I

D430A-f: 5′-TCATAAG**T**TTAG**C**TAATAAATATCTAAATGATTATA -3′

D430A-r: 3′- AAAAAAATAATTTACAGTATTC**A**AATC**G**ATTATTTAT -5′

*Bst*NI

K432A-f: 5′-CATAAGC**CTG**GATAAT**GC**ATATCTAAATGATTATAATAATA-3′

K432A-r: 3′-AAAAATAATTTACAGTATTC**GGAC**CTATTA**CG**TATAGATTT-5′

*Hae*III

Y433A-f: 5′- GATAATAA**GGCC**CTAAATGATTATAATAATATTA -3′

Y433A-r: 3′- CAGTATTCGAATCTATTATT**CCGG**GATTTAC -5′

*Sca*I

D436A-f: 5′-GATAATAA**GTACT**TAAATG**C**TTATAATAATATTAGTAAAATG-3′

D436A-r: 3′-CAGTATTCGAATCTATTATT**C**AT**GA**ATTTAC**G**AATATTATT-5′

*Bst*BI

Y437A-f: 5′-TAAATGAT**GC**TAATAATATT**TCG**AAAATGGATTTTTTTATAACTA-3′

Y437A-r :3′-TCTATTATTTATAGATTTACTA**CG**ATTATTATAA**AGCT**TTTACC-5′

*Sna*BI

P510A-f: 5′- TTAGTATCGCTGC**T**AC**G**TATAAAACTCAAGTG -3′

P510A-r: 3′- ATTTTCAGAATCATAGCGACG**A**TG**C**ATATTTTGA-5′

*Pst*I

T512A-f: 5′- CCTGCA**G**CATATAAAACTCAAGT -3’

T512A -r: 3′- AATCATAGGGACGT**C**GTATATTTT -5′

*Rsa*I

Y513A -f: 5′CTGCAACA**GC**TAAAACTCAAGTGTA**C**ACGTTTGCTTGGACA -3′

Y513A -r: 3′-TCATAGGGACGTT**GC**GATTTTGAGTTCACAT**G**TGCAAACG -5′

*Sna*BI

K514A -f: 5′- CCCT GC**T**AC**G**TAT**GC**AACTCAAGTGTATACG -3′

K514A -r: 3′- AGAATCATAGGGAG**A**TG**C**ATA**CG**TTGAGTTC-5′

*Sna*BI

T515A -f**:** 5′- CCCTGC**T**AC**G**TATAAA**G**CTCAAGTGTATACGT -3′

T515A -r: 3′- GAATCATAGGGACG**A**TG**C**ATATTT**C**GAGTTCAC-5′

3.7.2 Cry4Ba primers

All synthetic oligonucleotide primers were purchased from Sigma Proligo (Singapore). The sequences of all oligonucleotides are shown below. [a]Recognition sites introduced for restriction enzyme analysis are underlined. Bold letters indicate mutated nucleotide residues; f and r represent forward and reversed primers, respectively.

*Dpn*I

R230Q/D454A -f**:** 5′- CTGATGT**G**AT**C**G**C**TTATAACAGTAACAGGG -3′

R203Q/D454A -r: 3′- ATATATATTTTTGACTACA**C**TA**G**C**G**AATATTGTC-5′

*Dpn*I

R230Q/D454E -f**:** 5′- CTGATGT**G**AT**C**GA**A**TATAACAGTAACAGGG -3′

R203Q/D454E -r: 3′- GATATATTTTTGACTACA**C**TA**G**CT**T**ATATTGTC -5′

*Hinf*I

R230Q/D454R -f**:** 5′- CTGATGT**G**AT**TCG**TTATAACAGTAACAGGG -3′

R203Q/D454R -r: 3′- CGATATATTTTTGACTACA**C**TA**AGC**AATATTGT -5′

*Dpn*I

R230Q/D454K -f**:** 5′- CTGATGT**G**ATC**A**A**G**TATAACAGTAACAGGG -3′

R203Q/D454K -r: 3′- GATATATTTTTGACTACA**C**TAG**T**T**C**ATATTGTC -5′

CHAPTER IV
METHODS

4.1 Plasmid extraction by CTAB method [69]

A single colony was inoculated in 3 ml LB broth containing 100 µg/ml ampicillin and grown at 37°C with 250 rpm shaking for 16-20 hr. The pellet was collected in a 1.5 ml microcentrifuge tube by centrifugation at 12,000g for 30 sec and resuspended in 200 µl of STET buffer (8% sucrose, 5% Triton X-100, 50 mM EDTA, 50 mM Tris-HCl, pH 8.0). The cell mixture was added with 10 µl of freshly prepared lysozyme solution (10 mg/ml) and incubated for 10 min at room temperature. The mixture was boiled at 95°C for exactly 45 sec and immediately centrifuged at 12,000 rpm for 15 min at room temperature. The pellet (chromosomal DNA) was removed with steriled toothpick. Plasmids and low molecular weight residual DNAs were recovered by adding 20 µl of 5% CTAB into supernatant. The solution was mixed by vortex and centrifuged at 12,000 rpm for 10 min at room temperature. Then, the pellet was resuspended in 300 µl of 1.2 M NaCl. In order to eliminate RNA, 10 µl of RNase A (10 mg/ml) was added and incubated at 37°C for 30 min. Protein was removed by adding 300 µl of chloroform, vigorous inversion and centrifugation at 12,000 rpm for 5 min at room temperature. The clear aqueous phase was transfered to a new microcentrifuge tube. The plasmid DNAs were precipitated with 2 volumes of absolute ethanol at -20°C for 30 min and centrifuged at 12,000 rpm for 15 min at room temperature. The final DNA pellets were washed with 70% ethanol and centrifuged at 12,000 rpm for 5 min. After removal of the supernatant following with air dry, the pellet was resuspended in 20 µl of distilled water.

4.2 Agarose gel electrophoresis of DNA

The appropriate amount of agarose powder was dissolved in either 1X TBE buffer (89 nM Tris-HCl, 89 mM boric acid, 25 mM EDTA, pH 8.0) or TAE buffer (40 mM Tris-HCl, 40 mM acetic acid, 25 mM EDTA, pH 8.0) under boiling temperature to ensure the homogeneity of the gel solution. When the gel mixture was cooled down to about 55°C, the mixture was poured into the mold to solidify at room temperature. DNA sample was mixed with gel-loading dye (0.1% bromophenol blue, 15% (w/v) Ficoll 400, 50 mM EDTA) at ratio 1:5 (v/v) and then the mixture was loaded in to a well of the agarose gel submerged in TBE or TAE buffer. After electrophoresis with constant voltage at set 80 V was completed, the gel was stained in 2 µg/ml ethidium bromide solution for 5 min and destained in water for 10 min. The DNA patterns were visualised under UV light and digitalised by the Geldoc® system. The amount of DNA was estimated by comparing the stained DNA bands with the standard DNA markers of known concentration under UV light.

4.3 *In vitro* site-directed mutagenesis

The method was based on Stratagene's QuickChange™ Site-Directed Mutagenesis Kit. The method principle as shown in **Fig. 4.1** utilises a supercoiled, double-standed DNA (dsDNA) plasmid containing an insert of the gene of interest and two synthetic oligonucleotide primers containing the desired mutation. The oligonucleotide primers, each complementary to opposite strands of the plasmid, extend during temperature cycling by Phusion DNA polymerase which replicates both plasmid strands with high fidelity (50X greater than that of ordinary *Taq* DNA polymerase) and high polymerization speed (15-30 sec/1 kb).

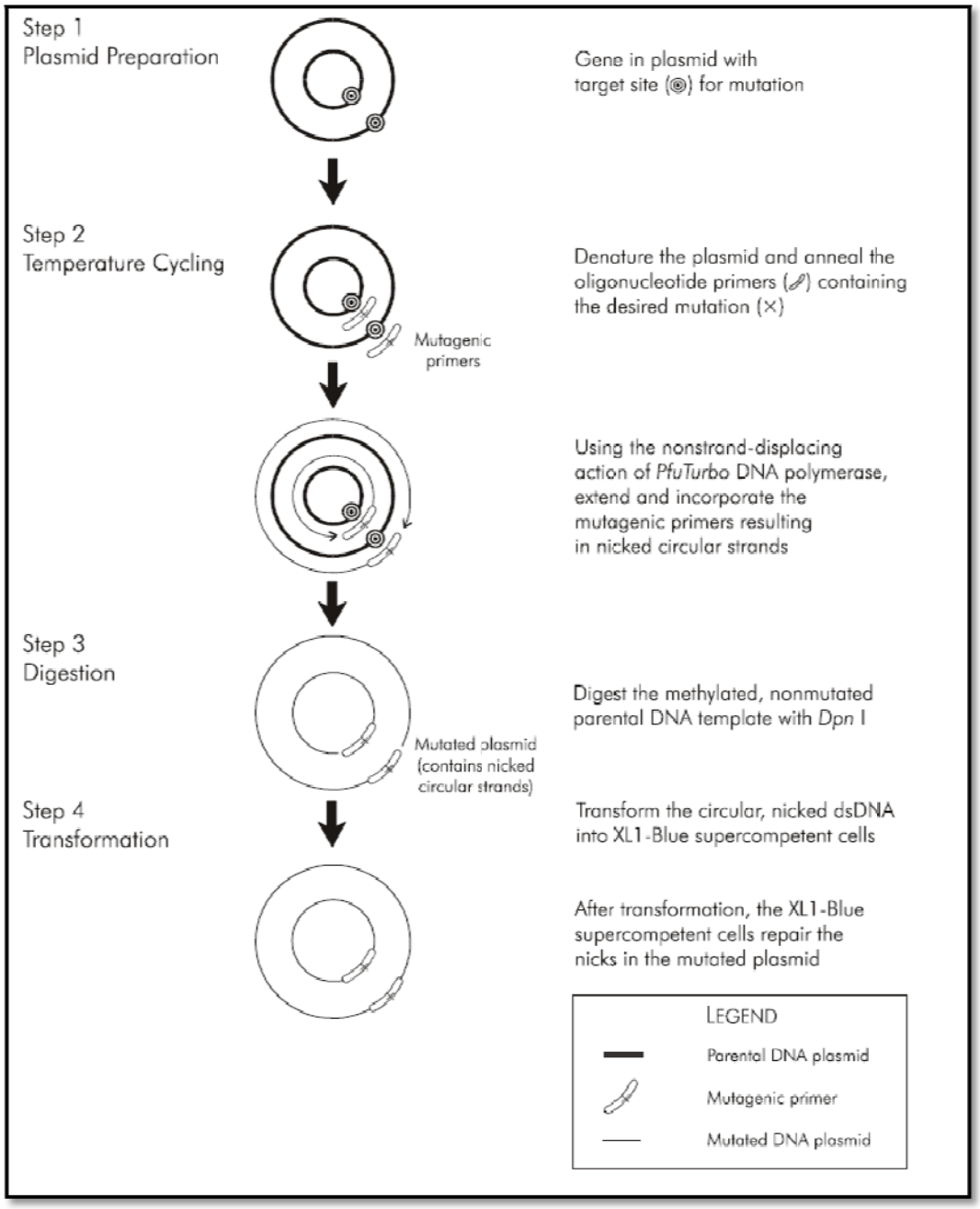

Figure 4.1: Overview of the QuikChange site-directed mutagenesis method

(Stratagene's Quick Change kit)

4.3.1 Setting up and cycling the PCR reactions

The mutagenic pairs of oligonucleotides (Method 3.7.1 to 3.7.2) were designed and synthesised (Proligo, Singapore) in order to substitute each residues with desired amino acids. Based on Stratagene's QuickChange Site-Directed Mutagenesis Kit, the PCR reaction was prepared in a 0.25 ml PCR tube containing 50 µl of a reaction mixture.

DNA template	50	ng
dNTPs	50	µM each
Forward primer	10	pmol
Reverse primer	10	pmol
5x Phusion^{TM} HF buffer	10	µl
Phusion DNA polymerase	1	U
Sterilized distilled water making final volume to 50 µl		

The temperature cycling parameters for the site-direct mutagenesis were shown in **Figure. 4.2** and **Table**. **4.2**. After the amplification reaction was finished, the PCR products were examined on 0.8% agarose gel electrophoresis.

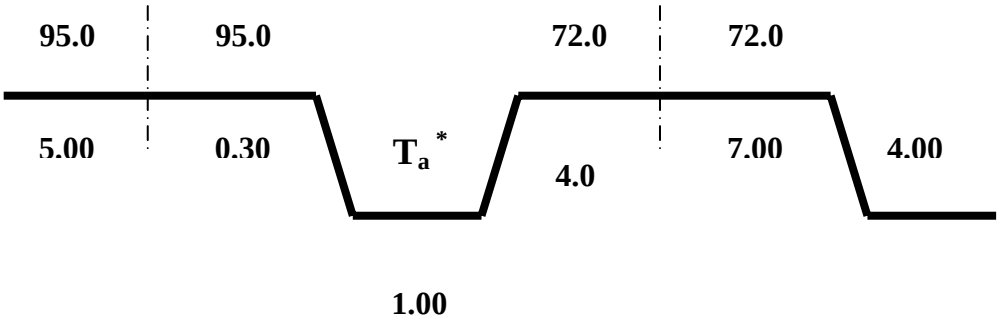

T_a * - The annealing temperature (T_a) as shown in Table 4.1 and 4.2

Figure 4.2: Temperature parameters for site-directed mutagenesis method

Table 4.1: Annealing temperature (T_a) for each Cry4Aa mutant primers

Mutant	T_a(°C)
D430A	50
K432A	50
Y433A	50
D436A	45
Y437A	45
P510A	45
T512A	45
Y513A	45
K514A	45
T515A	45

Table 4.2: Annealing temperature (T_a) for each Cry4BAa mutant primers

Mutant	T_a(°C)
R203Q/D454A	50
R203Q/D454E	50
R203Q/D454R	50
R203Q/D454K	45

4.4 Digestion of PCR products with *Dpn*I

The amplified reaction was incubated with 10U of *Dpn*I restriction endonuclease and incubate at 37°C for 1 hr to digest the parental DNA template and to select for mutation containing synthesized DNA. *Dpn*I restriction endonuclease is specific for methylated and hemimethylated DNA (5'-G^{me}A↓TC-3'). DNA, which is isolated from almost all *E. coli* strains, is *dam* methylated and it would be therefore susceptible to *Dpn*I digestion. The *Dpn*I-digested PCR products were analyzed by agarose gel electrophoresis (0.8% gel) before being transformed into *E.coli* competent cells.

4.5 Preparation of competent *E. coli* cells by calcium chloride method [70]

A single colony of *E. coli* strain JM109 was inoculated into 3 ml of LB broth and incubated at 37°C with 250 rpm shaking for 16-20 hr. The culture was inoculated into fresh LB broth to obtain 1% of cell concentration and then incubated at 37°C until the OD_{600} was 0.3-0.5. The culture was chilled on ice for 10 min. Cell were recovered by centrifugation at 3,000g for 10 min at 4°C and the cell pellets were resuspended in 10 ml of ice-cold 0.1M $CaCl_2$. Cell were centrifuged at 3,000g for 10 min at 4°C again and the cell pellet were resuspended in 10 ml of chilled 0.1M $CaCl_2$ and centrifuged again at the same condition for washing the pellet. The cell pellet were resuspended in 2 ml of ice-cold 0.1M $CaCl_2$ and add 900 µl of sterile glycerol was added to the solution and mixed gently. The resulting competent cells were split into 200 µl aliquots and store at -80°C until need. The efficiency of the competent cell was determined by transforming 10 ng of pUC12 into 200 µl of the competent cell suspension.

4.6 Transformation of plasmid DNA into competent cells

The *Dpn*I-digested PCR product was mixed with 200 µl of competent cells. The mixture was immediately chilled on ice for 30 min, following by incubation at 42°C for 90 sec, and then immediately placed on ice for 5 min. 800 µl of LB broth was added into the transformed cells, gently mixed and incubated at 37°C for 1 hr. Transormed cells were collected by centrifugation at 3,000 g for 2 min. Medium was decanted and the cell pellets were gently resuspended in 200 µl of LB broth. The transformed cell was spread gently over the surface of the LB agar plate containing 100 µg/ml ampicillin by a sterile glass rod. The agar plate was incubated at 37°C for 16-20 hr until *E.coli* colonies were clearly seen on agar plate.

4.7 Mutagenic plasmid screening

Restriction endonuclease analysis was used to screen for each mutant plasmid based on a recognition site silently introduced into each pair of mutagenic oligonucleotide primers. The digestion reaction was performed in 20 µl of a mixture that is composed of 0.5-1µg of DNA sample, an appropriate 1X restriction enzyme digestion buffer, 1X bovine albumin serum and sterilised distilled water to make up to the 20 µl total volume. The digestion reaction was incubated at recommended temperature for 3 hr with appropriate enzymes. To visualise the reaction patterns, electrophoresis of digested DNA was carried out in the horizontal 0.8% agarose gel in TBE buffer at 100 V for 1-2 hr.

4.8 DNA sequencing analysis

In order to verify nucleotide sequence of the mutant plasmids, 100 ng of each mutant plasmid, together with 10 pmole of oligonucleotide primer (Cry4Ba/Y266A-f: 5’ GCCAGTGCGGATCCACGTC 3’ and Cry4Aa/D200P-f: 5’TGATTGCCCGTACTAC TATAACATACTAG 3’) was submitted to Macrogen Inc. (Korea) to perform DNA sequencing. The resulting sequences were aligned with that of the wild type using ClustalX.

4.9 Expression of toxins

A single colony of *E. coli* JM109 containing either wild-type or each mutant plasmid was inoculated into 3 ml LB broth containing 100 µg/ml ampicillin. The cultures were incubated at 37°C with 250 rpm shaking for 16-20 hr. The overnight culture was inoculated into new LB broth containing 100 µg/ml ampicillin and grown at 37°C with 250 rpm shaking until the OD_{600} was 0.3-0.5. Then, protein expression was induced with IPTG at a final concentration of 0.1 mM at either 37°C for 4 hr or 30°C for 10 hr. After 4-hr or 10-hr induction, the cultures cell were placed on ice and harvested by centrifugation at 6,000 g for 10 min. 0.1 OD_{600} of *E. coli* (~ 10^7 cells) was analysed on 12.5% SDS-polyacrylamide gel electrophoresis.

4.10 SDS-polyacrylamide gel electrophoresis (SDS-PAGE)

Protein sample was prepared by mixing the sample with 4x loading buffer (8% SDS, 4 mM EDTA, 40% glycerol, 0.4% bromophenol blue, 100 mM DTT, 200 mM Tris-HCl, pH 6.8) in the ratio of 3:1 (v/v) and heated at 100° for 10 min. The heated samples were vigorously mixed using vortex and centrifuged at 12,000 rpm for 10 min to precipitate any insoluble materials. The supernatant were loaded on each well of SDS-polyacrylamide gel.

SDS-polyacrylamide gel was prepared using mini-Protein II electrophoresis system (BIORAD) according to the formulation in **Table 4.3**. The gel system in SDS-PAGE is composed of separating and stacking gels. The separating gel consists of 3.3% crosslinker, 10%, 12.5% or 15% gel, 0.375 M Tris-HCl (pH 8.8) and 0.1% SDS. The stacking gel contains 3.3% crosslinker, 5% gel, 0.125 M Tris-HCl (pH 6.8) and 0.1% SDS. The gel was run in Tris-glycine buffer (192 mM glycine, 0.1% SDS, 25 mM Tris-HCl, pH 8.3). Electrophoresis was performed with constant voltage at 100 V at room temperature.

After elctrophoresis, the protein bands on the gel were visualised by soaking in staining solution (0.1% Coomassie Brilliant Blue R250, 10% ethanol, 10% glacial acetic acid) for 40 min. The gel was then soaked in destaining solution (10% ethanol, 10% glacial acetic acid) for overnight or until the background was clear.

4.11 Partial purification of protoxin inclusions

After the large-scale expression of the protoxin inclusions in 700 ml of LB broth that containing 100 µg/ml ampicillin, the culture was harvested by centrifugation at 6,000g for 10 min at 4°C. The cell suspension was lysed by using a French Pressure cell at 10,000 psi. The protoxin inclusions were collected by centrifugation at 12,000 rpm for 10 min at 4°C. The supernatant was discarded, the pellet was resuspended and incubated in 30 ml of 100 mM KH_2PO_4 (pH 6.5) containing 0.1% Triton X-100 and 1 M NaCl. After incubation for 30 min, the pellets were collected by centrifugation and washed in cold 100 ml KH_2PO_4 (pH 6.5) and then in cold distilled water. The partially purified toxin inclusions were resuspended in distilled water to give a desired concentration of protein.

4.12 Determination of protein concentration

Protein concentrations were determined by using Bio-Rad protein assay reagent kit (Bio-Rad, USA). The calibration curves were constructed from a standard protein, bovine serum albumin (BSA). BSA standards were prepared by making dilution ranging from 1, 2, 3, 4 and 5 µg of BSA in 50 µl distilled water.

Each standard protein solution was mixed with 200 µl of Bradford dye reagent in a 96-well flat bottom microtitre plate (Costar, USA) and measured absorbance at 595 nm (SpectraMax 250 with Softmax Pro software; Molecular Devices, Sunnyvale, CA). 50 µl of protein sample was used and the protein concentration was calculated from the standard curve.

4.13 Solubilisation and proteolytic activation of protoxin inclusions

Partially purified inclusions were suspended in 50 mM Na_2CO_3, pH 10.0 and incubated at 37°C for 1 hr. Any insoluble protoxin inclusions were removed by centrifugation at 12,000 rpm for 10 min at room temperature. The sample were analysed on SDS-PAGE (12.5% gel). A soluble protoxins were mixed with trypsin (tosyl-phenylalanine chloromethyl ketone treated, Sigma) at a ratio of 1:20 (w/w,

enzyme/ protein) at 37°C for 16 hr. The trypsin digestion patterns were analysed on SDS-PAGE (15% gel).

4.14 Mosquito- larvicidal activity assay

Larvicidal activity assay was performed in a 24-well microtitre plate (15.6 mm well diameter, Costar). Each well contained 20 larvae (2-day old *Cu. quinquefasciatus* larvae) in 1,400 µl of distilled water. Then 400 µl of *E. coli* suspension (10^8 cells) expressing the Cry4Aa, Cry4Ba or a mutant protoxin was added into each well. A total of 100 larvae were used per each *E. coli* clone. Percent mortality was recorded after 24-hr incubation room temperature (25°C). At least three independent experiments were performed. *E. coli* cells expressing Cry4Aa, Cry4Ba or mutant protoxin were prepared according to Method 4.9.

The 50% lethal concentration (LC50) calculation was perform by incubating 1 ng, 10 ng, 100 ng, 1 µg or 10 µg of each protoxin inclusion with 2-day old *Cu. quinquefasciatus* larvae. A total of 100 larvae were used per each *E. coli* clone. At least three independent experiments were performed. LC50 was calculated using Finney's Probit Analysis [71].

Table 4.3: Formulation for SDS-polyacrylamide gel

Separating gel (10-15%)

%gel	10	12	15
40% acrylamide stock solution (ml)	2.5	3	3.75
1.5 M Tris-HCl (pH 8.8) (ml)	2.5	2.5	2.5
Distilled Water (ml)	4.8	4.3	3.55
10% SDS (µl)	100	100	100
TEMED (µl)	4	4	4
10% ammonium persulfate (µl)	100	100	100
Total (ml)	10	10	10

Table 4.3: Formulation for SDS-polyacrylamide gel (cont.)

Stacking gel (5%)

%gel	**5**	**5**	**5**
40% acrylamide stock solution (ml)	0.5	1	1.5
0.5 M Tris-HCl (pH 6.8) (ml)	0.5	1	1.5
Distilled water (ml)	2.92	5.84	8.76
10% SDS (µl)	40	80	120
TEMED (µl)	4	8	12
10% ammonium persulfate (µl)	40	80	120
Total (ml)	4	8	12

4.15 Protein purification

The activated toxin was purified by using size-exclusion FPLC (Superose-12 HR 10/30 column). The column was equilibrated with 50 mM Na_2CO_3 (pH 10.0) at flow rate of 0.4 ml/min for 2 column volume before operation. During the equilibrating step, the activated toxin sample was centrifuged at 12,000 rpm for 15 min and the supernatant was transferred into a new tube. The sample was injected into column and collected as 1-ml fraction at the flow rate of 0.4 ml/min. The fractions containing a purified 65-kDa activated toxin were pooled together and analysed by SDS-PAGE (15% gel).

4.16 Immunohistochemical method

4.16.1 *In vitro* receptor binding assay

Head and tail of 5-day old *Cu. quinquefasciatus* larvae were cut out on Petri-dish containing ice-cold fixative solution (4% paraformaldehyde, 5% sucrose, 1X PBS pH 7.4). The fixative solutions containing the dissected larvae were incubated at 4°C for 2 hr. Then, the fixative solutions were replaced with 10% sucrose fixative solution. The fixed larvae were dehydrated in a serial of ethanol baths and cleared in xylene bath. The larvae were subsequently infiltrated in three paraffin baths at 65°C under evacuation to absolutely remove the clearing solution. The infiltrated larvae were placed on mold and the melted paraffin was filled. The mold was removed to the cold place. After the paraffin solidified, the larvae were sectioned into 10-µm slices and placed on glass slide coated with 3-aminopropyltriethoxysilane.

The slide containing the sectioned larvae was incubated at 1 60°C hr. The section was then deparaffinated in two baths containing xylene and then in two baths containing absolute ethanol for 3 min in each bath. The section was hydrated in a series of ethanol baths (95%, 70%, 50% and 30%) and soaked in tap water for 5 min. To block the endogenous peroxidase, the section was incubated with 1X PBS, pH 7.4, containing 3% H_2O_2 and 0.1% Triton X-100 for 30 min at room temperature. The slide was washed 3 times with washing buffer (1X PBS, pH 7.4, containing 1% Triton X-

100) for 5 min each. The section was incubated with normal goat serum for blocking non-specific protein binding at dilution of 1:200 for 45 min at room temperature in humidified chamber.

In immunohistochemical detection step (**Fig. 4.3**), the larval sections were incubated with 200 µl of 12.5 µg/ml purified toxin for 45 min at room temperature in humidified chamber. 50 mM Na_2CO_3, pH 9.0, which was used as elution buffer in toxin purification step was used as a negative control. The sections were washed 3 times with washing buffer for 5 min each. The sections were then incubated with 200 µl of the primary antibodies (Rabbit anti 4B-R203Q or Rabbit anti 4A-R235Q 1:100 dilution in 1X PBS, pH 7.4) at room temperature in humidified chamber for 45 min. The sections were washed 3 times with washing buffer for 5 min each. Then, the sections were incubated with the secondary antibody (Goat anti rabbit IgG (H+L) conjugated with biotin 1:8,000 dilution in 1X PBS, pH 7.4) for 45 min at room temperature in humidified chamber. The sections were washed 3 times with washing buffer for 5 min each. Then, the sections were incubated with 200 µl of 5 µg/ml streptavidin conjugated with horseradish peroxidase diluted with 1X PBS, pH 7.4, at room temperature for 45 min in humidified chamber. The sections were washed 3 times with washing buffer for 5 min each, followed by 1X PBS, pH 7.4, for 5 min. The binding of toxin on the larval sections was detected as dark brown color after the addition of 3, 3'-diaminobenzidine (Vector, USA) for 5 min and the reaction was stopped with distilled water. Finally, the sections were mounted with permount solution and viewed under 40X magnification of light microscope.

4.16.2 *In vivo* receptor binding assay

In vivo assay was performed in a 6-well microtitre plate (34.8 mm well diameter, Costar), each well of which contained 25 larvae (5-day old *Cu. quinquefasciatus* larvae) in 5 ml of distilled water. Then, 50 µg/ml Cry4Aa, Cry4Ba or a mutant protoxin inclusion was added into a well. A total of 25 larvae was used per each clone. After 1-hr incubation at room temperature, all larvae were transferred to another plate that contained tap water. head and tail of larvae fed with toxin inclusion were cut out on Petri-dish containing ice-cold fixative solution (4% paraformaldehyde, 5% sucrose, PBS-150 mM NaCl, 8.56 mM Na_2HPO_4, 1.42 mM $NaH_2PO_4.H_2O$, pH

7.4). All the remaining steps of this *in vivo* receptor binding assay are the same as those mentioned in section 4.16.1 (*in vitro* receptor binding assay).

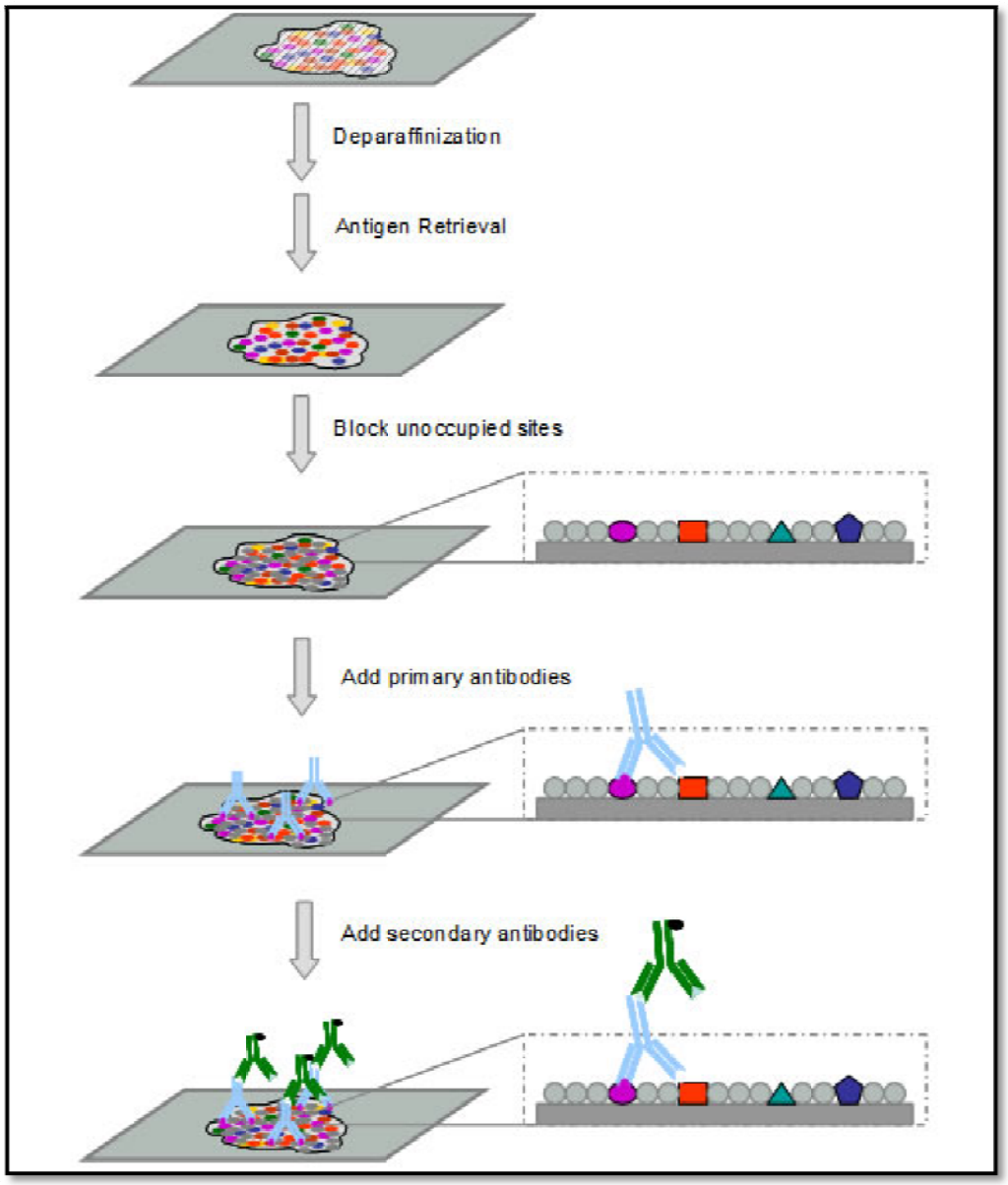

Figure 4.3: Immunohistochemistry method

CHAPTER V
RESULT I: MUTAGENESIS OF THE β6 - β7 SURFACE-EXPOSED LOOP OF THE Cry4Aa TOXIN

5.1 Constructions of the β6-β7 loop mutant plasmids

Five loop residues (D^{430}, K^{432}, Y^{433}, D^{436} and Y^{437}) in the β_6-β_7 loop of the Cry4Aa toxin were initially substituted with alanine by using PCR-based site-directed mutagenesis. The oligonucleotide primers (**Material 3.7.1**) were designed by introducing the mutated nucleotides and a restriction enzyme recognition site for distinguishing between the template and the mutant plasmid. Following the thermal cycle reactions with various annealing temperatures (**Table 4.1** and **4.2**), all of the PCR-amplified plasmids gave a 7.4-kb major DNA band on the ethidium bromide-stained agarose gel (**Fig**. **5.1**). In order to eliminate the parental DNA template, the PCR products were digested with *Dpn*I endonuclease. Then, 10 µl of *Dpn*I-treated PCR products were analysed on agarose gel electrophoresis. It was found that the bands of 7.4-kb plasmids still appeared (**Fig. 5.2**).

The *Dpn*I-treated PCR products were subsequently transformed into *E. coli* JM109 competent cells. Using of restriction analysis, 10-20 transformants from each mutation were screened for the presence of the mutant plasmids. After treated with an appropriate restriction endonuclease, the digested DNA fragments of each mutant plasmid clearly showed a correct restriction pattern from that of the wild-type plasmid as shown in **Fig. 5.3A** - **5.7A**. Each mutant plasmid was confirmed in the mutated region by DNA sequencing and the sequencing chromatograms are shown in **Fig. 5.3B** - **5.7B**. The results revealed that all mutants contain nucleotide changes at the desired positions.

5.2 Expression of the β6-β7 loop mutant toxins

When the plasmids encoding the wild-type or mutant Cry4Aa protoxins under control of the *tac* promoter were expressed in *E. coli* upon IPTG induction (**Method 4.9**), all the mutant (D430A, K432A, Y433A, D436A and Y437A) were produced as 130-kDa protoxin inclusion at levels comparable with that of the wild-type (**Fig. 5.8**).

5.3 Inclusion purification and solubilisation of the β6-β7 loop mutants

Toxin inclusion of all mutants (D430A, K432A, Y433A, D436A and Y437A) were partially purified as described in **Method 4.11** After the fractions were washed with distilled water, protein concentrations of the partially purified inclusions were determined by using the Bradford protein assay.

To determinate the degree of solubility, the inclusions of each mutant toxin (1 mg/ml) were solubilised in carbonate buffer pH 10.0, at 37°C for 1 hr as described in **Method 4.13** The amounts of the 130-kDa soluble proteins in the supernatant were then compared with that of the proteins in total fraction by SDS-PAGE analysis (**Fig. 5.8-5.9**). It can be seen that all of the 130-kDa mutant protoxins were significantly soluble (>80%).

5.4 Proteolytic processing of the β6-β7 loop mutants

After solubilization of the wild type Cry4Aa and its mutants (D430A, K432A, Y433A, D436A and Y437A) protoxins, they were digested with TCPK-treated trypsin (**Method 4.13**). The proteolytic patterns were compared on SDS-PAGE. Similar to the wild type, the major proteolytic products of ca. 47 and ca. 21 kDa were observed in all mutants as shown in **Fig. 5.10**. The results suggested that the mutants fold with the native conformation.

5.5 Mosquito-larvicidal activity of the β6-β7 loop mutants

To examine the effect of amino acid substitutions on larvicidal activity, *E. coli* whole cells expressing each mutant toxin were tested for their toxicity against *C. quinquafasciarus* larvae (**Method 4.13**). The percentage of dead larvae recorded after 24-hr incubation at room temperature is shown in **Fig. 5.11**. It was found that toxicity of all mutants (D430A, K432A, Y433A, D436A and Y437A) was slightly lower than that of the wild type.

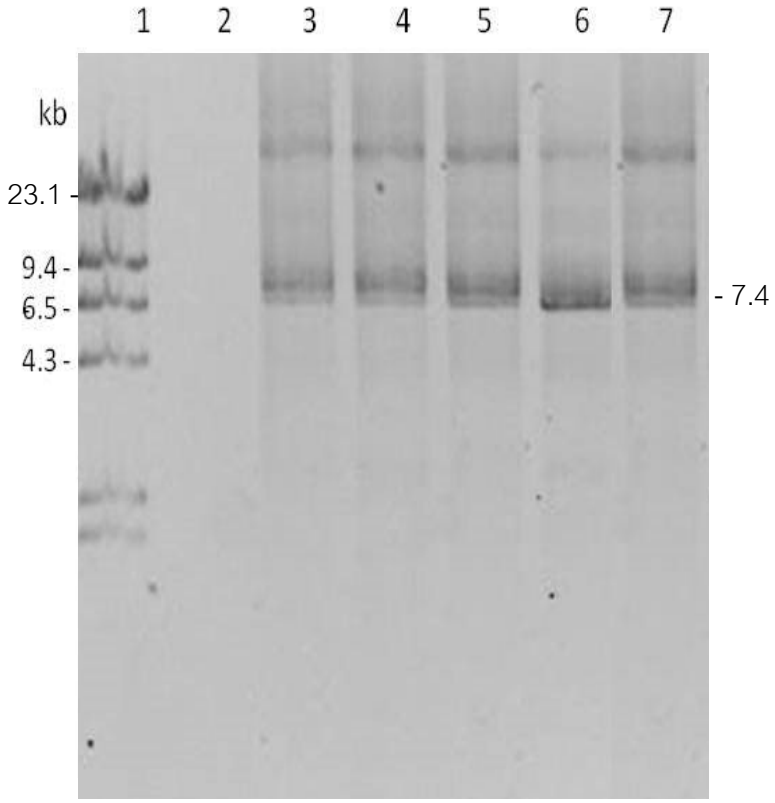

Figure 5.1: PCR amplification of Cry4Aa mutant plasmids: pD430A, pK432A, pY433A, pD436A and pY437A

Lane 1: *Hind*III-digested λ DNA markers
Lane 2: The PCR product of negative control
Lane 3: The PCR product of the mutant D430A plasmid
Lane 4: The PCR product of the mutant K432A plasmid
Lane 5: The PCR product of the mutant Y433A plasmid
Lane 6: The PCR product of the mutant D436A plasmid
Lane 7: The PCR product of the mutant Y437A plasmid

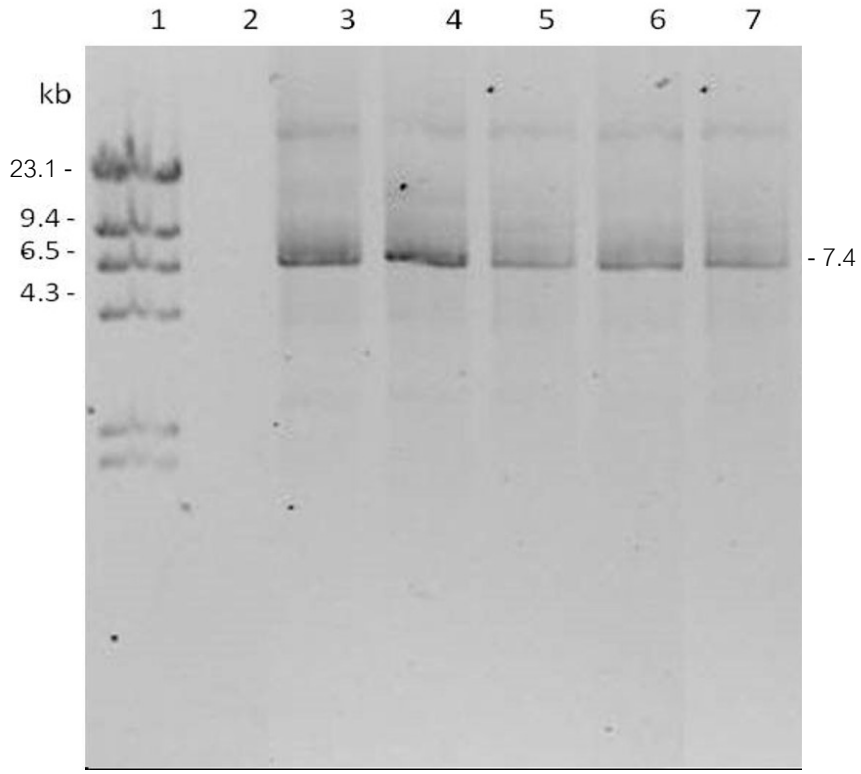

Figure 5.2: *Dpn*I digestion of the PCR products of Cry4Aa mutant plasmids: pD430A, pK432A, pY433A, pD436A and pY437A.

Lane 1: *Hind*III-digested λ DNA markers
Lane 2: The *Dpn*I-digested PCR product of negative control
Lane 3: The *Dpn*I-digested PCR product of the pD430A plasmid
Lane 4: The *Dpn*I-digested PCR product of the pK432A plasmid
Lane 5: The *Dpn*I-digested PCR product of the pY433A plasmid
Lane 6: The *Dpn*I-digested PCR product of the pD436A plasmid
Lane 7: The *Dpn*I-digested PCR product of the pY437A plasmid

(A) **(B)**

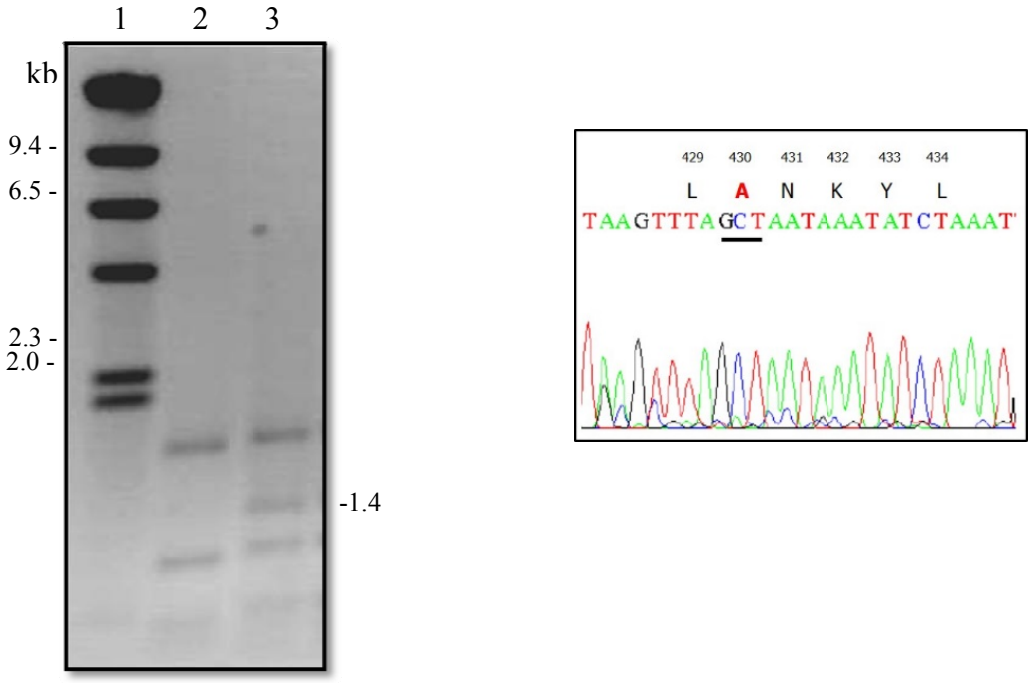

Figure 5.3: Restriction endonuclease and DNA sequence analysis of pD430A

(A) 1.2% agarose gel electrophoresis (ethidium bromide-stained) of *Dde*I digestion patterns of the template and mutated plasmids.

Lane 1: *Hind*III-digested λ DNA markers

Lane 2: The *Dde*I-digested wild-type plasmid, pMEx-B4A

Lane 3: The *Dde*I-digested mutant plasmid, pD430A

(B) DNA sequencing chromatogram of pD430A, using D200P-f as a sequencing primer. Part of the sense strand sequence is shown. Underlined letters indicate mutated nucleotide residues.

(A) **(B)**

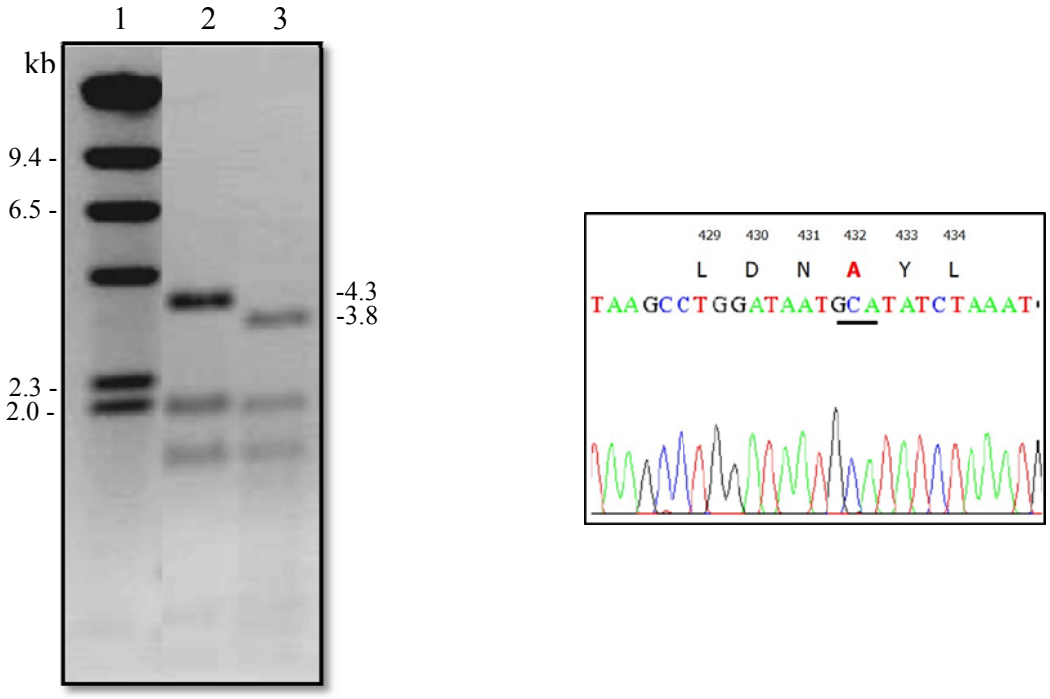

Figure 5.4: Restriction endonuclease and DNA sequence analysis of pK432A

(A) 1.2% agarose gel electrophoresis (ethidium bromide-stained) of *Bst*NI digestion patterns of the template and mutated plasmids.

Lane 1: *Hind*III-digested λ DNA markers

Lane 2: The *Bst*NI-digested wild-type plasmid, pMEx-B4A

Lane 3: The *Bst*NI-digested mutant plasmid pK432A

(B) DNA sequencing chromatogram of pK432A, using D200P-f as a sequencing primer. Part of the sense strand sequence is shown. Underlined letters indicate mutated nucleotide residues.

(A) **(B)**

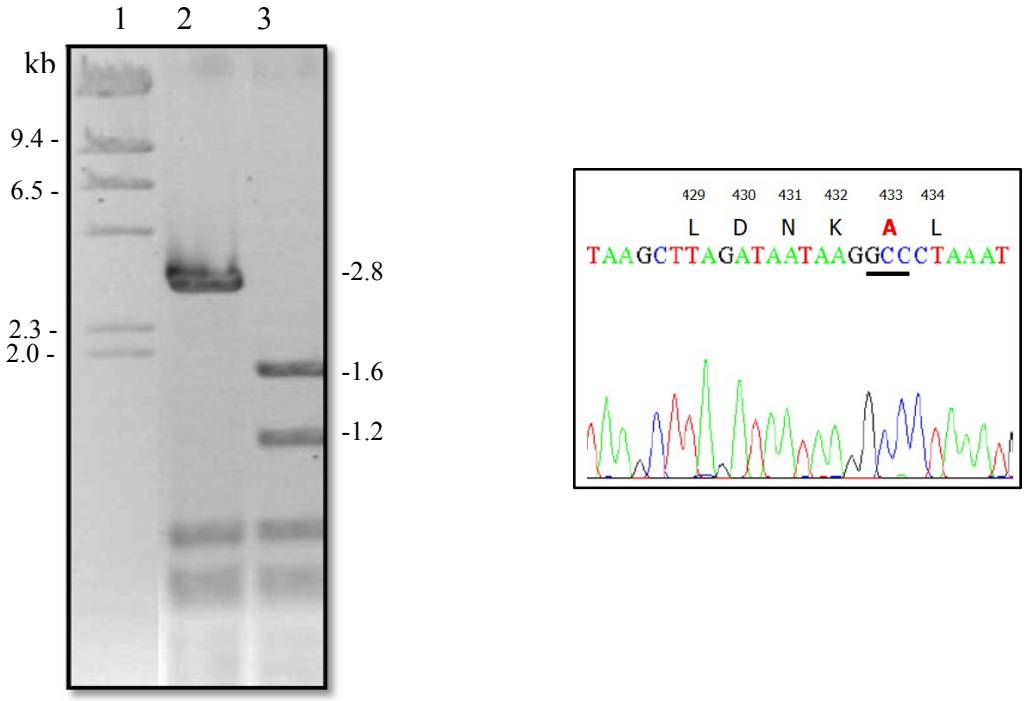

Figure 5.5: Restriction endonuclease and DNA sequence analysis of pY433A

(A) 1.2% agarose gel electrophoresis (ethidium bromide-stained) of *Hae*III digestion patterns of the template and mutated plasmids.

Lane 1: *Hind*III-digested λ DNA markers

Lane 2: The *Hae*III-digested wild-type plasmid, pMEx-B4A

Lane 3: The *Hae*III-digested mutant plasmid pY433A

(B) DNA sequencing chromatogram of pK432A, using D200P-f as a sequencing primer. Part of the sense strand sequence is shown. Underlined letters indicate mutated nucleotide residues.

(A) **(B)**

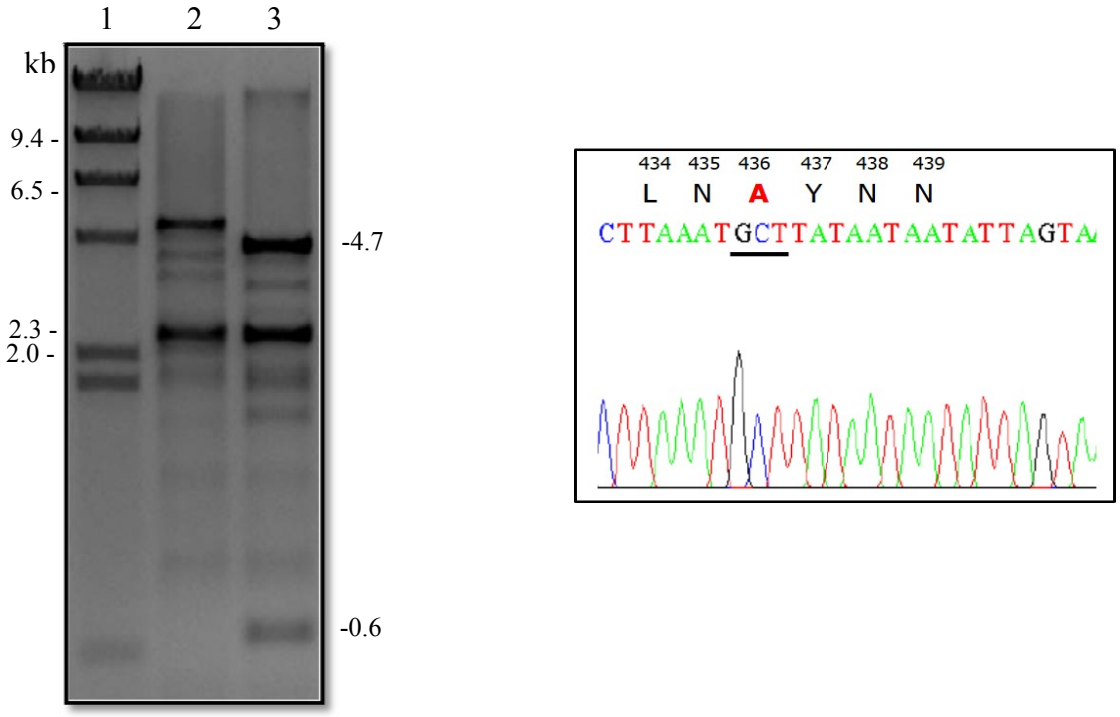

Figure 5.6: Restriction endonuclease and DNA sequence analysis of pD436A

(A) 1.2% agarose gel electrophoresis (ethidium bromide-stained) of *Sca*I digestion patterns of the template and mutated plasmids.

Lane 1: *Hind*III-digested λ DNA markers

Lane 2: The *Sca*I-digested wild-type plasmid, pMEx-B4A

Lane 3: The *Sca*I-digested mutant plasmid pD436A

(B) DNA sequencing chromatogram of pD436A, using D200P-f as a sequencing primer. Part of the sense strand sequence is shown. Underlined letters indicate mutated nucleotide residues.

(A) **(B)**

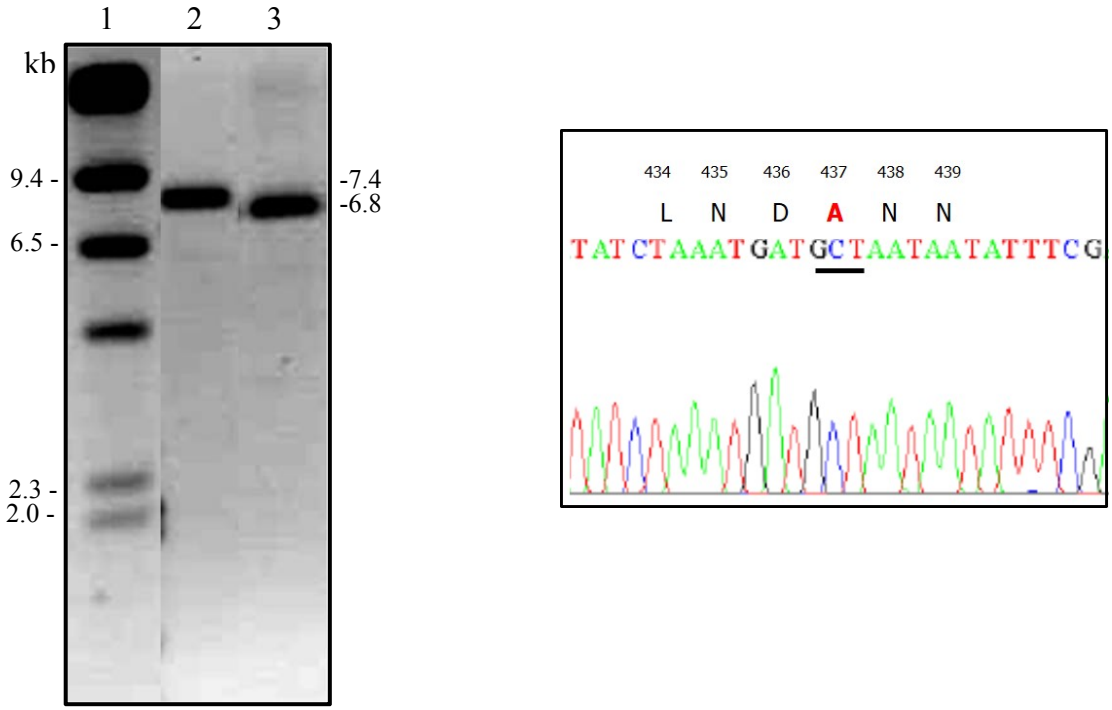

Figure 5.7: Restriction endonuclease and DNA sequence analysis of pY437A

(A) 1.2% agarose gel electrophoresis (ethidium bromide-stained) of *BstB*I digestion patterns of the template and mutated plasmids.

Lane 1: *Hind*III-digested λ DNA markers

Lane 2: The *BstB*I-digested wild-type plasmid, pMEX-B4A

Lane 3: The *BstB*I-digested mutant plasmid pY437A

(B) DNA sequencing chromatogram of pY437A, using D200P-f as a sequencing primer. Part of the sense strand sequence is shown. Underlined letters indicate mutated nucleotide residues.

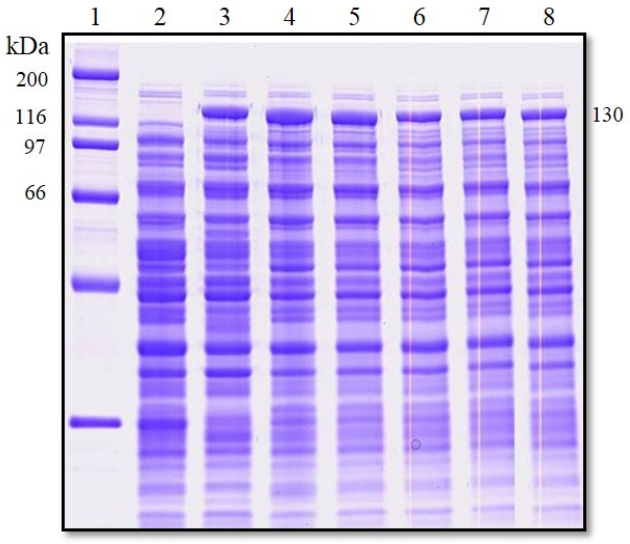

Figure 5.8: Expression of Cry4Aa and its mutants: D430A, K432A, Y433A, D436A and Y437A

Lane 1: standard protein marker

Lane 2: crude lysates of *E. coli* cells containing pMEx8 (negative control)

Lane 3: crude lysates of *E. coli* cells containing pMEx-B4A

Lane 4: crude lysates of *E. coli* cells containing mutant pD430A

Lane 5: crude lysates of *E. coli* cells containing mutant pK432A

Lane 6: crude lysates of *E. coli* cells containing mutant pY433A

Lane 7: crude lysates of *E. coli* cells containing mutant pD436A

Lane 8: crude lysates of *E. coli* cells containing mutant pY437A

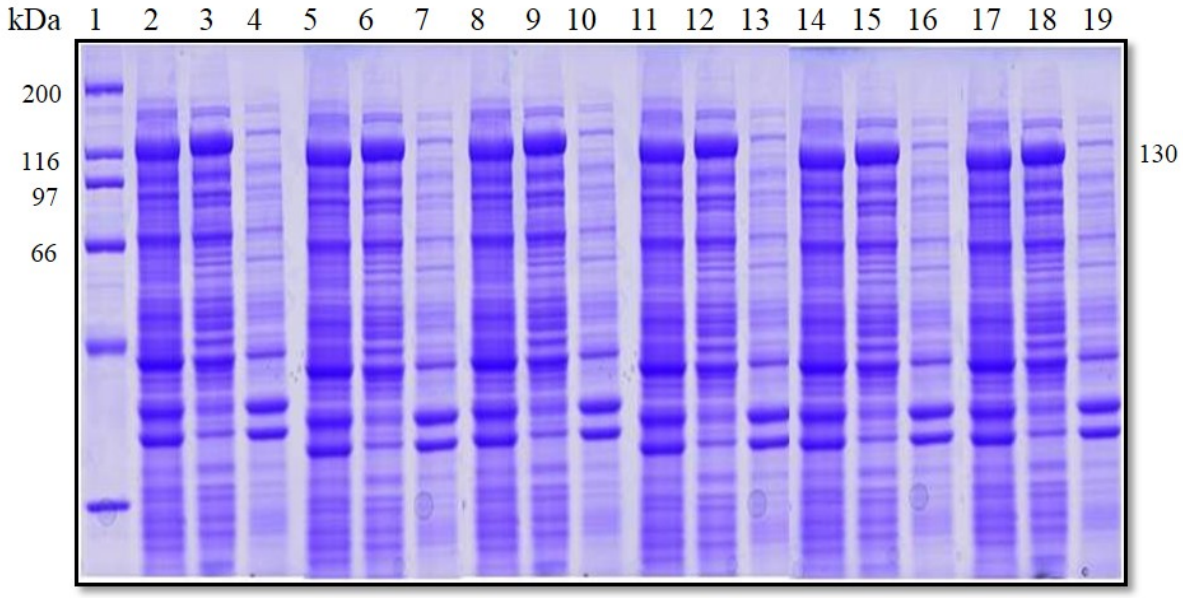

Figure 5.9: Solubility of Cry4Aa and its mutants: D430A, K432A, Y433A, D436A and Y437A

The figure shows coomassie brilliant blue-stained SDS-PAGE (12.5% gel) comparing the solubility of the wild type and its mutant inclusions in 50 mM Na_2CO_3 (pH 9.0).

Lane 1: standard protein marker

Lanes 2-4: total, soluble and pellet fraction of pMEx-B4A, respectively

Lanes 5-7: total, soluble and pellet fraction of D430A, respectively

Lanes 8-10: total, soluble and pellet fraction of K432A, respectively

Lanes 11-13: total, soluble and pellet fraction of Y433A, respectively

Lanes 14-16: total, soluble and pellet fraction of D436A, respectively

Lanes 17-19: total, soluble and pellet fraction of Y437A, respectively

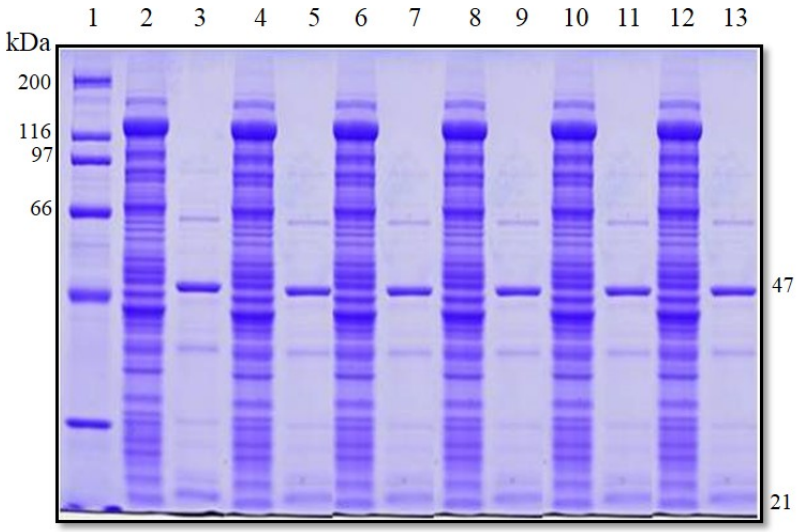

Figure 5.10: Proteolytic processing of Cry4Aa and its mutants: D430A, K432A, Y433A, D436A and Y437A

The figure shows coomassie brilliant blue-stained SDS-PAGE (15% gel) comparing trypsin digested products of wild type and its mutant toxins. The major expected bands of ca. 47 kDa and ca. 21 kDa fragments are indicated with the labels.

Lane 1: standard protein marker
Lanes 2-3: solubilised and trypsin treated products of pMEx-B4A, respectively
Lanes 4-5: solubilised and trypsin treated products of D430A, respectively
Lanes 6-7: solubilised and trypsin treated products of K432A, respectively
Lanes 8-9: solubilised and trypsin treated products of Y433A, respectively
Lanes 10-11: solubilised and trypsin treated products of D436A, respectively
Lanes 12-13: solubilised and trypsin treated products of Y437A, respectively

Toxin	%Mortality(n=3)						
	Cry4Aa	D430A	K432A	Y433A	D436A	Y437A	pMEX-8
mean	91.3	84.7	86.3	86.3	87.7	87	1.0
SEM	0.7	0.3	1.7	0.9	0.33	0.6	0.6

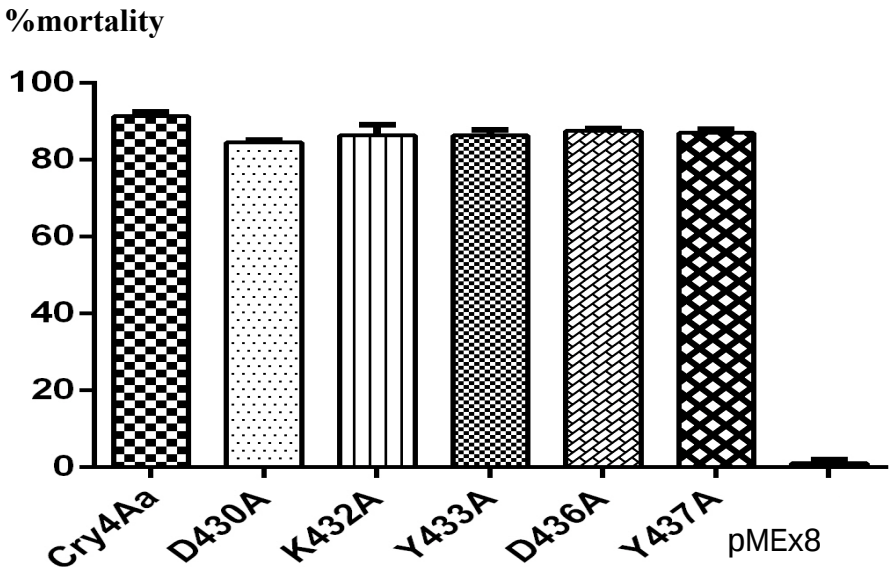

Figure 5.11: Larvicidal activity of *E. coli* cells containing the Cry4Aa toxin or its mutant toxins: D430A, K432A, Y433A, D436A and Y437A

The figure shows toxicity of *E. coli* cells containing the Cry4Aa wild-type or its mutant toxins against *Cu. quinquefasciatus*. The control samples were *E. coli* cells containing the pMEx8 vector. Error bars represent standard error of the mean from five independent experiments.

CHAPTER VI
RESULT II: MUTAGENESIS OF THE β10-β11 SURFACE-EXPOSED LOOP OF THE Cry4Aa TOXIN

6.1 Construction of the β10-β11 loop mutant plasmids

Selected residues (Pro^{510}, Thr^{512}, Tyr^{513}, Lys^{514} and Thr^{515}) in the β_{10}-β_{11} loop of the Cry4Aa toxin were replaced with alanine by using PCR-based site-directed mutagenesis. The pMEx-B4A plasmid containing the *cry4Aa* gene was used as template and the oligonucleotide primers (**Material 3.7.1**) were used as mutagenic primers to substitute these individual residues with alanine. After amplification (**Method 4.3.1**), all of the PCR-amplified plasmids were analysed on agarose gel electrophoresis (**Fig. 6.1**). In order to eliminate the parental DNA template, the PCR products were digested with *Dpn*I endonuclease and 10 µl of *Dpn*I-treated PCR products were analysed on agarose gel electrophoresis. It was found that the bands of 7.4-kb plasmids still appeared (**Fig. 6.2**).

6.2 Screening of the β10-β11 loop mutant plasmids

The *Dpn*I-treated PCR products were then transformed into *E. coli* JM109 competent cells (**Method 4.5**). 10-20 ampicillin resistant colonies were randomly selected and screened for the desired loop mutant plasmids by restriction endonuclease digestion in comparison with the wild type plasmid as shown in **Fig. 6.3A-6.7A**. Each mutant plasmid was confirmed in the mutated region by DNA sequencing and the sequencing chromatograms are shown in **Fig. 6.3B-6.7B**. The results revealed that all mutants contain nucleotide changes at the desired positions.

6.3 Expression of the β10-β11 loop mutant toxins

All the verified mutant plasmids, (pP510A, pT512A, pY513A, pK514A and pT515A) were expressed in *E.coli* cells with 0.1 mM IPTG induction at 37°C for 4 hr. Crude lysates of *E.coli* cells (0.1 OD_{600}) expressing each mutant toxin were analysed for protein expression levels on SDS-PAGE (12.5% gel) in comparison with the crude lysates of the cells expressing the Cry4Aa wild type. As shown in **Fig. 6.8**, all the loop mutant clones were expressed as 130-kDa protoxin with levels similar to the wild type.

6.4 Inclusion purification and solubilisation of the β10-β11 loop mutant toxins

Toxin inclusions of all mutants (P510A, T512A, Y513A, K514A and K514A) were partially purified as described in **Method 4.11** After the fractions were washed with distilled water, protein concentrations of the partially purified inclusions were determined by using the Bradford protein assay. To determine the degree of solubility, inclusions of the five mutant were solubilised in 50 mM carbonate buffer pH 10.0, at 37°C for 1 hr. As can be seen in **Fig. 6.9**, all the mutants showed the same solubility as the wild type.

6.5 Proteolytic processing of the β10-β11 loop mutant toxins

All five soluble protoxins were digested with TCPK-treated trypsin at a ratio of 1:20 (enzyme: protoxin, w/w) at 37°C for 16 hr (**Method 4.13**). The 130-kDa solubilised mutant protoxins showed the same trypsin digestion patterns as that of the wild type (**Fig. 6.10**), suggesting that all the mutant protoxins folded with their native conformation.

6.6 Mosquito-larvicidal activity of the β10-β11 loop mutant toxins

Mosquito bioassays were performed to determine the effect of amino acid substitutions on toxicity. *E. coli* cells expressing each individual toxin were tested for their toxicity against *C. quinquefasciatus* larvae. The percentage of dead larvae recorded after 24-hr incubation is shown in **Fig. 6.11**. It was found that only K514A mutant showed a reduction of larvicidal activity to about 40% whereas the four other mutants showed the same larvicidal activity as the wild type at 90%.

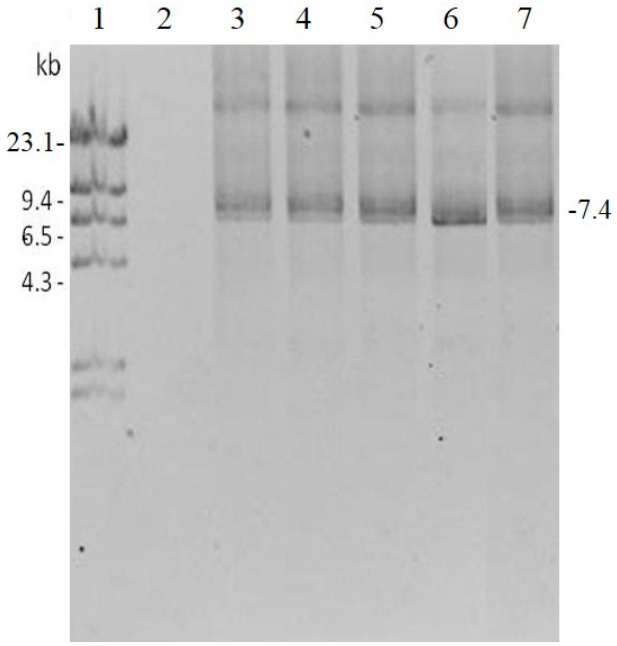

Figure 6.1: PCR amplification of Cry4Aa mutant plasmids: pP510A, pT512A, pY513A, pK514A and pT515A

Lane 1: *Hind*III-digested λ DNA markers
Lane 2: The PCR product of negative control
Lane 3: The PCR product of the pP510A plasmid
Lane 4: The PCR product of the pT512A plasmid
Lane 5: The PCR product of the pY513A plasmid
Lane 6: The PCR product of the pK514A plasmid
Lane 7: The PCR product of the pT515A plasmid

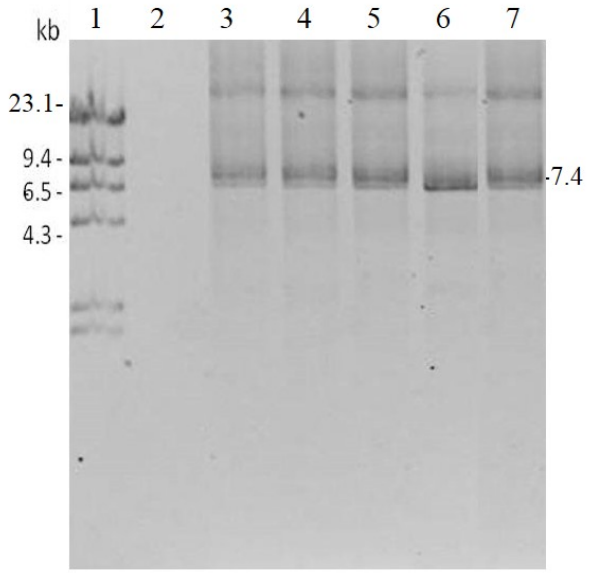

Figure 6.2: *Dpn*I digestion of the PCR products of Cry4Aa mutant plasmids: pP510A, pT512A, pY513A, pK514A and pT515A

Lane 1: *Hind*III-digested λ DNA markers
Lane 2: The *Dpn*I-digested PCR product of negative control
Lane 3: The *Dpn*I-digested PCR product of pP510A plasmid
Lane 4: The *Dpn* I-digested PCR product of pT512A plasmid
Lane 5: The *Dpn* I-digested PCR product of pY513A plasmid
Lane 6: The *Dpn* I-digested PCR product of pK514A plasmid
Lane 7: The *Dpn* I-digested PCR product of pT515A plasmid

(A) **(B)**

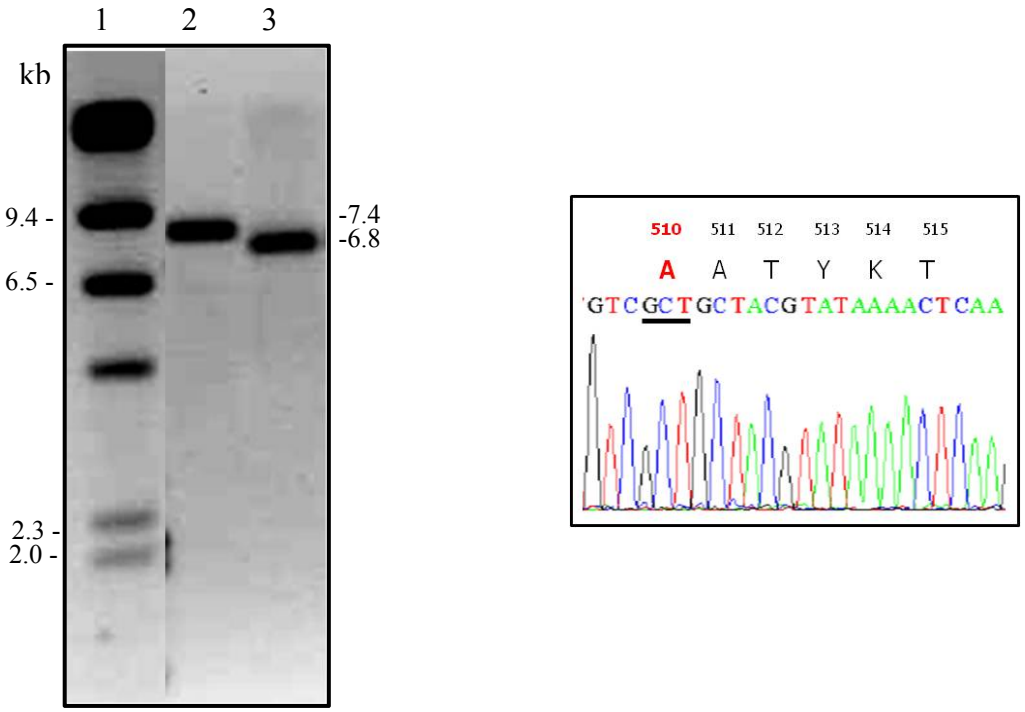

Figure 6.3: Restriction endonuclease and DNA sequence analysis of pP510A

(A) 1.2% agarose gel electrophoresis (ethidium bromide-stained) of *Sna*BI digestion patterns of the template and mutated plasmids.

Lane 1: *Hind*III-digested λ DNA markers

Lane 2: The *Sna*BI digested wild-type plasmid, pMEx-B4A

Lane 3: The *Sna*BI digested mutant plasmid, pP510A

(B) DNA sequencing chromatogram of pP510A, using D200P-f as a sequencing primer. Part of the sense strand sequence is shown. Underlined letters indicate mutated nucleotide residues.

(A) **(B)**

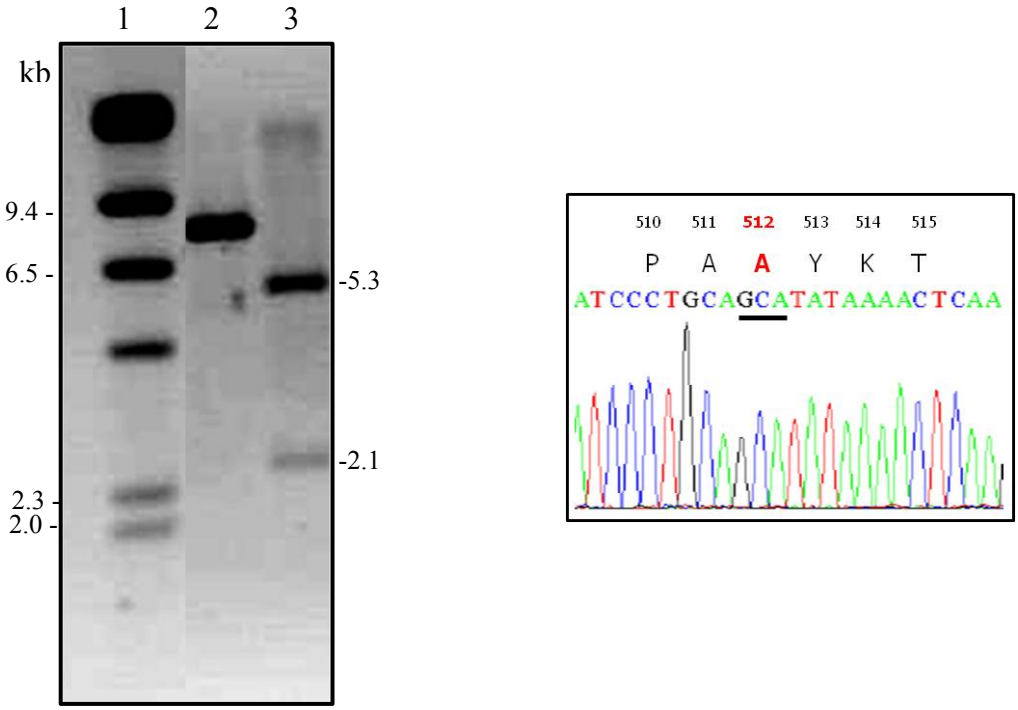

Figure 6.4: Restriction endonuclease and DNA sequence analysis of pT512A

(A) 1.2% agarose gel electrophoresis (ethidium bromide-stained) of *Pst*I digestion patterns of the template and mutated plasmids.

Lane 1: *Hind*III-digested λ DNA markers

Lane 2: The *Pst*I digested wild-type plasmid, pMEx-B4A

Lane 3: The *Pst*I digested mutant plasmid, pT512A

(B) DNA sequencing chromatogram of pT512A, using D200P-f as a sequencing primer. Part of the sense strand sequence is shown. Underlined letters indicate mutated nucleotide residues.

(A) **(B)**

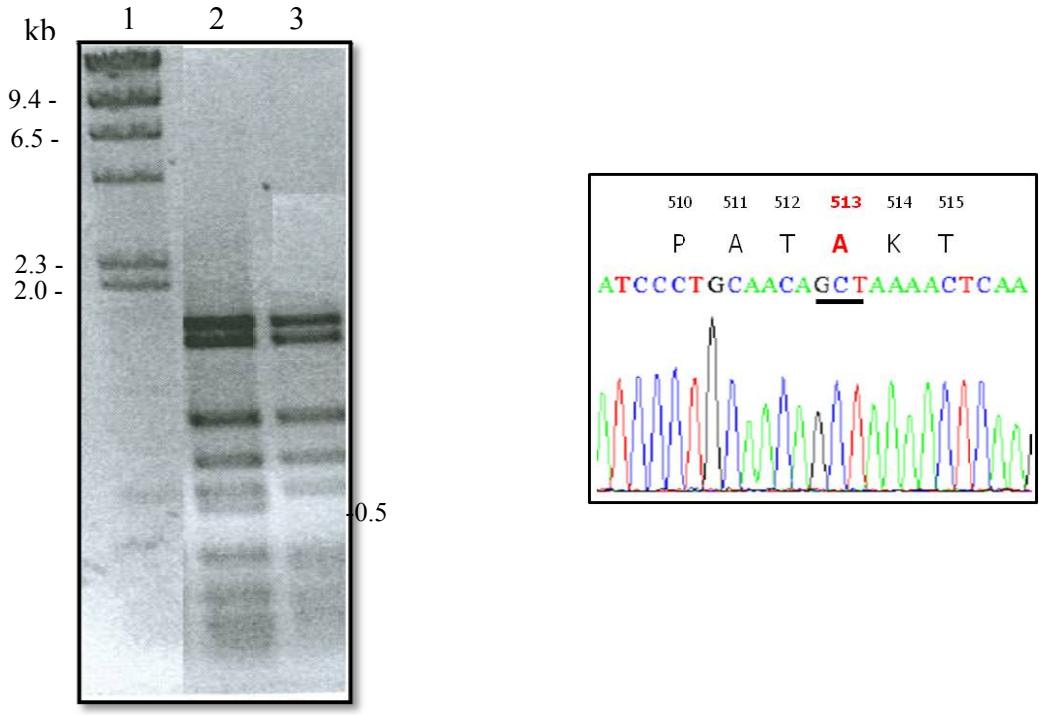

Figure 6.5: Restriction endonuclease and DNA sequence analysis of pY513A

(A) 1.2% agarose gel electrophoresis (ethidium bromide-stained) of *Rsa*I digestion patterns of the template and mutated plasmids.

Lane 1: *Hind*III-digested λ DNA markers

Lane 2: The *Rsa*I digested wild-type plasmid, pMEx-B4A

Lane 3: The *Rsa*I digested mutant plasmid, pT512A

(B) DNA sequencing chromatogram of pT512A, using D200P-f as a sequencing primer. Part of the sense strand sequence is shown. Underlined letters indicate mutated nucleotide residues.

(A) **(B)**

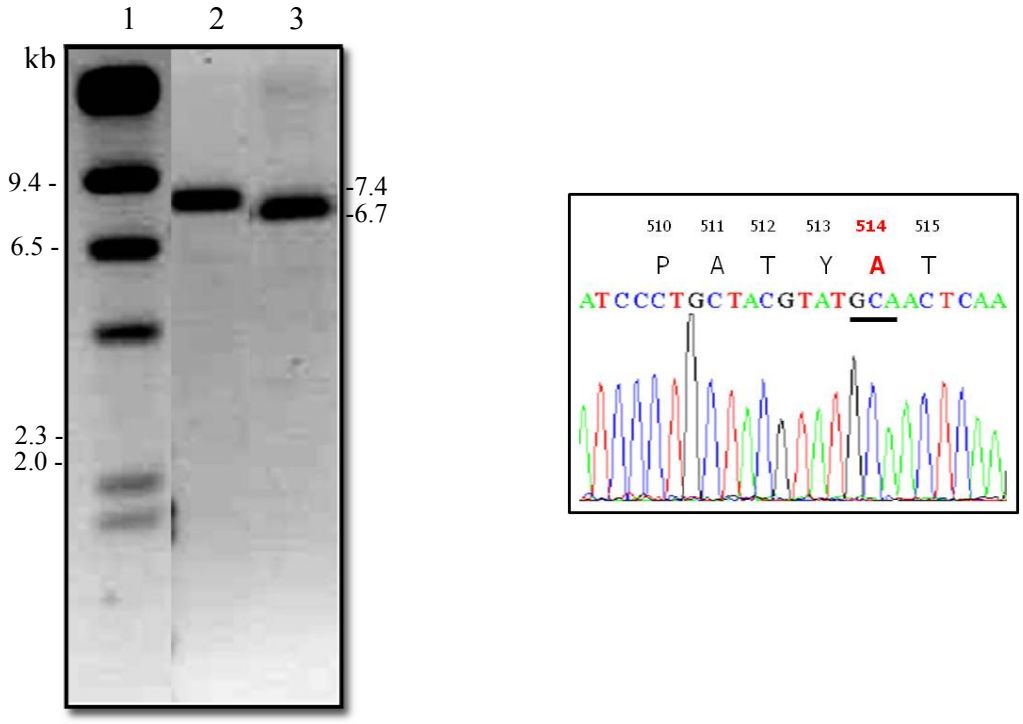

Figure 6.6: Restriction endonuclease and DNA sequence analysis of pK514A

(A) 1.2% agarose gel electrophoresis (ethidium bromide-stained) of *Sna*BI digestion patterns of the template and mutated plasmids.

Lane 1: *Hind*III-digested λ DNA markers

Lane 2: The *Sna*BI digested wild-type plasmid, pMEx-B4A

Lane 3: The *Sna*BI digested mutant plasmid pK514A

(B) DNA sequencing chromatogram of pK514A, using D200P-f as a sequencing primer. Part of the sense strand sequence is shown. Underlined letters indicate mutated nucleotide residues.

(A) **(B)**

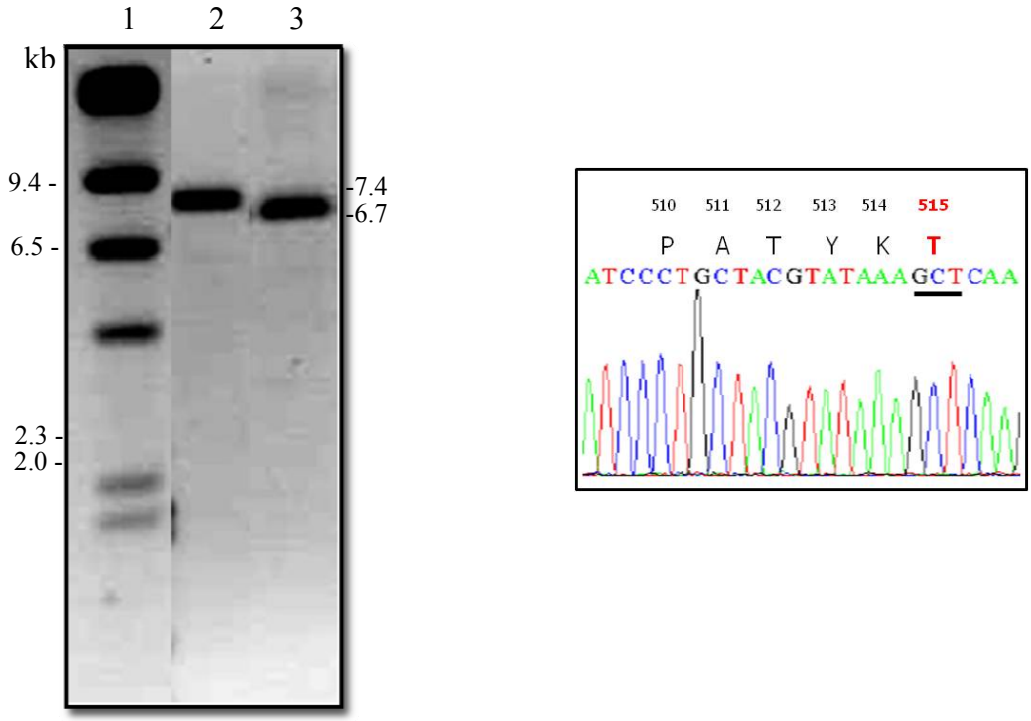

Figure 6.7: Restriction endonuclease and DNA sequence analysis of pT515A

(A) 1.2% agarose gel electrophoresis (ethidium bromide-stained) of *Sna*BI digestion patterns of the template and mutated plasmids.

Lane 1: *Hind*III-digested λ DNA markers

Lane 2: The *Sna*BI digested wild-type plasmid, pMEx-B4A

Lane 3: The *Sna*BI digested mutant plasmid pT515A

(B) DNA sequencing chromatogram of pT515A, using D200P-f as a sequencing primer. Part of the sense strand sequence is shown. Underlined letters indicate mutated nucleotide residues.

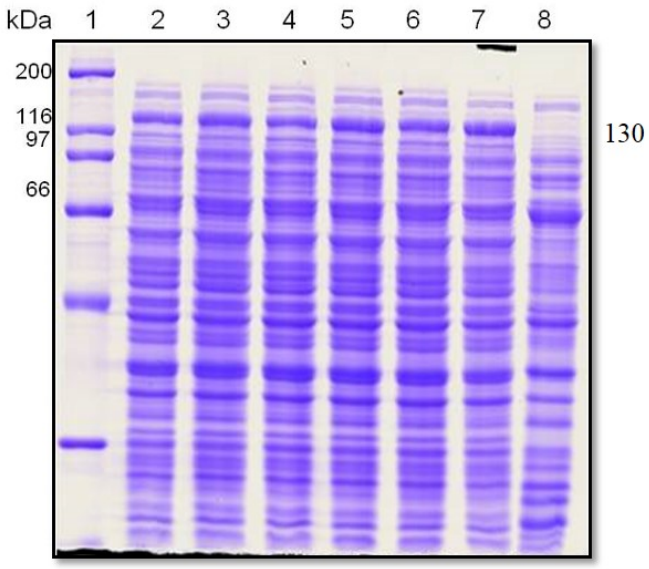

Figure 6.8: Expression of Cry4Aa and its mutants: P510A, T512A, Y513A, K514A and T515A

Lane 1: Standard protein marker

Lane 2: Crude lysates of *E. coli* cells containing pMEx-B4A

Lane 3: Crude lysates of *E. coli* cells containing pP510A plasmid

Lane 4: Crude lysates of *E. coli* cells containing pT512A plasmid

Lane 5: Crude lysates of *E. coli* cells containing pY513A plasmid

Lane 6: Crude lysates of *E. coli* cells containing pK514A plasmid

Lane 7: Crude lysates of *E. coli* cells containing pT515A plasmid

Lane 8: Crude lysates of *E. coli* cells containing pMEx8 (negative control)

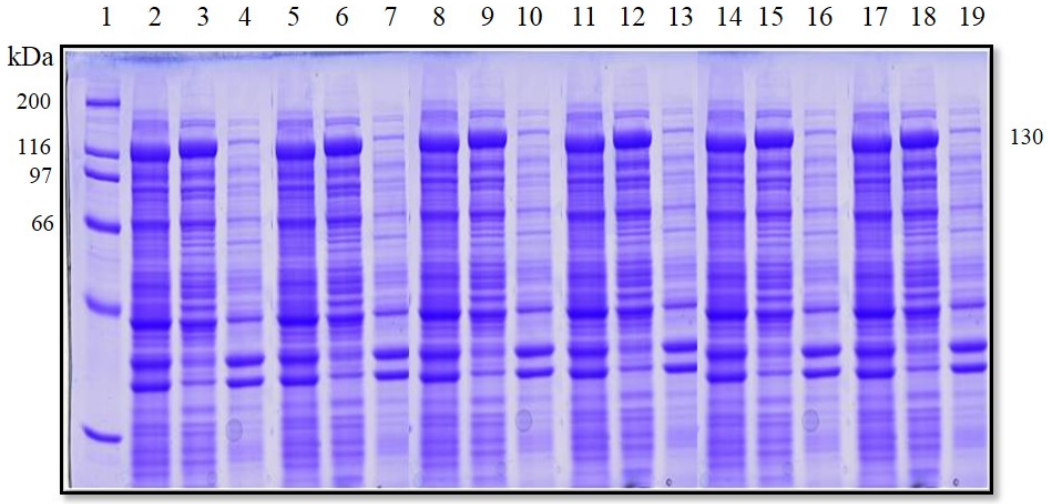

Figure 6.9: Solubility of Cry4Aa and its mutants: P510A, T512A, Y513A, K514A and T515A

The figure shows coomassie brilliant blue-stained SDS-PAGE (12.5% gel) comparing the solubility of the wild type and its mutant inclusions in 50mM Na_2CO_3 (pH 9.0).

Lane 1: Standard protein marker

Lanes 2-4: Total, soluble and pellet fraction of pMEX-B4A, respectively

Lanes 5-7: Total, soluble and pellet fraction of P510A, respectively

Lanes 8-10: Total, soluble and pellet fraction of T512A, respectively

Lanes 11-13: Total, soluble and pellet fraction of Y513A, respectively

Lanes 14-16: Total, soluble and pellet fraction of K514A, respectively

Lanes 17-19: Total, soluble and pellet fraction of T515A, respectively

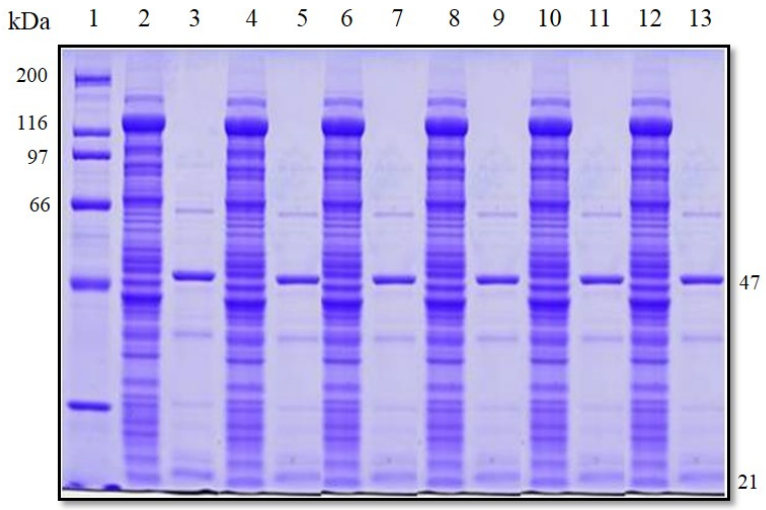

Figure 6.10: Proteolytic processing of Cry4Aa and its mutants: P510A, T512A, Y513A, K514A and T515A

The figure shows coomassie brilliant blue-stained SDS-PAGE (15% gel) comparing trypsin digested products of wild type and its mutant toxins. The major expected bands of ca. 47 kDa and ca. 21 kDa fragments are indicated with the labels.

Lane 1: standard protein marker

Lanes 2-3: solubilised and trypsin treated products of pMEx-B4A, respectively

Lanes 4-5: solubilised and trypsin treated products of P510A, respectively

Lanes 6-7: solubilised and trypsin treated products of T512A, respectively

Lanes 8-9: solubilised and trypsin treated products of Y513A, respectively

Lanes 10-11: solubilised and trypsin treated products of K514A, respectively

Lanes 12-13: solubilised and trypsin treated products of T515A, respectively

	%Mortality(n=3)						
	Cry4Aa	P510A	T512A	Y513A	K514A	T515A	pMEX-8
mean	89.3	85.3	88.7	89.0	46.3	88.0	1.0
SEM	0.7	6.2	5.6	4.0	1.7	6.0	0.6

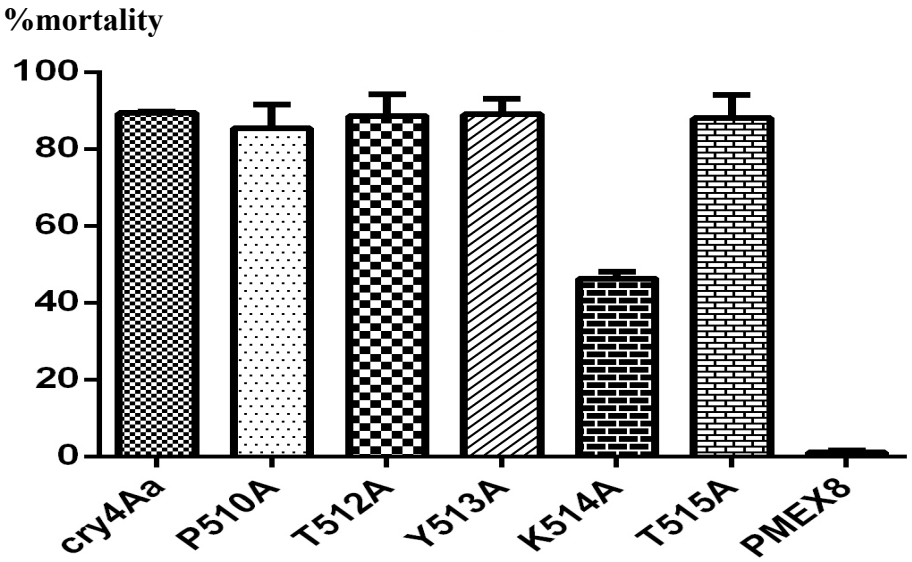

Figure 6.11: Larvicidal activity of *E. coli* cells containing the Cry4Aa toxin or its mutant toxins: P510A, T512A, Y513A, K514A and T515A.

The figure shows toxicity of *E. coli* cells containing the Cry4Aa wild-type or its mutant toxins against *Cu. quiquefasciatus* larvae. The control samples were *E. coli* cells containing the pMEx8 vector. Error bars represent standard error of the mean from three independent experiments.

CHAPTER VII
RESULT III: INVOLVEMENT IN TOXICITY OF THE β10 - β11 RECEPTOR-BINDING LOOP OF THE Cry4Ba TOXIN

7.1 Construction of the β10-β11 loop mutant plasmids

Previously, single alanine substitution of Asp^{454} which is located at the tip of Cry4Ba β10-β11 loop revealed a non-involvement of this residue in toxicity against *Ae. aegypti* larvae [6]. However, it was shown that replacement of Asp^{454} with variety of tripeptides can raise toxicity against *Culex* larvae [10]. Here, importance of the Asp^{454} was further elucidated *via* site-directed mutagenesis. The pR203Q plasmid was used as template and the oligonucleotide primers (**Material 3.7.2**) were used as mutagenic primers to substitute this residue with alanine, lysine, arginine and glutamic acid. After amplification, all the PCR-amplified products were analysed on agarose gel electrophoresis as shown in **Fig. 7.1**. As can be seen that all the PCR products appeared to contain a major band of 6.3-kb.

7.2 Screening of the β10-β11 loop mutant plasmids

In order to eliminate the nonmutated parental DNA template, the PCR products were digested with *Dpn*I endonuclease and 10 µl of *Dpn*I-digested PCR products were analysed on agarose gel electrophoresis. It was found that the bands of 6.3-kb plasmid still appeared (**Fig 7.2**).

Each *Dpn*I-digested PCR product was then transformed into *E. coli* JM109 cells (**Method 4.5**). 10-20 transformants from each mutant were screened for the presence of the mutant plasmids. After treated with an appropriate restriction endonuclease, the digested DNA fragments of the mutant plasmids could be clearly distinguished from those of the template plasmid as shown in **Fig. 7.3A-7.6A.**

The tentative mutant clones that showed correct restriction patterns were further verified of their mutated region by automated DNA sequencing (**Method 4.8**). The DNA sequencing results revealed that all of the mutant clones showed nucleotide changes at the desired positions (**Fig. 7.3B-7.6B**).

7.3 Expression of the β10-β11 loop mutant toxins

When all the verified mutant plasmids (pR203Q/D454A, pR203Q/D454E, pR203Q/D454R and pR203Q/D454K) under control of the *LacZ* promoter were expressed in *E.coli* JM109 cells upon IPTG induction (**Method 4.9**). Crude lysates *E. coli* cells (0.1 OD_{600}) expressing each mutant toxin were analysed for protein expression levels on SDS-PAGE (12.5% gel) in comparison with the crude lysates of the cells expressing the R203Q template. As shown in **Figure 7.7**, all the loop mutant clones were expressed as 130-kDa protoxin with levels similar to that of the R203Q template.

7.4 Solubilisation and proteolytic processing of the β10-β11 loop mutant toxins

Experiments were further carried out to assess the solubility of the mutant inclusions in comparison with the R203Q template and the Cry4Ba wild-type protein. The toxin inclusions of all mutants (R203Q/D454A, R203Q/D454E, R203Q/D454R and R203Q/D454K) were solubilized in carbonate buffer, pH 9.0 (**Method 4.13**). As can be seen that all the 130-kDa mutant protoxins showed the same solubility as the R203Q template and the Cry4Ba wild-type protein (**Fig. 7.8 to 7.9**).

As previously demonstrated, the 130-kDa R203Q mutant toxin was cleaved by trypsin into ca. 65-kDa fragment [5, 72]. All mutants were also examined for their proteolytic stability by digestion with TPCK-treated trypsin and were found to produce trypsin-resistant fragment of ca. 65 kDa similar to the R203Q template protoxin (**Fig. 7.10**).

7.5 Mosquito-larvicidal activity of the β10-β11 loop mutant toxins

To determine mutational effects on toxicity, *E.coli* cells expressing each mutant toxin and protoxin inclusion were tested for their relative biological activity against *Cu. quinquefasciatus* mosquito larvae. The percentage of dead larvae recorded after 24-hr incubation at room temperature is shown in **Fig. 7.11**. It was found that R203Q/D454R and R203Q/D454K showed ~50% toxicity which is higher than that of the wild-type Cry4Ba toxin (~ 16%) whereas R203Q/D454E showed the same larvicidal activity as that of the wild type Cry4Ba toxin. The 50% lethal concentration (**Table 7.1**) revealed that R203Q/D454R and R203Q/D454K mutations resulted in more than five-time increase in toxicity when compared with the wild-type Cry4Ba toxin.

7.6 Purification of the β10-β11 loop mutant toxins

After solubilisation and trypsin digestion in 50 nM Na_2CO_3 (pH 9.0), the 65-kDa activated Cry4Aa wild-type, Cry4Ba wild type and Cry4Ba mutant toxins (R203Q, R203Q/D454A, R203Q/D454E, R203Q/D454R and R203Q/D454K) were subjected to size-exclusion FPLC (superpose 12 GL 10/300 column), which was equilibrated with carbonated buffer (pH 9.0). It was found that purified activated toxins (65-kDa) were eluted as a peak at the time of 25 minutes (indicated by arrow in **Fig. 7.12A to 7.18A**). These peak fractions were then analysed on SDS-PAGE (**Fig. 7.12B to 7.18B**) and used for further experiment.

7.7 Binding activity of the β10-β11 loop mutant toxins

In vitro binding assay was performed by using *Cu. quinquefasciatus* sections based on the method of immunohistochemistry (**Method 4.16.1**). Cry4Aa, Cry4Ba, R203Q, R203Q/D454A, R203Q/D454E, R203Q/D454R and R203Q/D454K were selected to examine for their binding activity. Rabbit anti 4B-R203Q and Rabbit anti 4A-R235Q, that specifically recognise the Cry4Ba and Cry4Aa, respectively, were used in the binding assay. The immunohistochemical staining revealed that the purified R203Q/D454R and R203Q/D454K showed a higher signal intensity of the dark brown color products of 3, 3'-diaminobenzidine substrate detected on the apical region of the midgut epitherial cell sections when compared to the purified Cry4Ba toxin. But R203Q/D454E showed a slightly reduction in signal intensity of dark brown color. No signal of the dark brown products was observed when a midgut section is incubated with antibody conjugation in the control reaction (**Fig. 7.19**).

In vivo binding assay was performed by using *Cu. quinquefasciatus* sections according the method of immunohistochemistry (**Method 4.16.2**). The Cry4Aa, Cry4Ba, R203Q, R203Q/D454A, R203Q/D454E, R203Q/D454R and R203Q/D454K were selected to examine for their binding activity. Similar to the result from *in vitro* binding assay, a higher intensity of the dark brown was observed for R203Q/D454R and R203Q/D454K while R203Q/D454E showed a slightly reduction in signal intensity when compared to the Cry4Ba wild type (**Fig. 7.20**).

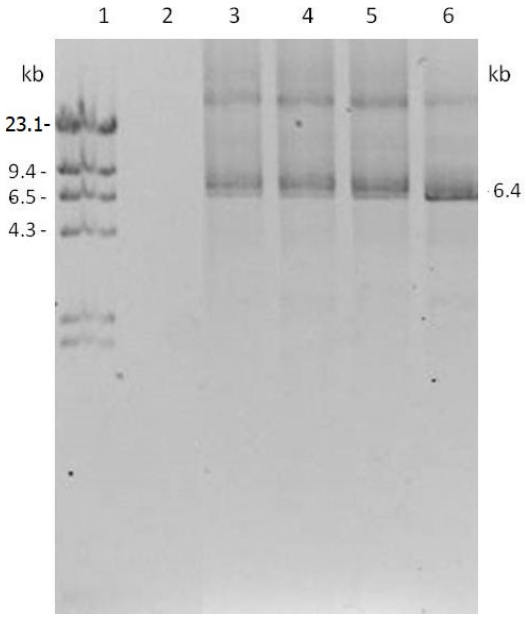

Figure 7.1: PCR amplification of Cry4Ba mutant plasmids: pR203Q/D454A, pR203Q/D454E, pR203Q/D454R and pR203Q/D454K

Lane 1: *Hind*III-digested λ DNA markers
Lane 2: the PCR product of negative control
Lane 3: the PCR product of the pR203Q/D454A plasmid
Lane 4: the PCR product of the pR203Q/D454E plasmid
Lane 5: the PCR product of the pR203Q/D454R plasmid
Lane 6: the PCR product of the pR203Q/D454K plasmid

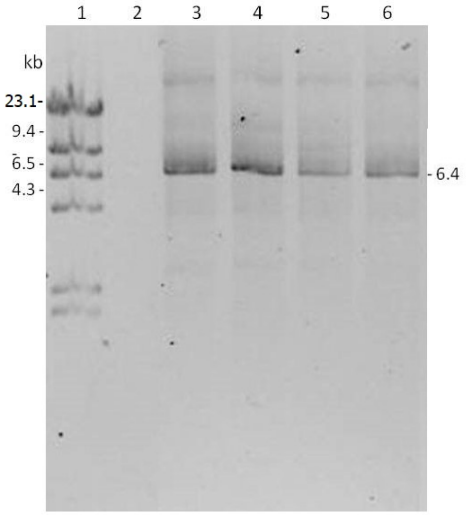

Figure 7.2: *Dpn*I digestion of the PCR products of Cry4Ba mutant plasmids: pR203Q/D454A, pR203Q/D454E, pR203Q/D454R and pR203Q/D454K

Lane 1: *Hind*III-digested λ DNA markers
Lane 2: The *Dpn*I-digested PCR product of negative control
Lane 3: The *Dpn*I-digested PCR product of the pR203Q/D454A plasmid
Lane 4: The *Dpn*I-digested PCR product of the pR203Q/D454E plasmid
Lane 5: The *Dpn*I-digested PCR product of the pR203Q/D454R plasmid
Lane 6: The *Dpn*I-digested PCR product of the pR203Q/D454K plasmid

(A) **(B)**

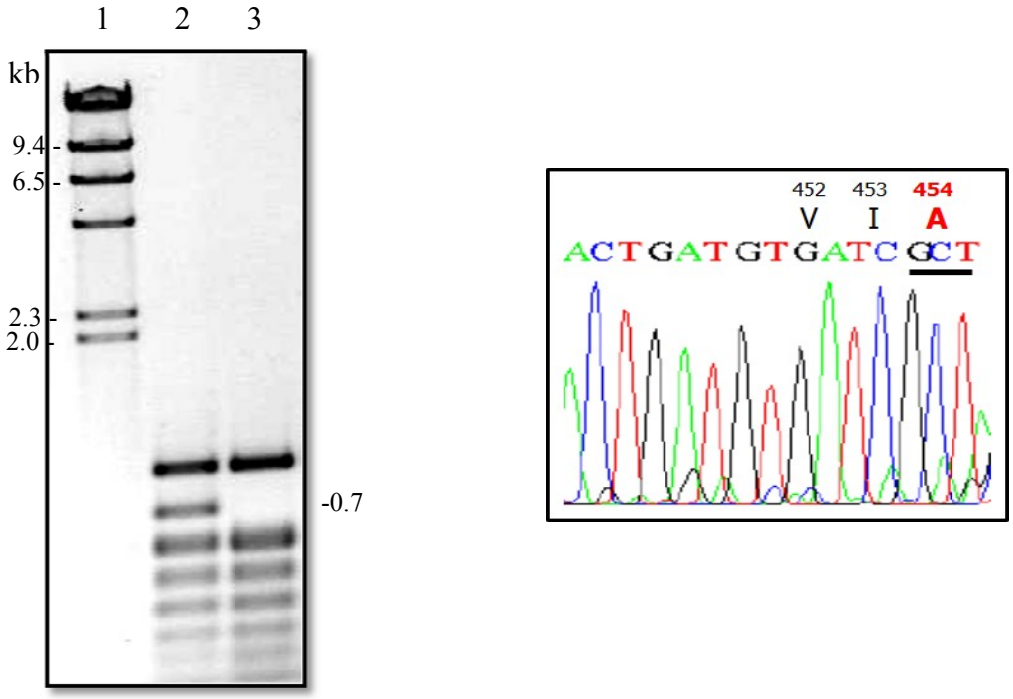

Figure 7.3: Restriction endonuclease and DNA sequence analysis of pR203Q/D454A

(A) 1.2% agarose gel electrophoresis (ethidium bromide-stained) of *Dpn*I digestion patterns of the template and mutated plasmids.

Lane 1: *Hind*III-digested λ DNA markers

Lane 2: The *Dpn*I digested template, R203Q

Lane 3: The *Dpn*I digested mutant plasmid, pR203Q/D454A

(B) DNA sequencing chromatogram of pR203Q/D454A, using Y266A-f as a sequencing primer. Part of the sense strand sequence is shown. Underlined letters indicate mutated nucleotide residues.

(A) **(B)**

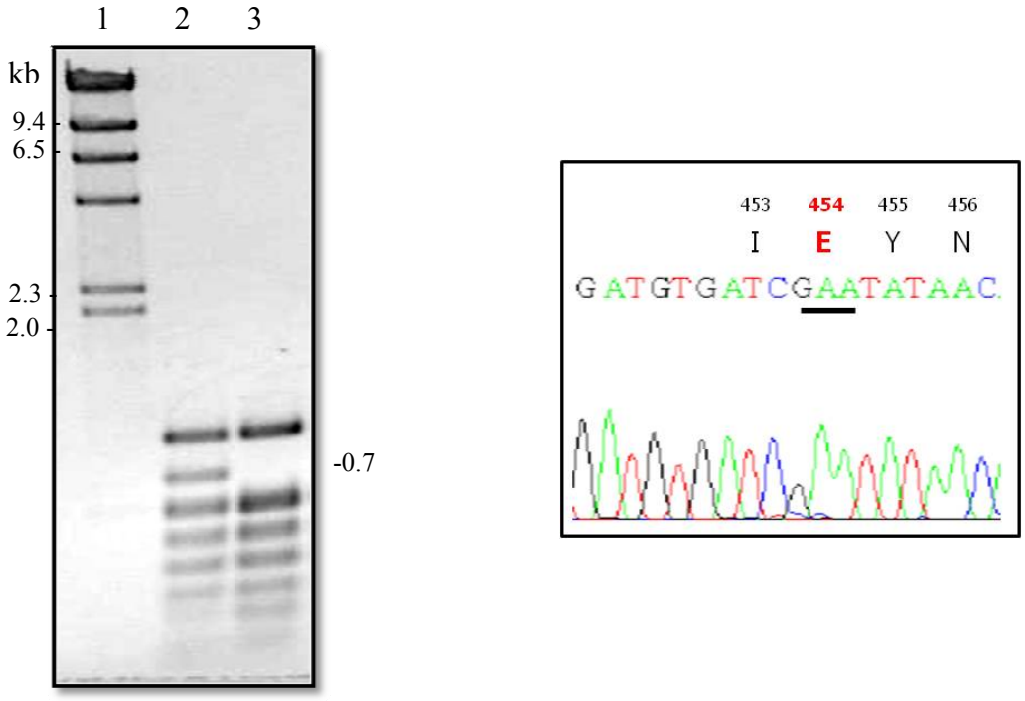

Figure 7.4: Restriction endonuclease and DNA sequence analysis of pR203Q/D454E

(A) 1.2% agarose gel electrophoresis (ethidium bromide-stained) of *Dpn*I digestion patterns of the template and mutated plasmids.

Lane 1: *Hind*III-digested λ DNA markers

Lane 2: The *Dpn*I digested template, R203Q

Lane 3: The *Dpn*I digested mutant plasmid, pR203Q/D454E

(B) DNA sequencing chromatogram of pR203Q/D454E, using Y266A-f as a sequencing primer. Part of the sense strand sequence is shown. Underlined letters indicate mutated nucleotide residues.

(A) **(B)**

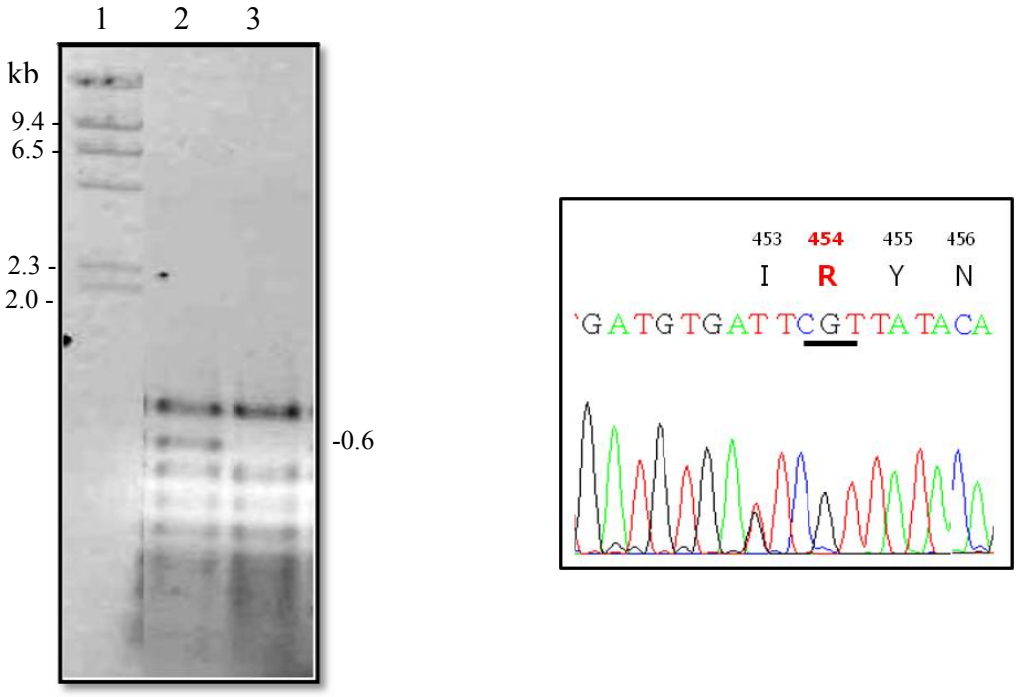

Figure 7.5: Restriction endonuclease and DNA sequence analysis of pR203Q/D454R

(A) 1.2% agarose gel electrophoresis (ethidium bromide-stained) of *Hinf*I digestion patterns of the template and mutated plasmids.

Lane 1: *Hind*III-digested λ DNA markers

Lane 2: The *Hinf*I digested template, R203Q

Lane 3: The *Hinf*I digested mutant plasmid, pR203Q/D454R

(B) DNA sequencing chromatogram of pR203Q/D454R, using Y266A-f as a sequencing primer. Part of the sense strand sequence is shown. Underlined letters indicate mutated nucleotide residues.

(A) **(B)**

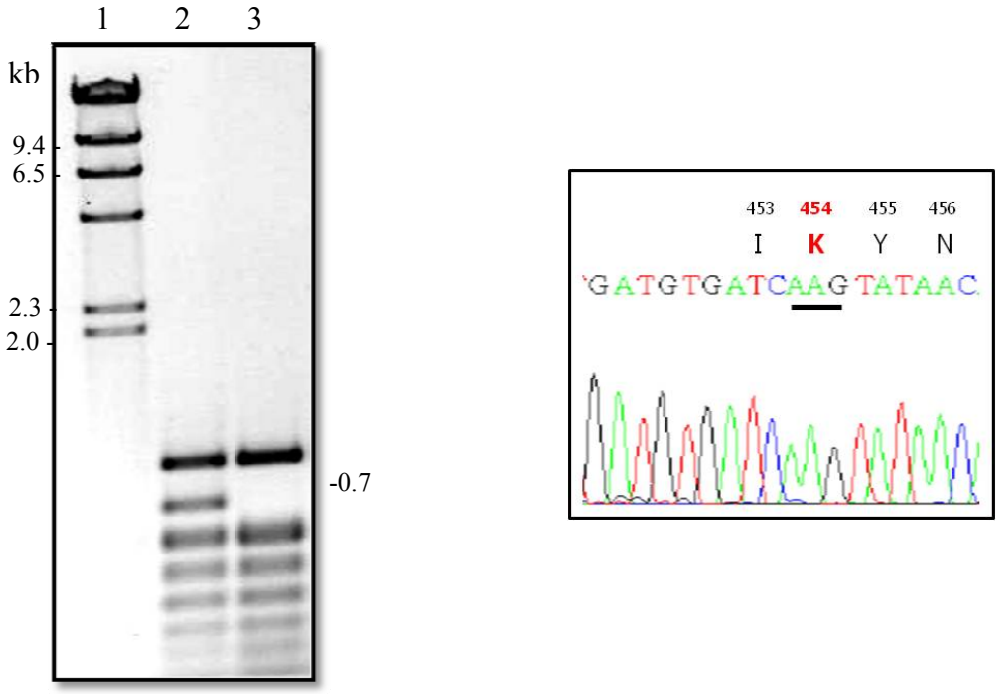

Figure 7.6: Restriction endonuclease and DNA sequence analysis of pR203Q/D454R

(A) 1.2% agarose gel electrophoresis (ethidium bromide-stained) of *Dpn*I digestion patterns of the template and mutated plasmids.

Lane 1: *Hind*III-digested λ DNA markers

Lane 2: The *Dpn*I digested template, R203Q

Lane 3: The *Dpn*I digested mutant plasmid, pR203Q/D454K

(B) DNA sequencing chromatogram of pR203Q/D454K, using Y266A-f as a sequencing primer. Part of the sense strand sequence is shown. Underlined letters indicate mutated nucleotide residues.

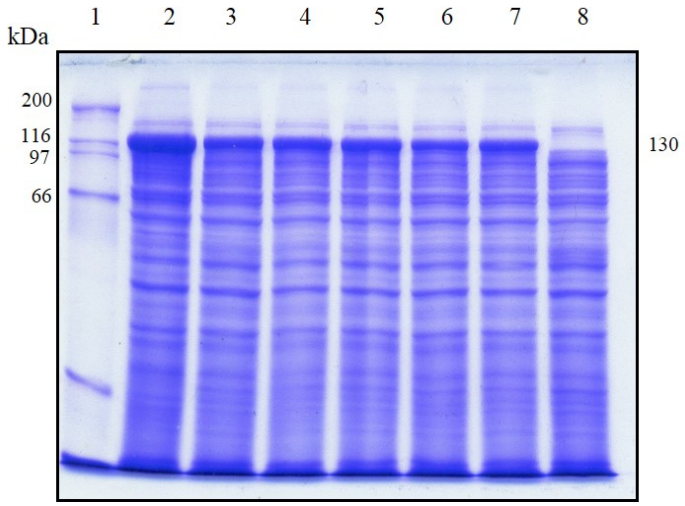

Figure 7.7: Expression of Cry4Ba and its mutants: R203Q, R203Q/D454A, R203Q/D454E, R203Q/D454R and R203Q/D454K

Lane 1: standard protein marker

Lane 2: crude lysates of *E. coli* cells containing pMU388 (the Cry4Ba wild type)

Lane 3: crude lysates of *E. coli* cells containing plasmid, pR203Q

Lane 4: crude lysates of *E. coli* cells containing pR203Q/D454A plasmid

Lane 5: crude lysates of *E. coli* cells containing pR203Q/D454E plasmid

Lane 6: crude lysates of *E. coli* cells containing pR203Q/D454R plasmid

Lane 7: crude lysates of *E. coli* cells containing pR203Q/D454K plasmid

Lane 8: crude lysates of *E. coli* cells containing pUC12 (negative control)

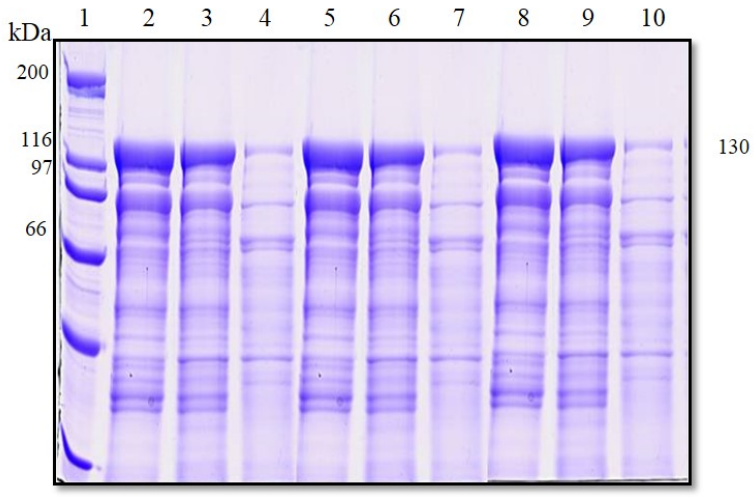

Figure 7.8: Solubility of Cry4Ba and its mutants: R203Q/D454A and R203Q/D454E

The figure shows coomassie brilliant blue-stained SDS-PAGE (12.5% gel) comparing the solubility of the wild type and its double mutant inclusions in 50 mM Na_2CO_3 (pH 9.0).

Lane 1: Standard protein marker

Lanes 2-4: Total, soluble and pellet fraction of pMU388, respectively

Lanes 5-7: Total, soluble and pellet fraction of R203Q/D454A, respectively

Lanes 8-10: Total, soluble and pellet fraction of R203Q/D454E, respectively

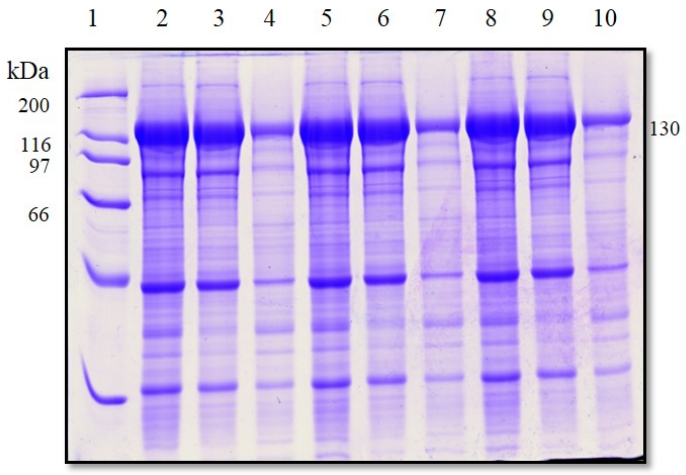

Figure 7.9: Solubility of Cry4Ba and its mutants: R203Q/D454R and R203Q/ D454K

The figure shows coomassie brilliant blue-stained SDS-PAGE (12% gel) comparing the solubility of the wild type and its mutant inclusions in 50 mM Na_2CO_3 (pH 9.0).

Lane 1: standard protein marker

Lanes 2-4: total, soluble and pellet fraction of pMU388, respectively

Lanes 5-7: total, soluble and pellet fraction of R203Q/D454R, respectively

Lanes 8-10: total, soluble and pellet fraction of R203Q/D454K, respectively

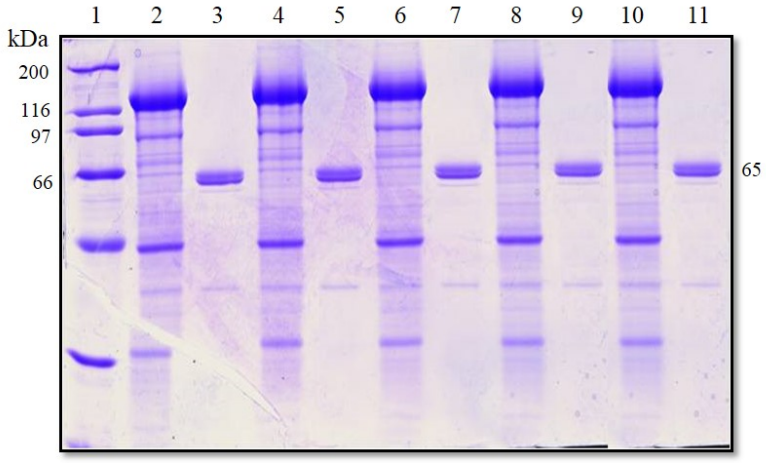

Figure7.10: Proteolytic processing of R203Q, R203Q/D454A, R203Q/D454E, R203Q/D454R and R203Q/D454K

The figure shows coomassie brilliant blue-stained SDS-PAGE (15% gel) comparing trypsin digested products of wild type and its mutant toxins. The major expected bands of ca. 65 kDa are indicated with the bold labels.

Lane 1: standard protein marker

Lanes 2-3: solubilised and trypsin-treated products of R203Q template, respectively

Lanes 4-5: solubilised and trypsin-treated products of R203Q/D454A, respectively

Lanes 6-7: solubilised and trypsin-treated products of R203Q/D454E, respectively

Lanes 8-9: solubilised and trypsin-treated products of R203Q/D454R, respectively

Lanes 10-11: solubilised and trypsin-treated products of R203Q/D454K, respectively

	%Mortality(n=3)						
	pMU388	R203Q	R203Q/ D454A	R203Q/ D454E	R203Q/ D454R	R203Q/ D454K	pUC12
mean	16.3	16.7	21.0	11.0	52.7	53.3	0.7
SEM	0.9	1.2	1.2	1.0	0.3	2.3	0.3

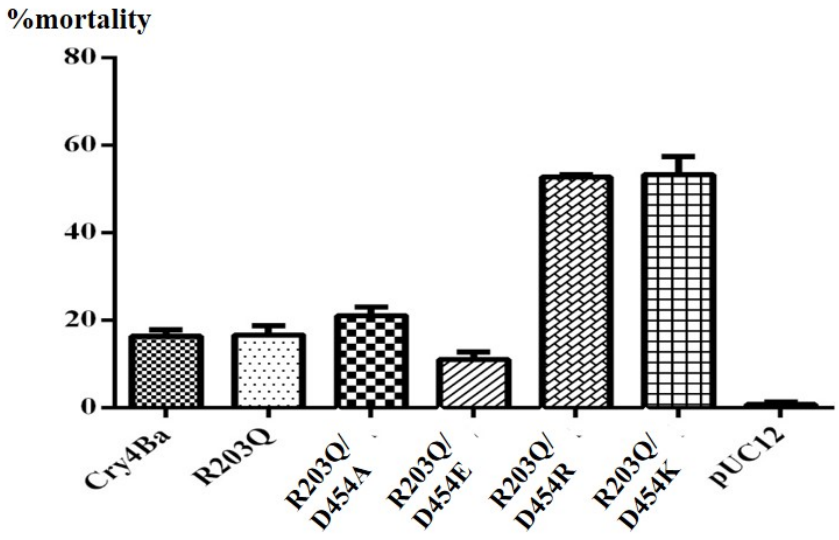

Figure 7.11: Larvicidal activity of *E. coli* cells containing the Cry4Ba, R203Q, R203Q/D454A, R203Q/D454E, R203Q/D454R and R203Q/D454K

The figure shows toxicity of *E. coli* cells containing each individual toxin. The control samples were *E. coli* cells containing the pMEx8 vector. Error bars represent standard error of the mean from three independent experiments.

Table 7.1: Mosquito larvicidal activities (LC50) of each individual partial purified proteins

Clones	LC50 (µg/ml)
Cry4Aa	0.02 (0.004-0.05)[a]
Cry4Ba	1.20 (1.1-4.8)
R203Q	0.80 (0.5-1.5)
R203Q/D454A	0.70 (0.4-1.3)
R203Q/D454E	≥50[b]
R203Q/D454R	0.10 (0.07-0.4)
R203Q/D454K	0.20 (0.07-0.3)

Cry4Aa, Cry4Ba wild-type and Cry4Ba mutant toxins (R203Q, R203Q/D454A, R203Q/D454E, R203Q/D454R and R203Q/D454K). LC50, 50% lethal, concentration. [a]The values in parentheses are 95% confidence limits. [b]The 95% confidence limits could not be determined.

(A) **(B)**

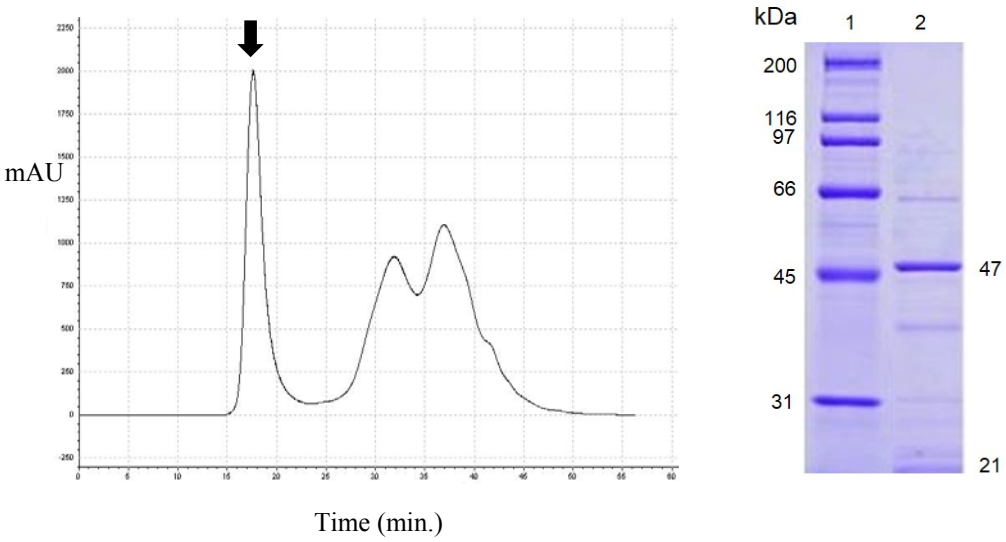

Figure 7.12: Chromatogram analysis of purified Cry4Aa toxin

(A) FPLC chromatogram from size-exclusion chromatography of purified Cry4Aa toxin. The peak corresponding to the purified 65-kDa Cry4Aa toxin is indicated.

(B) Coomassie brilliant blue-stained SDS-PAGE (15% gel) of the purified fraction of the Cry4Aa toxin.

Lane 1: Molecular mass standards

Lane 2: The purified fractions of ca. 47 and 21 kDa of Cry4Aa toxin

(A) **(B)**

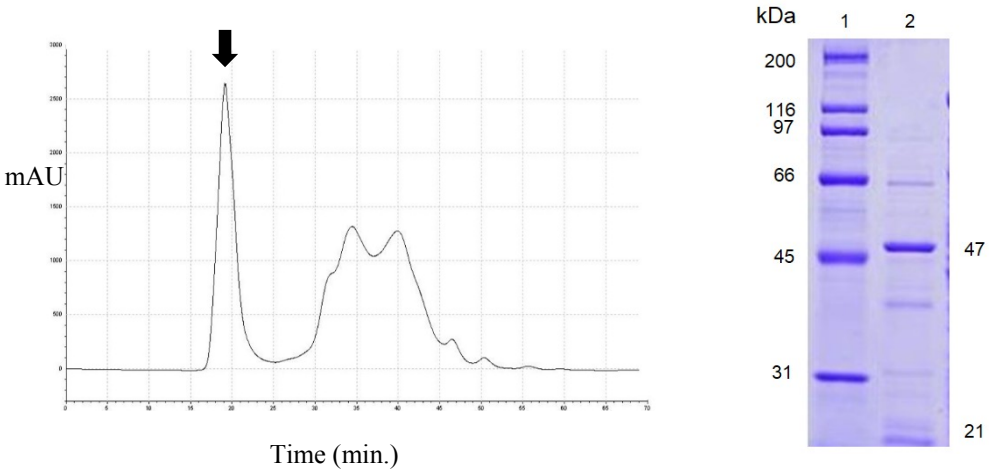

Figure 7.13: Chromatogram analysis of purified Cry4Ba toxin

(A) FPLC chromatogram from size-exclusion chromatography of purified Cry4Ba toxin. The peak corresponding to the purified 65-kDa Cry4Ba toxin is indicated

(B) Coomassie brilliant blue-stained SDS-PAGE (15% gel) of the purified fraction of the Cry4Ba toxin.

Lane 1: Molecular mass standards

Lane 2: The purified fractions of the ca. 47 and 21 kDa of Cry4Ba toxin

(A) **(B)**

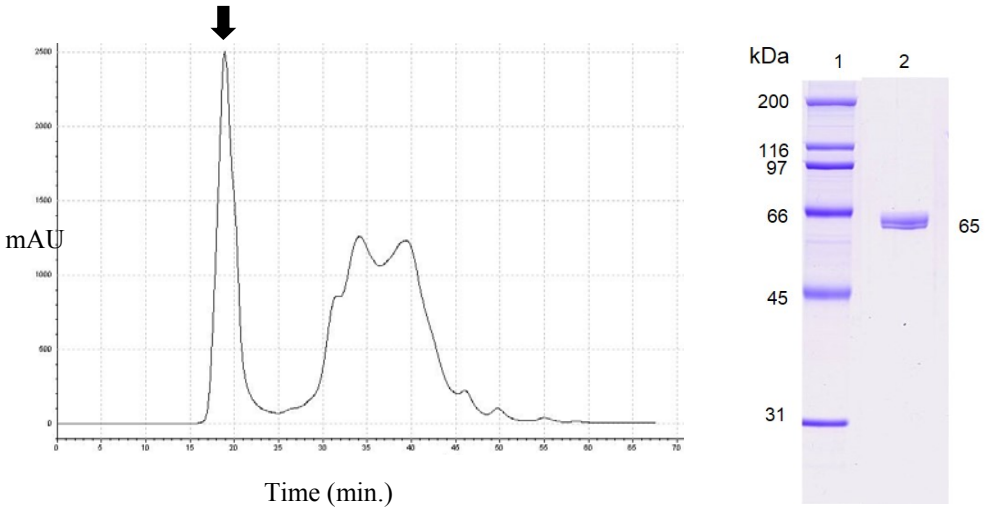

Figure 7.14: Chromatogram analysis of purified R203Q mutant toxin

(A) FPLC chromatogram from size-exclusion chromatography of purified R203Q mutant toxin. The peak corresponding to the purified 65-kDa R203Q mutant toxin is indicated.

(B) Coomassie brilliant blue -stained SDS-PAGE (15% gel) of the purified fraction of D454E mutant toxin

Lane 1: Molecular mass standards

Lane 2: The purified fraction of 65 kDa of R203Q mutant toxin

(A) **(B)**

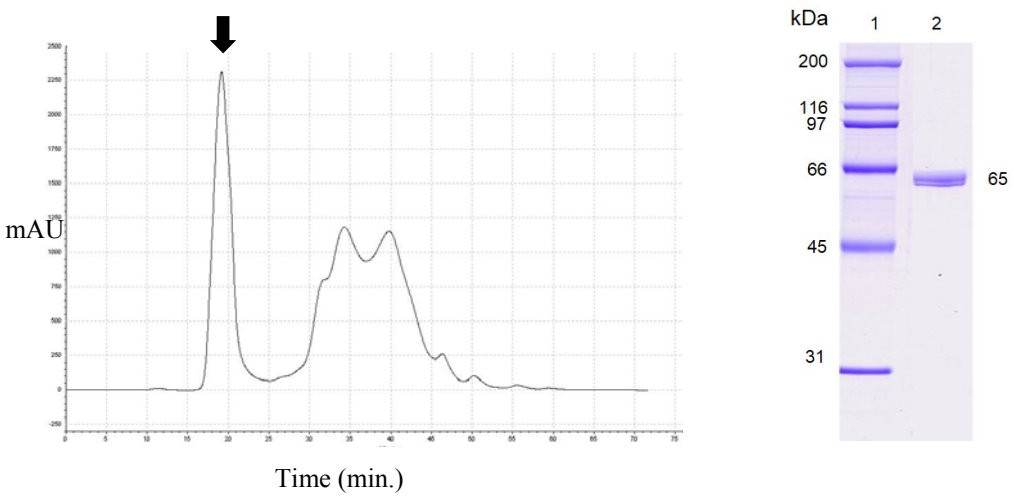

Figure 7.15: Chromatogram analysis of purified R203Q/D454A mutant toxin

(A) FPLC chromatogram from size-exclusion chromatography of purified R203Q/D454A mutant toxin. The peak corresponding to the purified 65-kDa R203Q/D454A mutant toxin is indicated.

(B) Coomassie brilliant blue-stained SDS-PAGE (15% gel) of the purified fraction of R203Q/D454A mutant toxin.

Lane 1: Molecular mass standards

Lane 2: The purified fraction of 65 kDa of R203Q/D454A mutant toxin

(A) **(B)**

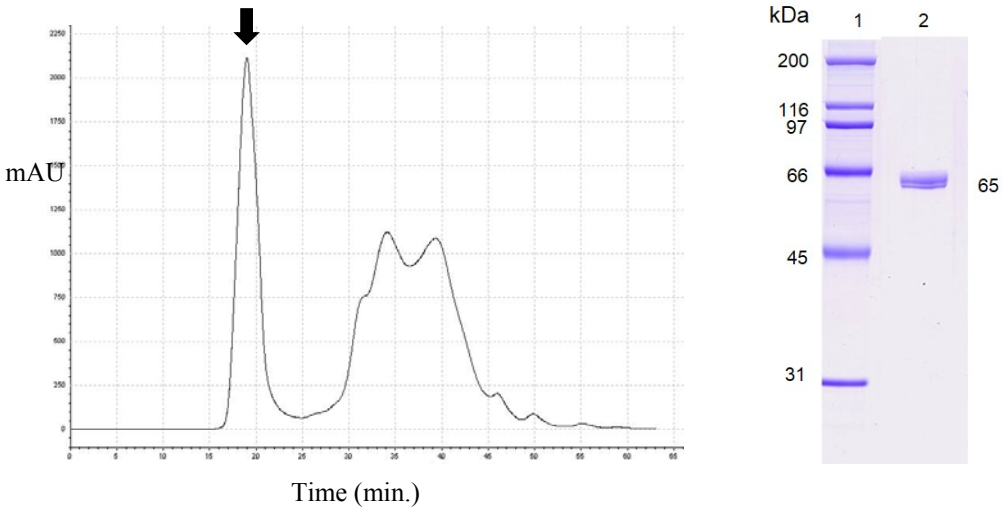

Figure 7.16: Chromatogram analysis of purified R203Q/D454E mutant toxin

(A) FPLC chromatogram from size-exclusion chromatography of purified R203Q/D454E mutant toxin. The peak corresponding to the purified 65-kDa R203Q/D454E mutant toxin is indicated.

(B) Coomassie brilliant blue-stained SDS-PAGE (15% gel) of the purified fraction of R203Q/D454E mutant toxin

Lane 1: Molecular mass standards

Lane 2: The purified fraction of 65 kDa of R203Q/D454E mutant toxin

(A) **(B)**

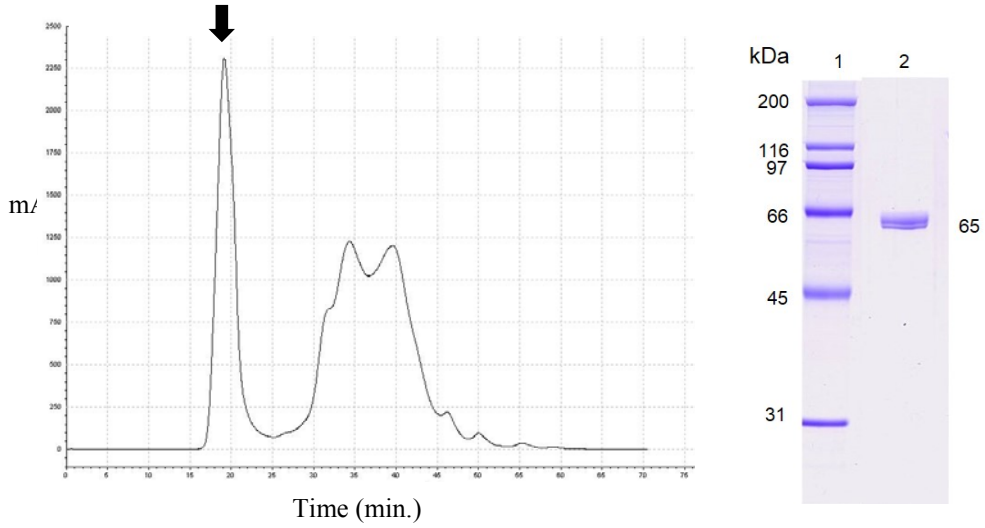

Figure 7.17: Chromatogram analysis of purified R203Q/D454R mutant toxin

(A) FPLC chromatogram from size-exclusion chromatography of purified R203Q/D454R mutant toxin. The peak corresponding to the purified 65-kDa R203Q/D454R mutant toxin is indicated

(B) Coomassie brilliant blue-stained SDS-PAGE (15% gel) of the purified fraction of R203Q/D454R mutant toxin

Lane 1: Molecular mass standards

Lane 2: The purified fraction of 65 kDa of R203Q/D454R mutant toxin

(A) **(B)**

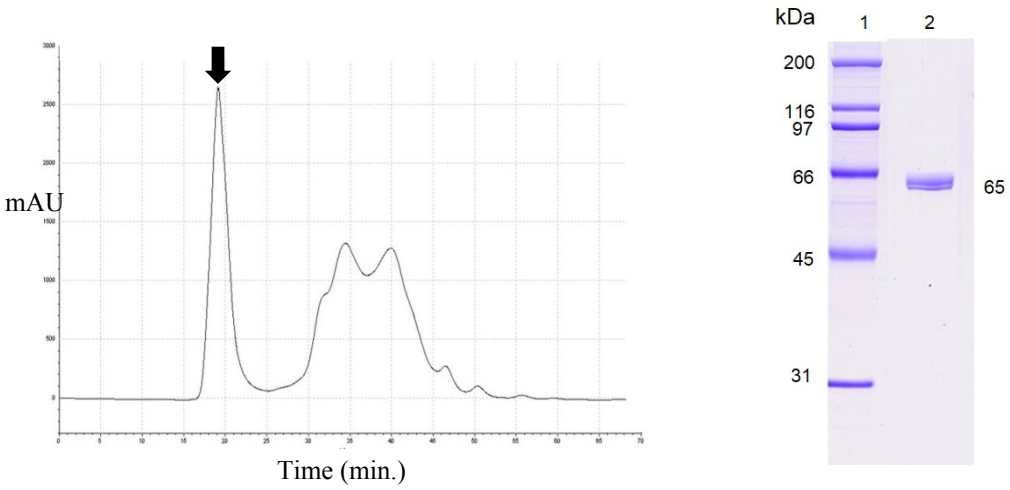

Figure 7.18: Chromatogram analysis of purified R203Q/D454K mutant toxin

A) FPLC chromatogram from size-exclusion chromatography of purified R203Q/D454K mutant toxin. The peak corresponding to the purified 65-kDa R203Q/D454K mutant toxin is indicated.

B) Coomassie brilliant blue-stained SDS-PAGE (15% gel) of the purified fraction of R203Q/D454K mutant toxin.

Lane 1: Molecular mass standards

Lane 2: The purified fraction of 65 kDa of R203Q/D454K mutant toxin

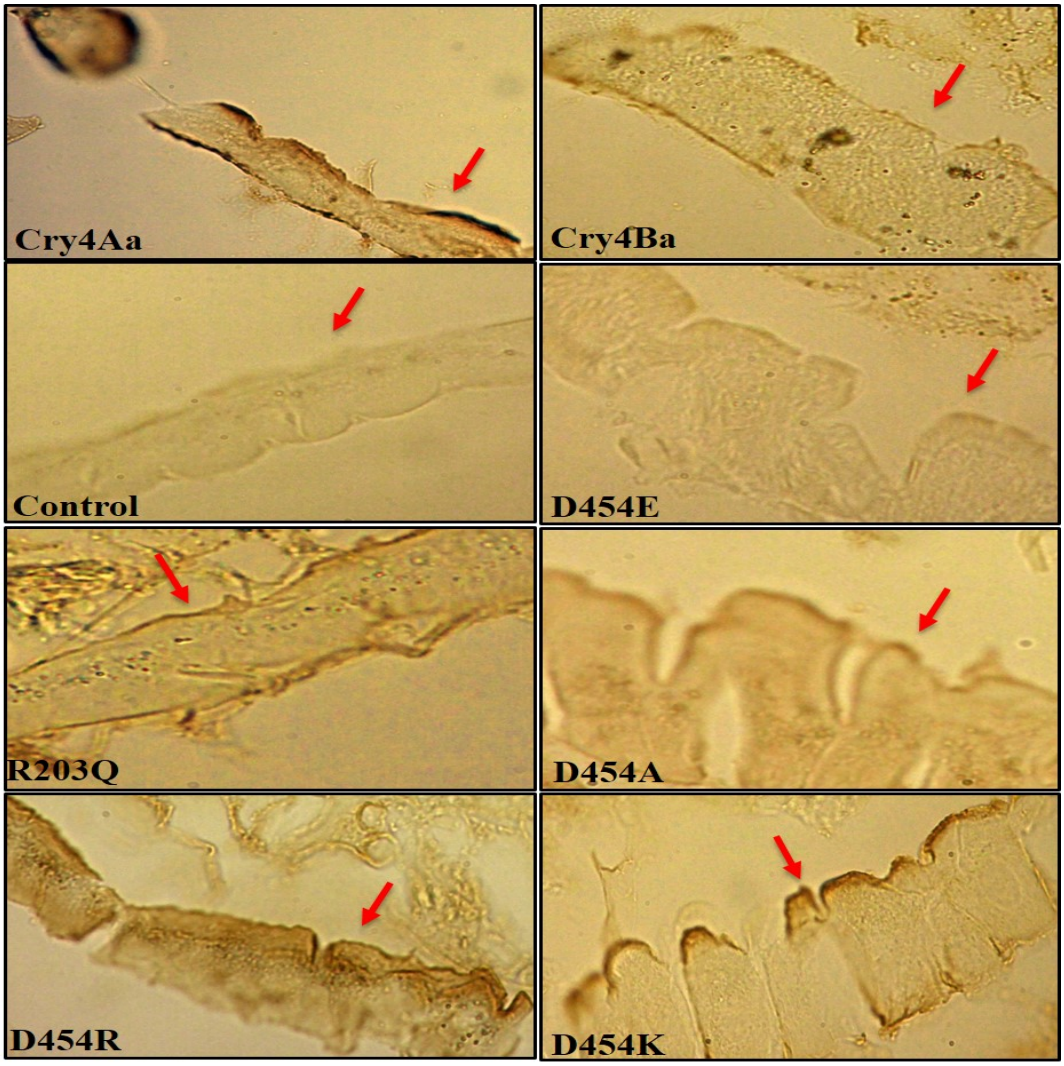

Figure 7.19: Immunohistochemical staining (overlay toxin) of the Cry4Aa, Cry4Ba and its mutant toxins

Arrows indicate bound toxins on larval section, showing brown color product of 3' 3-diaminobenzidine substrate.

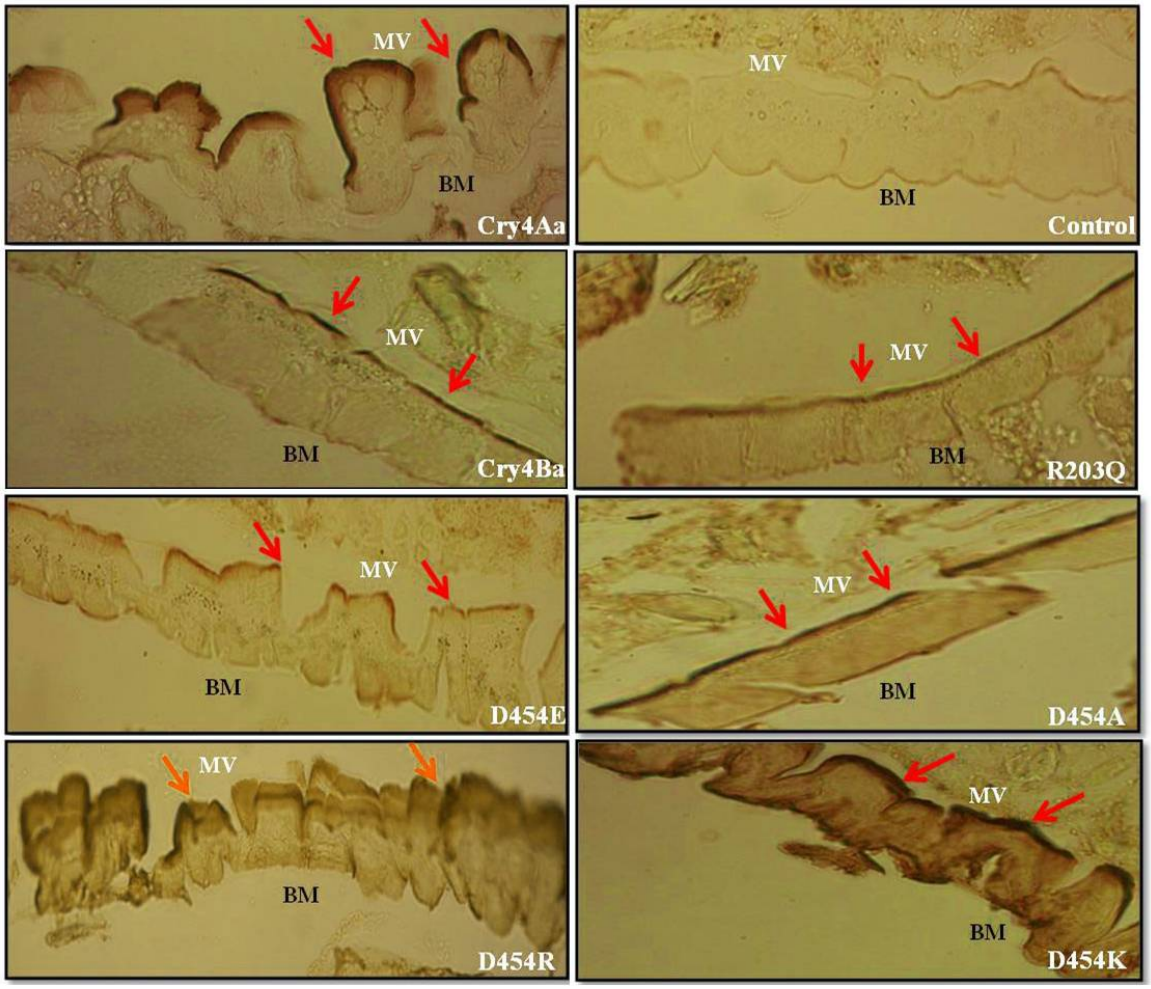

Figure 7.20: Immunohistochemical staining (feeding toxin to *Culex* sp. larvae) of the Cry4Aa, Cry4Ba and mutant toxins

Arrow indicate bound toxins on larval section, showing brown color product of 3' 3-diaminobenzidine substrate, BM; basement membrane and MV; microvilli.

CHAPTER VIII
DISCUSSION

Domain II, the most divergent part among the *Bt* Cry toxins, has been demostrated to be involved in the interaction with toxin binding sites in the midgut of the susceptible insect larvae. The interaction of domain II with the binding sites is thought to take place through the surface-exposed loops. It has been shown that mutagenesis of some residues localised in these loops leads to a reduction in binding of the toxin to their receptor and consequently, decrease in toxicity.

8.1 Involvement of the β6-β7 loop and β10-β11 loop residues of Cry4Aa toxin in toxicity

Selected residues Asp^{430}, Lys^{432}, Tyr^{433}, Asp^{436} and Tyr^{437} in the β6-β7 loop, (**Fig. 1.2**) and all residues (Pro^{510}, Thr^{512}, Tyr^{513}, Lys^{514} and Thr^{515}) in the β10-β11 loop (**Fig. 1.3**) were changed individually to alanine *via* PCR-based site-directed mutagenesis. As can be seen that, all the 130-kDa mutant protoxins were highly expressed in *E. coli* upon IPTG induction at levels similar to that of the Cry4Aa wild-type toxin (see **Fig. 5.8** and **6.8**) and showed same solubility in carbonate buffer (pH 9.0) and trypsin digestion patterns as the Cry4Aa wild type (see **Fig.5.9-5.10** and **Fig. 6.9-6.10**). This indicates that all mutants did not have an adverse effect on protein folding, as protein misfolding can lead to low level of protein expression due to proteolytic degradation [63].

The toxicity results showed that only Lys^{514} in the β10-β11 loop exhibited reduction of larvicidal activity to approximately 50% when compared with Cry4Aa wild-type toxin (**Fig. 6.11**). This result suggested that positively charged residue at position 514 plays a critical role in larvicidal activity of the Cry4Aa toxin. The positively charged residue at position 514 which is at the apex of the β10-β11 loop

might interact with a receptor on the larval gut epithelial cells *via* electrostatic interactions.

8.2 Involvement in toxicity of charged residue in the β10-β11 loop of Cry4Ba toxin

Previously, Tuntitippawan *et. al.* [6] showed that Asp^{454} at the apex of the β10-β11 loop of Cry4Ba toxin is not involved in toxicity against *Aedes* larvae. However, it was shown that replacement of this D^{454} with a variety of tripeptides can raise toxicity against *Culex* larvae [10]. In the present study, the role of Asp^{454} was examined by amino acid substitutions. Mutagenic analysis was performed *via* PCR-based site-directed mutagenesis. Asp^{454} was investigated for functional importance of its charged side chain by replacing with Ala (nonpolar residue), Glu (negatively charged residue), Arg (positively charged residue) and Lys (positively charged residue), using the Cry4Ba-R203Q mutant as template. Upon IPTG induction, the recombinant *E. coli* cells highly produced mutant toxins as inclusion bodies at level comparable with that of the wild-type toxin (see **Fig. 7.7**). All the mutants showed same solubility in carbonate buffer (pH 9.0) and trypsin digestion pattern as the R203Q template (see **Fig. 7.8-7.10**).

Upon mosquito larvicidal assay revealed that D454E mutant which maintains the negative charge of the Cry4Ba β10-β11 loop preserved the low *Culex* toxicity of the Cry4Ba wild-type toxin. Interestingly, D454R and D454K mutations resulted in a more than three time increase in *Culex* toxicity (**Fig. 7.11** and **Table 7.1**). As domain II surface exposed loops, including β10-β11 loop, were widely shown to be involved in Cry toxin-receptor binding. The substantial enhancement of Cry4Ba toxicity against *Culex* larvae due to such negative-to-positive substitutions suggested a requirement of a positive charge for toxin interactions with *Culex* receptors.

As mention earlier, the Cry4Aa toxin is highly toxic against *Culex* larvae while its closely related Cry4Ba toxin is inactive to such larvae. Consistent with their larvicidal activity, *in vitro* and *in vivo* binding analysis *via* immunohistochemical assay revealed that Cry4Aa toxin, but not Cry4Ba toxin, bound strongly to apical

brush border of the posterior midgut section of *Culex* larvae (**Fig. 7.19-7.20**). Similar to the *Culex*-active Cry4Aa toxin, only D454R and D454K mutant toxins whose *Culex* toxicity is significantly higher than that of the Cry4Ba wild type were found to interact potently with the *Culex* gut membrane, confirming an involvement of the positive charge at the Cry4Ba β10-β11 loop in toxin binding to *Culex* receptors. Although it was previously suggested that the length of the β10-β11 loop is an essential determinant for specificity [11], introduction of *Culex* toxicity to Cry4Ba *via* charge-inverting mutation in such loop indicated an involvement of charge in specificity. According to our result, the positive charge at the β10-β11 loop of both Cry4Ba and Cry4Aa toxin is likely a determinant of toxin-*Culex* receptor binding. A similar result was observed in GluA2 (a ligand-gated ionotropicglutamate receptor) when a charge-reversal mutation (R628E) cause an increase in affinity to its agonist [73]. Also, a study of aminoacyl-tRNA synthetase *via* a charge-swapping substitution (K279E) and calculation of free energy binding indicated that the positive charge of Lys^{279} is necessary for tRNA binding [74]. Interestingly, crystal structure of R47E (a mutant of cytochrome P450 BM-3) revealed that an adverse effect of such mutation on the protein binding to *N*-palmitoylglycine is likely related to a charge repulsion [75]. Altogether, it is possible that interaction of both Cry4Ba and Cry4Aa toxins with *Culex* receptor conceivably occur *via* ionic interaction when binding site on the toxins is positive and binding region on the *Culex* receptor is negative.

In conclusion, our data provide the first evidence that positively charged residue in the β10-β11 loop of two closely related toxins, Cry4Ba and Cry4Aa (**Fig. 8.1**), is essential for toxicity against *Culex* larvae. Furthermore, the positive charge at such loop of both toxins was suggested to be a critical determinant of toxin interaction with specific receptor located on *Culex* larval gut membrane. Further experiment, Tyr^{455} and Asn^{456} in domain II of Cry4Ba toxin were substituted with positively charged and Lys^{514} in domain II of Cry4Aa toxin was changed to negatively charged to check an involvement of charge residue in receptor binding interacton.

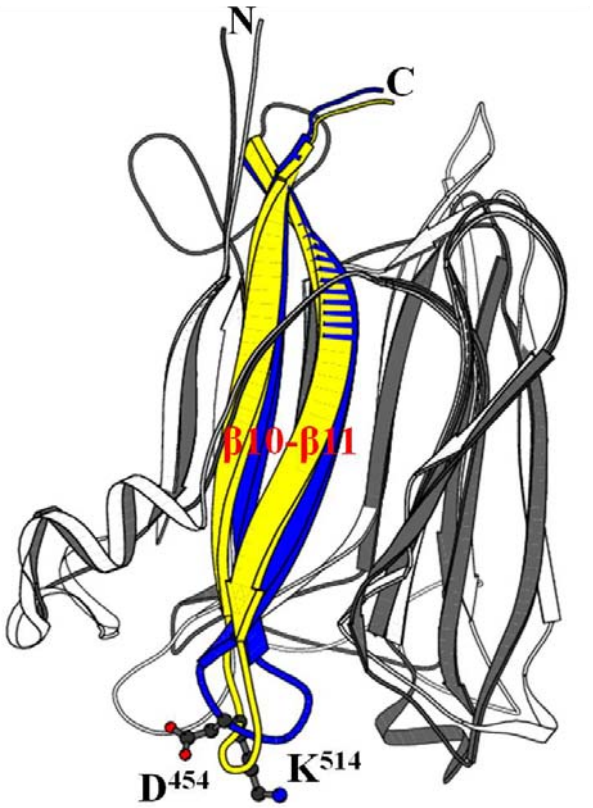

Figure 8.1: Superimposed domain II of Cry4Aa and Cry4Ba crystal structures

Cry4Aa is shown in yellow/white and Cry4Ba is show in blue/black colors. Loop charged residues (Asp^{454} of Cry4Ba and Lys^{514} of Cry4Aa) are shown in ball-and-stick representation.

CHAPTER IX
CONCLUSIONS

1. Selected Cry4Aa-loop residues (Asp^{430}, Lys^{432}, Tyr^{433}, Asp^{436} and Tyr^{437} in β6-β7 loop; Pro^{510}, Thr^{512}, Tyr^{513}, Lys^{514} and Thr^{515} in the β10-β11 loop) were changed to alanine by using PCR-based mutagenesis. All β6-β7 and β10-β11 loop-mutants were highly expressed as130 kDa protoxin in *E. coli* JM109 cells with yield similar to Cry4Aa wild-type toxin. In addition, all mutant protoxins were highly solubilised in 50 mM $NaCO_3$ (pH 9.0) and gave the products of 47 and 21 kDa upon trypsin digestion similar to Cry4Aa wild-type toxin. The bioassays showed that only alanine substitution of Lys^{514} in the β10-β11 loop reduced toxicity against *C. quinquefasciatus* larvae, sugeesting that positively charged in position 514 involved in Cry4Aa toxicity against *C. quinquefasciatus* larvae.

2. Amino acid substitution of Asp^{454} within the β10-β11 loop in domain II of the Cry4Ba toxin by using R203Q as a template were performed to investigate whether a charge-charge interaction is important for larvicidal toxicity. Bioassays revealed that replacement of Asp^{454} with positively charged residue, Arg or Lys, caused a significant increase in toxicity of Cry4Ba toxin against *C. quinquefasciatus* larvae, suggesting that the positive charge in the Cry4Ba- β10-β11 loop is essentially involved in toxin binding to *Culex* receptors.

REFERENCES

1.Federici, B.A., et al., Recombinant bacteria for mosquito control. J Exp Biol, 2003. 206(21): p. 3877-85.

2.Crickmore, N., et al., Revision of the nomenclature for the *Bacillus thuringiensis* pesticidal crystal proteins. Microbiol Mol Biol Rev, 1998. 62(3): p. 807-13.

3.Schnepf, E., et al., *Bacillus thuringiensis* and its pesticidal crystal proteins. Microbiol Mol Biol Rev, 1998. 62(3): p. 775-806.

4.Angsuthanasombat, C., et al., *Bacillus thuringiensis* Cry4A and Cry4B mosquito-larvicidal proteins: homology-based 3D model and implications for toxin activity. J Biochem Mol Biol, 2004. 37(3): p. 304-13.

5.Angsuthanasombat, C., N. Crickmore, and D.J. Ellar, Effects on toxicity of eliminating a cleavage site in a predicted interhelical loop in *Bacillus thuringiensis* CryIVB delta-endotoxin. FEMS Microbiol Lett, 1993. 111(2-3): p. 255-61.

6.Tuntitippawan, T., et al., Targeted mutagenesis of loop residues in the receptor-binding domain of the *Bacillus thuringiensis* Cry4Ba toxin affects larvicidal activity. FEMS Microbiol Lett, 2005. 242(2): p. 325-32.

7.Khaokhiew, T., C. Angsuthanasombat, and C. Promptmas, Correlative effect on the toxicity of three surface-exposed loops in the receptor-binding domain of the *Bacillus thuringiensis* Cry4Ba toxin. FEMS Microbiol Lett, 2009. 300(1): p. 139-45.

8.Moonsom, S., et al., Binding characteristics to mosquito-larval midgut proteins of the cloned domain II-III fragment from the *Bacillus thuringiensis* Cry4Ba toxin. J Biochem Mol Biol, 2007. 40(5): p. 783-90.

9.Abdullah, M.A. and D.H. Dean, Enhancement of Cry19Aa mosquitocidal activity against *Aedes aegypti* by mutations in the putative loop regions of domain II. Appl Environ Microbiol, 2004. 70(6): p. 3769-71.

10.Abdullah, M.A., et al., Introduction of Culex toxicity into *Bacillus thuringiensis* Cry4Ba by protein engineering. Appl Environ Microbiol, 2003. 69(9): p. 5343-53.

11.Boonserm, P., et al., Structure of the functional form of the mosquito larvicidal Cry4Aa toxin from *Bacillus thuringiensis* at a 2.8-angstrom resolution. J Bacteriol, 2006. 188(9): p. 3391-401.

12.Boonserm, P., et al., Crystal structure of the mosquito-larvicidal toxin Cry4Ba and its biological implications. J Mol Biol, 2005. 348(2): p. 363-82.

13.Yamamoto, T. and R.E. McLaughlin, Isolation of a protein from the parasporal crystal of *Bacillus thuringiensis* var. *Kurstaki* toxic to the mosquito larva, *Aedes taeniorhynchus*. Biochem Biophys Res Commun, 1981. 103(2): p. 414-21.

14.Dai, S.M. and S.S. Gill, In vitro and in vivo proteolysis of the *Bacillus thuringiensis* subsp. *israelensis* CryIVD protein by *Culex quinquefasciatus* larval midgut proteases. Insect Biochem Mol Biol, 1993. 23(2): p. 273-83.

15.Herrnstadt, C., et al., Nucleotide sequence and deduced amino acid sequence of a coleopteran-active delta-endotoxin gene from *Bacillus thuringiensis* subsp. *san diego*. Gene, 1987. 57(1): p. 37-46.

16.Hofte, H. and H.R. Whiteley, Insecticidal crystal proteins of *Bacillus thuringiensis*. Microbiol Rev, 1989. 53(2): p. 242-55.

17.Goldberg LJ, M.J., A bacterial spore demonstrating rapid larvicidal activity against *Anopheles sergentii, Uranotaenia unguiculata, Culex univitattus, Aedes aegypti* and *Culex pipiens*. Mosquito News, 1977. 37: p. 355-358.

18.Grochulski, P., et al., *Bacillus thuringiensis* CryIA(a) insecticidal toxin: crystal structure and channel formation. J Mol Biol, 1995. 254(3): p. 447-64.

19.Morse, R.J., T. Yamamoto, and R.M. Stroud, Structure of Cry2Aa suggests an unexpected receptor binding epitope. Structure, 2001. 9(5): p. 409-17.

20.Li, J.D., J. Carroll, and D.J. Ellar, Crystal structure of insecticidal delta-endotoxin from *Bacillus thuringiensis* at 2.5 A° resolution. Nature, 1991. 353(63): p. 815-21.

21.Galitsky, N., et al., Structure of the insecticidal bacterial delta-endotoxin Cry3Bb1 of *Bacillus thuringiensis*. Acta Crystallogr D Biol Crystallogr, 2001. 57(8): p. 1101-9.

22.Guo, S., et al., Crystal structure of *Bacillus thuringiensis* Cry8Ea1: An insecticidal toxin toxic to underground pests, the larvae of *Holotrichia parallela*. J Struct Biol, 2009. 168(2): p. 259-66.

23.Gazit, E., et al., The alpha-5 segment of *Bacillus thuringiensis* delta-endotoxin: in vitro activity, ion channel formation and molecular modelling. Biochem J, 1994. 304 (Pt 3): p. 895-902.

24.Gazit, E., et al., The structure and organization within the membrane of the helices composing the pore-forming domain of *Bacillus thuringiensis* delta-endotoxin are consistent with an "umbrella-like" structure of the pore. Proc Natl Acad Sci USA, 1998. 95(21): p. 12289-94.

25.Chen, X.J., et al., Mutations in domain I of *Bacillus thuringiensis* delta-endotoxin CryIAb reduce the irreversible binding of toxin to manduca sexta brush border membrane vesicles. J Biol Chem, 1995. 270(11): p. 6412-9.

26.Wu, S.J., et al., Enhanced toxicity of *Bacillus thuringiensis* Cry3A delta-endotoxin in coleopterans by mutagenesis in a receptor binding loop. FEBS Lett, 2000. 473(2): p. 227-32.

27.Smith, G.P. and D.J. Ellar, Mutagenesis of two surface-exposed loops of the *Bacillus thuringiensis* CryIC delta-endotoxin affects insecticidal specificity. Biochem J, 1994. 302 (2): p. 611-6.

28.Lu, H., F. Rajamohan, and D.H. Dean, Identification of amino acid residues of *Bacillus thuringiensis* delta-endotoxin CryIAa associated with membrane binding and toxicity to *Bombyx mori*. J Bacteriol, 1994. 176(17): p. 5554-9.

29.Masson L, T.B., Mazza A, Prefortaine G, Potvin L, Rossea R and Schwartz JL. , Mutagenenic analysis of a conserved region of Domain III in the Cry1Ac toxin of *Bacillus thuringiensis*. Appl Environ Microbio 2002. 68(1): p. 194-200

30.Jenkins, J.L., et al., Bivalent sequential binding model of a *Bacillus thuringiensis* toxin to gypsy moth aminopeptidase N receptor. J Biol Chem, 2000. 275(19): p. 14423-31.

31.Burton, S.L., et al., N-acetylgalactosamine on the putative insect receptor aminopeptidase N is recognised by a site on the domain III lectin-like fold of a *Bacillus thuringiensis* insecticidal toxin. J Mol Biol, 1999. 287(5): p. 1011-22.

32.Poncet, S., A. Delecluse, A. Klier, and G. Rapoport, Evaluation of synergistic interactions among the CryIVA, CryIVB, and CryIVD toxic components of *Bacillus thuringiensis* subsp. *israelensis* crystals. J. Invertebr. Pathol., 1995. 66.

33.Parker, M.W., F. Pattus, A. D. Tucker, and D. Tsernoglou., Structure of the membrane-pore-forming fragment of colicin A. Nature, 1989. 337: p. 93-96.

34.Wallace, A.J., T. J. Stillman, A. Atkins, S. J. Jamieson, P. A. Bullough, J. Green, and P. J. Artymiuk, E. coli hemolysin E (HlyE, ClyA, SheA): X-ray crystal structure of the toxin and observation of membrane pores by electron microscopy. Cell, 2000. 100: p. 265-276.

35.Delecluse, A., et al., Expression of cryIVA and cryIVB genes, independently or in combination, in a crystal-negative strain of *Bacillus thuringiensis* subsp. *israelensis*. Appl Environ Microbiol, 1993. 59(11): p. 3922-7.

36.Boonserm, P., D.J. Ellar, and J. Li, Crystallization and preliminary X-ray diffraction studies of a mosquito-larvicidal toxin from *Bacillus thuringiensis* subsp. *israelensis*. Acta Crystallogr D Biol Crystallogr, 2003. 59(3): p. 591-4.

37.Chayaratanasin, P., et al., High level of soluble expression in *Escherichia coli* and characterisation of the cloned *Bacillus thuringiensis* Cry4Ba domain III fragment. J Biochem Mol Biol, 2007. 40(1): p. 58-64.

38.Gill SS, C.E.a.P.P., The mode of action of *Bacillus thuringiensis* endotoxins. Annu Rev Entomol, 1992. 37: p. 615-636.

39.Aronson, A.I., et al., The solubility of inclusion proteins from *Bacillus thuringiensis* is dependent upon protoxin composition and is a factor in toxicity to insects. Appl Environ Microbiol, 1991. 57(4): p. 981-6.

40.McGaughey, W.H. and M.E. Whalon, Managing insect resistance to *Bacillus thuringiensis* toxins. Science, 1992. 258(5087): p. 1451-5.

41.Bietlot, H.P., et al., Characterization of the cysteine residues and disulphide linkages in the protein crystal of *Bacillus thuringiensis*. Biochem J, 1990. 267(2): p. 309-15.

42.Yamagiwa, M., et al., Activation process of dipteran-specific insecticidal protein produced by *Bacillus thuringiensis* subsp. *israelensis*. Appl Environ Microbiol, 1999. 65(8): p. 3464-9.

43.de Maagd, R.A., A. Bravo, and N. Crickmore, How *Bacillus thuringiensis* has evolved specific toxins to colonize the insect world. Trends Genet, 2001. 17(4): p. 193-9.

44.Hodgman, T.C. and D.J. Ellar, Models for the structure and function of the *Bacillus thuringiensis* delta-endotoxins determined by compilational analysis. DNA Seq, 1990. 1(2): p. 97-106.

45.CK., S.S.a.A., Delta endotoxins form cation-Selective channels in planar lipid bilayers. Biochem Biophy Res Commun 1990. 169(2): p. 765-772.

46.Pigott, C.R. and D.J. Ellar, Role of receptors in *Bacillus thuringiensis* crystal toxin activity. Microbiol Mol Biol Rev, 2007. 71(2): p. 255-81.

47.Yaoi, K., et al., Aminopeptidase N from *Bombyx mori* as a candidate for the receptor of *Bacillus thuringiensis* Cry1Aa toxin. Eur J Biochem, 1997. 246(3): p. 652-7.

48.Denolf, P., et al., Cloning and characterization of *Manduca sexta* and *Plutella xylostella* midgut aminopeptidase N enzymes related to *Bacillus thuringiensis* toxin-binding proteins. Eur J Biochem, 1997. 248(3): p. 748-61.

49.Valaitis, A.P., A. Mazza, R. Brousseau, and L. Masson, Interaction analyses of *Bacillus thuringiensis* Cry1A toxins with two aminopeptidases from gypsy moth midgut brush border membranes. Insect Biochem. Mol. Biol., 1997. 27: p. 529-539.

50.Banks, D.J., et al., *Bacillus thuringiensis* Cry1Ac and Cry1Fa delta-endotoxin binding to a novel 110 kDa aminopeptidase in *Heliothis virescens* is not N-acetylgalactosamine mediated. Insect Biochem Mol Biol, 2001. 31(9): p. 909-18.

51.Nakanishi, K., et al., Aminopeptidase N isoforms from the midgut of *Bombyx mori* and *Plutella xylostella* their classification and the factors that determine their binding specificity to *Bacillus thuringiensis* Cry1A toxin. FEBS Lett, 2002. 519(1-3): p. 215-20.

52.Vadlamudi, R.K., T.H. Ji, and L.A. Bulla, Jr., A specific binding protein from *Manduca sexta* for the insecticidal toxin of *Bacillus thuringiensis* subsp. *berliner*. J Biol Chem, 1993. 268(17): p. 12334-40.

53.Nagamatsu, Y., et al., Identification of *Bombyx mori* midgut receptor for *Bacillus thuringiensis* insecticidal CryIA(a) toxin. Biosci Biotechnol Biochem, 1998. 62(4): p. 718-26.

54.Hua, G., et al., Binding analyses of *Bacillus thuringiensis* Cry delta-endotoxins using brush border membrane vesicles of *Ostrinia nubilalis*. Appl Environ Microbiol, 2001. 67(2): p. 872-9.

55.Fernandez, L.E., et al., A GPI-anchored alkaline phosphatase is a functional midgut receptor of Cry11Aa toxin in *Aedes aegypti* larvae. Biochem J, 2006. 394(Pt 1): p. 77-84.

56.Dechklar, M., et al., Functional expression in insect cells of glycosylphosphatidy linositol-linked alkaline phosphatase from *Aedes aegypti* larval midgut: a *Bacillus thuringiensis* Cry4Ba toxin receptor. Insect Biochem Mol Biol, 2011. 41(3): p. 159-66.

57.Thammasittirong, A., et al., *Aedes aegypti* membrane-bound alkaline phosphatase expressed in *Escherichia coli* retains high-affinity binding for *Bacillus thuringiensis* Cry4Ba toxin. Appl Environ Microbiol, 2011. 77(19): p. 6836-40.

58.Lee, M.K., et al., Location of a *Bombyx mori* receptor binding region on a *Bacillus thuringiensis* delta-endotoxin. J Biol Chem, 1992. 267(5): p. 3115-21.

59.Kwak, I.S., H. Lu, and D.H. Dean, Exploration of receptor binding of *Bacillus thuringiensis* toxins. Mem Inst Oswaldo Cruz, 1995. 90(1): p. 75-9.

60.Rajamohan, F., et al., Single amino acid changes in domain II of *Bacillus thuringiensis* CryIAb delta-endotoxin affect irreversible binding to *Manduca sexta* midgut membrane vesicles. J Bacteriol, 1995. 177(9): p. 2276-82.

61.Rajamohan, F., et al., Role of domain II, loop 2 residues of *Bacillus thuringiensis* CryIAb delta-endotoxin in reversible and irreversible binding to *Manduca sexta* and *Heliothis virescens*. J Biol Chem, 1996. 271(5): p. 2390-6.

62.Rajamohan, F., et al., Mutations at domain II, loop 3, of *Bacillus thuringiensis* CryIAa and CryIAb delta-endotoxins suggest loop 3 is involved in initial binding to lepidopteran midguts. J Biol Chem, 1996. 271(41): p. 25220-6.

63.Almond, B.D. and D.H. Dean, Structural stability of *Bacillus thuringiensis* delta-endotoxin homolog-scanning mutants determined by susceptibility to proteases. Appl Environ Microbiol, 1993. 59(8): p. 2442-8.

64.Liang, Y. and D.H. Dean, Location of a lepidopteran specificity region in insecticidal crystal protein CryIIA from *Bacillus thuringiensis*. Mol Microbiol, 1994. 13(4): p. 569-75.

65.Widner, W.R. and H.R. Whiteley, Location of the dipteran specificity region in a lepidopteran-dipteran crystal protein from *Bacillus thuringiensis*. J Bacteriol, 1990. 172(6): p. 2826-32.

66.Barusrux, S., et al., *Ex vivo* cytotoxicity of the *Bacillus thuringiensis* Cry4B delta-endotoxin to isolated midguts of *Aedes aegypti* larvae. J Biochem Mol Biol, 2003. 36(3): p. 294-8.

67.Lailak, C., et al., *Bacillus thuringiensis* Cry4Ba toxin employs two receptor-binding loops for synergistic interactions with Cyt2Aa2. Biochem Biophys Res Commun, 2013. 435(2): p. 216-21.

68.P, U., Investigation of functional motifs of *Bacillus thuringiensis* Cry4 toxin. (Ph.D thesis) Mahidol University, 2001.

69.Del Sal G, M.G., Scheider C., A one-tube plasmid DNA mini-preparation for sequencing. Nucleiac Acid Res, 1988. 16(20): p. 9878.

70.Sambrook J, M.T., Fritsch EF., Molecular cloning: a laboratory manual. Newyork, USA: Cold spring harbor laboratory press. 2001.

71.DJ, F., Probit analysis. Cambridge University Press, Cambridge, United Kingdom, 1971.

72.Thamwiriyasati, N., et al., Crystallization and preliminary X-ray crystallographic analysis of a full-length active form of the Cry4Ba toxin from *Bacillus thuringiensis*. Acta Crystallogr Sect F Struct Biol Cryst Commun, 2010. 66(6): p. 721-4.

73.Catalano, J., et al., Structural evidence: a single charged residue affects substrate binding in cytochrome P450 BM-3. Biochemistry, 2013. 52(39): p. 6807-15.

74.Bartholow, T.G., et al., Strictly conserved lysine of prolyl-tRNA Synthetase Editing domain facilitates binding and positioning of misacylated tRNA(Pro.). Biochemistry, 2014. 53(6): p. 1059-68.

75.Harms, J.E., et al., A charge-inverting mutation in the linker region of a-amino-3-hydroxy-5-methyl-4-isoxazolepropionic acid (AMPA) receptors alters agonist binding and gating kinetics independently of allosteric modulators. J Biol Chem, 2014.

BIOGRAPHY

NAME	Miss Sarinporn Visitsattapongse
DATE OF BIRTH	14 April 1982
PLACE OF BIRTH	Bangkok, Thailand
INSTITUTES ATTENDED	Mahidol University, 2000-2003: Bachelor of Science (Biology) Mahidol University, 2004-2006: Master of Science (Molecular Genetics and Genetic engineering) Mahidol University, 2007-2013: Doctor of Philosophy (Medical technology)
RESEARCH GRANTS	The Commission on Higher Education, Ministry of Education, Thailand, 2007-2010
HOME ADDRESS	36/67 Soi Prachasongkro 23, Prachasonkro Rd, Dindang, Bangkok, Thailand Email: appkung@gmail.com